Sudan University of Science and Technology
College of Graduate studies

Change of the Electrical Magnetic and Optical Properties of Nano Sodium Chloride Due to the Change of its Nano Structure

تغيير الخواص الكربية والمغنطيسية والضوئية لكلوريد الصوديوم النانوي نتيجة لتغير تركيبته النانوية

A thesis Submitted in Fulfillment of the Requirements for the Degree of Doctor of Philosophy in Physics

By

Mahmoud Hassan Osman Fadl

Supervisor

Prof. Dr. Mubarak Dirar Abd-Alla

2022

الآيـــــة

قَالَ تَعَالَىٰ:

﴿ ۞ ٱللَّهُ نُورُ ٱلسَّمَٰوَٰتِ وَٱلْأَرْضِ ۚ مَثَلُ نُورِهِۦ كَمِشْكَوٰةٍ فِيهَا مِصْبَاحٌ ۖ ٱلْمِصْبَاحُ فِى زُجَاجَةٍ ۖ ٱلزُّجَاجَةُ كَأَنَّهَا كَوْكَبٌ دُرِّىٌّ يُوقَدُ مِن شَجَرَةٍ مُّبَٰرَكَةٍ زَيْتُونَةٍ لَّا شَرْقِيَّةٍ وَلَا غَرْبِيَّةٍ يَكَادُ زَيْتُهَا يُضِىٓءُ وَلَوْ لَمْ تَمْسَسْهُ نَارٌ ۚ نُّورٌ عَلَىٰ نُورٍ ۗ يَهْدِى ٱللَّهُ لِنُورِهِۦ مَن يَشَآءُ ۚ وَيَضْرِبُ ٱللَّهُ ٱلْأَمْثَٰلَ لِلنَّاسِ ۗ وَٱللَّهُ بِكُلِّ شَىْءٍ عَلِيمٌ ﴿٣٥﴾ ﴾

سـورة النـور الآيـة (٣٥)

Dedication

I would like to dedicate this work to the Soul of my Father who was my first teacher, I learned even how to speak and how to walk from him, He taught me to be honest and to ambitious. Also I would like to dedicate my work to my mother whose I love dearly and owe everything, and to my lovely and kindness Brothers… In addition my work is dedicated to the following: 1/To all my great teachers.

2/ To all colleagues, friends, and everyone who helped.

3/ Also to everyone who helped me during this research by anyway.

Mahmoud

Acknowledgement

I would like to thank God for helping me and giving me life, health and time to accomplish this work .Thanks to Sudan University of Science and Technology, department of physics for permission to do this research . for permission to do the experimental at physics lab.

I extend my gratitude to my supervisor **Prof. D r. Mubarak Dirar Abdulla** who gave me much useful advice, and support which has encouraged me throughout this whole process.

I would like to thank **Dr. Ali Sulaiman** of Omdurman Islamic University for his academic advice and **Dr. Abdalsakhi sulaiman** of alneelain University of Science & Technology for helping me during the experimental part of this research .

And to everyone who have helped me with his valuable advice and efforts.

April 2022

Abstract

Nano science represents one of the most popular powerful tools for controlling and changing the physical properties of matter. It is now widely used in many applications. One of the most popular known one is the field of electronics, where the optical and electrical properties of matter are important. This encourages to do this work.

In this work 8 Na Cl samples were prepared and crushed for different micro sizes and nano sizes using crushing machine. Before that the samples where purified by being dissolved in water that flows through sever and dried using drying machine. Their optical, electrical and magnetic properties were investigated by UV, FTIR and XRD. The ultraviolet - visible (UV) determines absorption coefficient, energy gap and conductivity. Fourier transform infra-red spectrometer (FTIR) determines the chemical energy bonds. The X-ray diffraction (XRD) technique determines the crystal structure as well as the nana structure.

The crushing of Nacl into small particles having different micro sizes shows that this causes their physical properties to change. It was found that their nano size increases upon increasing their micro size, where each micro particle consists of aggregates of nano crystals. The absorption coefficient, crystal spacing increases upon increasing the nano and micro size. The energy gap decreases upon increasing the nano and micro size. The optical conductivity also increases for a wide range of wavelengths. The electric conductivity, permittivity, refractive index and magnetic permeability decreases for short wavelengths and increases for long wave lengths upon increasing the nano and micro size.

المستخلص

يعتبر علم النانو من أحد أفضل وأكفأ الطرق للتحكم ولتغيير خواص المادة الفيزيائية. وهو يستخدم الان على نطاق واسع في العديد من التطبيقات. ويعتبر مجال الإلكترونيات من احد افضل المجالات المعروفة حيث تكون الخواص الضوئية والكهربية مهمة. وهذا ما دفع للقيام بهذا العمل. في هذا العمل حضرت وسحقت 8 عينات من كلوريد الصوديوم بإبعاد مايكروية ونانوية مختلفة وذلك باستخدام جهاز سحن. وقبل ذلك نقيت العينات بإذابتها في ماء ثم تمريرها عبر غربال ثم جففت بجهاز تجفيف. ثم درست خواصها الضوئية والكهربية باستخدام الاشعة فوق البنفسجية وتحت الحمراء وحيود الاشعة السينية. حيث حدد مطياف الأشعة فوق البنفسجية معامل الامتصاص وفجوة الطاقة والموصلية. في حين حدد مطياف تحويل فورير للاشعة تحت الحمراء روابط الطاقة الكيميائية. اما تقنية حيود الاشعة السينية فقد حددت واوجدت التركيب البلوري بنفس قدر التركيب النانوي. بينت عملية سحق كلوريد الصوديوم لجسيمات ذات احجام مايكروبة مختلفة ان خواصها الفيزيائية تتغير. وقد وجد ان البعد النانوي يزيد بزيادة البعد المايكروي حيث يحوي اي جسيم مايكروي على مجموعة من البلورات النانوية. حيث يزيد معامل الامتصاص والمسافة بين البلورات بزيادة البعد المايكروي والنانوي. اما فجوة الطاقة فتقل بزيادة البعد المايكروي والنانوي. وتزيد الموصلية أيضا لمدى واسع من الأطول الموجية. حيث تقل الموصلية الكهربية والسماحية الكهربية ومعامل الانكسار والنفاذية المغنطيسية للأطوال الموجية القصيرة وتزيد للأطوال الموجية الطويلة عند زيادة البعد النانوي والمايكروي.

Table of Contents

List of Tables

List of Figures

List of Abbreviations

Abbreviations	Full name
IC	Integrated Circuits
XRD	X-ray Diffraction
UV	Ultra Violet - visible spectrometer
NNI	National Nanotechnology Initiative
CNT	Carbon Nanotube
ITs	Information Technologies
SWNTs	Single-Wall Nanotubes
MWNTs	Multi -Wall Nanotubes
SWCNTs	Single-Walled Carbon Nanotubes
MWCNT	Multi - Walled Carbon Nanotubes
LCD	Liquid-Crystal Display
NED	Nano- Emission Display
NAA	Neutron Activation Analysis
ICPMS	Inductively Coupled Plasma Mass Spectrometry
DSS-ET AAS	Direct Solid Sampling Electro thermal Atomic Absorption Spectrometry
ICP-MS	Inductively Coupled Plasma Mass Spectrometry
ICP OES	Inductively Coupled Plasma Optical Emission Spectrometry
FET	Field -Effect Transistors
FTIR	Fourier Transform Infrared Spectroscopy

Chapter One

Introduction

1.1 Nano science

The physical property of matter plays an important role in civilization. This includes electric, magnetic, thermal and mechanical properties. These properties are widely used in industry for fabrication of electronic devices like mobile phones, computers and solar cells [1]. The magnetic properties are used mainly in generating electricity and for fast trains. The mechanical properties are used for the body of cars, buildings and factories [2]. To understand the properties of matter its very important to understand the nature of atoms. Atoms are the building blocks of matter. The nature of atoms can be under stood using quantum laws, like Schrodinger, Klien-Gordon, and Dirac equations [3,4]. Quantum laws describe the behavior of elementary particles, atoms and small tiny particles on the scale of nano. Nano materials or consists of isolated particles that have dimensions in the range (1nm_300nm) where 1 Nano meter (1nm) is one of 100 million parts of 1 meter [5]. The behavior of the Nano material is found to be different from that of the bulk matter. This comes from the fact that nanometers are formed from Nano isolated particles which does not interact with each other [6]. This means that Nano materials have different physical properties from the bulk matter these properties include optical, mechanical, electrical, magnetic and thermal properties [7]. The new properties of Nano materials open a new horizon in technology. It enables scientists to control some physical properties of material to be used in energy, electronics, industry and medicine.

1.2 Research Problem

There are many problems facing the world concerning energy and industry. This needs controlling and searching for materials that have specific physical properties to solve these problems. Nano science can do this because it enables controlling the properties of matter. This needs knowing the mechanisms that control the physical properties of matter. This requires doing intensive work to see how to control the physical properties of nano material.

1.3 Aim of the Work

The aim of this work is to study the optical, electrical and magnetic properties of nano sodium chloride (Nacl) with different micro and nano sizes.

1.4 Thesis Layout

The thesis consists of many chapters. Chapters one and two are concerned with introduction and theoretical background. Chapters three and four are devoted for materials and methods beside results discussion and conclusion.

Chapter Two

Theoretical Background and Previous Studies

2.1 Introduction

The physical properties of matter are important in industry. In this chapter the crystal structure, optical, and electrical properties of matter are exhibited.

2.2 Crystals

Crystals are materials in which atoms or molecules are arranged regularly in one, two or three dimensions. The crystal structure consists of regular points cold lattice. When one put on each lattice point the so cold unit cell the crystal is formed. The unit cell consists of one atom or many interacting atoms that have the same structure and shape. The geometry of crystal structure can be described using the Bravais Lattice. A Baravais lattice is the three dimensional matrix of points which, together with the atoms or molecules situated at the points, form the crystal structure. A Bravais Lattice consists of all points generated by the vectors [9].

$$R= \sum n_i, a_i, \quad i= 1,2,3 \qquad \textbf{(2.1)}$$

Where a_i is a vector and n_i take on all integral values. The a_i which generate the Bravais Lattice is know as a primitive vector.

In the simple cubic structure, which has an atom at each corner of a cube of dimension the Bravais Lattice can be determined by three mutually orthogonal vectors.

$$a_1=ax,\ a_2 =ay,\ a_3=az \qquad \textbf{(2.2)}$$

one usually distinguishes simple (Brava's) Lattices and Lattices with a basis. To describe a unit cell, one needs to specify, its three dimension a,b and c and three angles α, β, λ.

2.3 Atomic spectra and Optical properties

Electromagnetic waves and photons are emitted from atoms when the electrons jump and transferee from one of the excited states to one of the lower states. The resulting emission is cold atomic spectra. The atomic spectra include visible light, x-rays and gamma rays. The electromagnetic waves can be scattered, transmitted, absorbed, refracted or reflected.

2.3.1 Scattering

Scattering process takes place when the incident electromagnetic beam enters bulk matter and collides with atoms and molecules. In this case photons collide with atoms and change their direction and energy. The scattering process leads to gain energy by the medium. This energy can be converted into heat energy or can excite atoms.

Small-Angle Scattering (SAS)

The small angle scattering is a scattering technique based on the deflection of a beam of particles, or an electromagnetic or acoustic wave, away from the original trajectory after it interferes with structures that are much larger than the wavelength of the radiation. The deflection is small (0.1-100 for SAS), hence the name. Small angle scattering SAS technique can give information about the size and orientation of structures in a sample [10].

Tyndall Effect

The Tyndall effect is the scattering of light by particles in colloidal systems such as emulsion or suspensions. It is named after 19th-century Irish scientist John Tyndall. The Tyndall effect is used to find the difference between types of mixtures, namely, solution, colloidal and suspension. For example, the Tyndall effect is seen when car headlamps are used in fog. According to [11], the light of shorter wavelength scatters better. Thus the color of scattered light has a bluish tint. This is also the reason why the sky

looks blue when viewed away from the sun. The blue light from the sun is scattered to a greater degree and is therefore visible far from its source.
This effect occurs because short wavelengths of light thit the air molecules in the earth's atmosphere and are reflected down to the earth surface. Longer wavelengths are less affected by the particles and pass on through the earth's atmosphere. Blue light scatters more rapidly than red light at sunset, and the path length of the sun through the atmosphere is longer at any other time of the day. This is because the blue components of the light have undergone multiple scattering events such that the intensity at such great seeing distance is minimal due to long path length.

Multiple scattering

Multiple scattering is realized in accordance with the laws of single scattering at each successive act. The final result is obtained by successive adding the results of simple scatterings taking into account the statistical nature of their occurrence. The radiation scattered by a particle may be scattered by another particle, and so on [12].

Thomson scattering

Thomson scattering is the type of electromagnetic scattering by charged particles in which the electric and magnetic components of the incident wave accelerate the particle. The accelerated particles emit radiation and the wave is scattered. The main cause of the acceleration of the particle is due to the electric field components of the incident wave. The particle will move in the direction of the oscillating electric field, resulting in electromagnetic dipole radiation. The moving particle radiates strongly in a direction perpendicular to its motion and that radiation will be polarized along the direction of its motion, depending on where an observer is located. The light scattered from a small volume element may be appear to be more or less polarized [13].

Compton scattering

Compton scattering is the type of scattering that occur as a result of change in the energy of the photon when it interacts with matter. The effect is important as it demonstrates that light cannot be explained purely as a wave phenomenon. The Compton scattering is described by the quantum Plank hypotheses Compton experiment convinced physicists that light can behave as a stream of particles whose energy is proportional to the frequency [14].

Brillion scattering

In Brillion scattering the light in a medium interacts with time dependent density variation and changes its frequency and trajectory . The density variation may be as a result of acoustic modes such as phonons or temperature gradient as described in classical physics. When the medium is compressed its index of refraction changes and light path necessarily bends. Brillion scattering is an interaction of light photons with acoustic or vibration quantum (phonons), with magnetic spin waves (magnons) or with other low frequency quasi particles interacting with light.

According to Matveev (1988), the interaction consists of an inelastic scattering process in which a phonon or magnon is either created (stokes process) or annihilation (anti stokes) the energy of the scattered light is slightly changed, that is decreased for a stokes process and increase for anti- stokes process. This shift known as Brillion shift is equal to the energy of the interacting phonon and magnon, and thus Brillion scattering can be used to measure phonon and magnon energies.

For intense beam (e. g laser light) travelling in a medium such as fiber, the variation in the electric field of the beam itself may produce acoustic vibration in the medium. The beam may undergo Brillion scattering from these vibrations, usually in opposite direction to the incoming beam [15].

Raman scattering

Raman scattering is the type of in-elastic scattering of a photon. When light is scattered from an atom or molecule, most photon have the same energy (frequency) and wavelength as the incident photons. A small part of the scattered light is scattered by an excitation, with the scattered photons having different form, and usually lower than a frequency of the incident photons. In a gas Raman scattering can occur with a change in vibration, rotational or electronic energy of a molecule [16].

Rayleigh scattering

Rayleigh scattering is strongly dependent on the viewing angle with a degree of dependence in turn dependent on photon wavelength; hence the shorter the wavelength, the stronger the light scattering. The sky is blue because of Rayleigh scattering which is stronger with shorter wavelengths. Blue-violet light has a shorter wavelength than red light, so blue-violent is scattered more strongly, resulting in a blue sky. The relative size of scattering particles is defined by the ratio of its characteristic dimension and wavelength.

where r is the radius of a spherical particle, λ is wavelength.

Rayleigh scattering occurs when light travels in transparent solids and liquids but is most prominently seen in gases. The amount of Rayleigh scattering that happens to a beam of light is dependent upon the size of the particles and the wavelength of the light; in particular, the scattering coefficient, and hence the intensity of the scattered light, varies for small size particles inversely with the fourth power of the wavelength. This wavelength dependence means that blue light is scattered much more than red light. In the atmosphere, the result is that blue light is scattered much more than glare at longer wavelengths, and so one sees blue light coming from all directions of the sky. At higher altitudes, high up in the mountain

or an airplane, we can observe that the sky is much darker because the amount of scattering particles is much lower. When the Sun is quiet on the horizon, the sunlight must pass through a much higher air mass to reach an observer on the ground. This causes much more scattering of blue light, but a relatively little scattering of red light, and results in a pronounced red-hued sky in the direction towards the sun, Rayleigh scattering can be defined as scattering in small size parameters regime . The amount of Rayleigh scattering that occurs to a beam of light is dependent upon the size of the particles and the wavelength of the sun in particular, and the scattering coefficient. Moreover, the intensity of the scattered light, varies for small size parameter inversely with fourth power of the wavelength, which means that the shorter wavelength of the blue light will scatter more than the longer wavelength of green and red light which gives the sky a blue appearance. However, when one looks towards the sun one sees colors that were not scattered away to longer wavelengths, such as red and yellow light. When the sun is near the horizon the volume of air through which sunlight must pass is significantly greater than when the sun is high in the sky. Accordingly, the gradient from a red-yellow sun to the blue is considerably sharper at sunrise and sunset. Rayleigh scattering was explained by Lord Rayleigh who described the details in 1871.The angular distribution of Rayleigh scattering given by the term (1+cos2q) is symmetric in the plane normal to the incident direction of the light, and so the forward scatter equally the backward scatter [17].

The Mie Theory

Scattering by spheres larger than the Rayleigh range is usually known as Mie scattering. In the Mie regime, the shape of the scattering center becomes much more significant, and the theory only applies well to spheres and, with some modification, spheroids, and ellipsoids. Closed-form

solutions for scattering by specific other simple shapes exist, but no general closed-form solution is known for arbitrary shapes (Ni et al., 2010). The wavelength dependence of Mie scattering is approximately described by $1/\lambda$ [18].

The Mie theory is formulated as follows: a linearly polarized plane wave propagating along the z-axis incident on a homogeneous spherical particle of an arbitrary size having refractive index m. The origin is taken at the center of the sphere and the x-axis in the plane of electric vibration of the incident wave. It was proposed that the external medium is assumed to be in the vacuum. The Mie theory provides an exact description of light scattering valid for spherical particles of an arbitrary size and refractive index. The method of solution consists of expanding incident field into an infinite series of terms, each of which corresponds to a specific spherical harmonics.

A similar expansion with arbitrary coefficient is carried out for the scattering waves. These coefficients, called the Mie coefficients are obtained by matching both fields on the surface of the sphere to satisfy the electromagnetic boundary conditions. The theory bear the additional provision that the particles be randomly distributed and separated from each other and are large compared to the wavelength of the incident radiation. Under these conditions, the total energy scattered is equal to the energy that is distributed by one particle multiply by their number.

An important property of the Mie scattering is that it has a weak dependence of the wavelength for particle having a considerably larger than the wavelength. And because of this the clouds are white and the sky is blue.

The sky, which is blue at the zenith, gradually becomes grey towards the horizon. When the atmosphere is foggy, the sky acquires a whitish tint. When an aeroplane flies very high, no sharp line of the horizon is usually

observed, since it is covered by the atmospheric haze. All these phenomena are due to the Mie scattering by the aerosols in the atmospheric air. The low or nearly complete polarization of fog is the consequence of a strong Mie scattering by tiny water drops. The sharp attenuation of light from the sun at dawn or dusk is also largely due to the Mie scattering [19].

According to Society, (2008), Mie theory is well illustrated by a recent implementation of a small Matlab Mie scattering program on a java enabled mobile phone.This allows the use of mobile phone as an active and portable educational tool helping students quickly and interactively obtain a good working kwowledge of the dependence of light scattering on particle size and refractive index.

Scattering, Absorption and Extinction Cross-section

The Mie formulation considers an incident wave of intensity

2.3.2 Absorption

Absorption process takes place when photons are incident on atoms to remove electrons from the ground state to one of excited states. When a beam of photons are incident on a material, the intensity I is given by :

$$I = I_o e^{-\alpha x} \qquad \textbf{(2.3)}$$

Where I_o represents the initial intensity, α is the absorption coefficient, x is the travelled distance and I is the final intensity after leaving the bulk matter.

Optical absorption measurements can be used determine the film thickness, the wavelength dependence of the refractive index and optical absorption coefficient [20].

2.3.3 Refraction

Refraction process takes place when electromagnetic waves transmit through the surface and move away from the original path when it enters the interface between two transparent media. Refraction depends on factors

such as the speed of light and the optical properties of the medium such as the density, atomic structure and band structure [21].

2.3.4 Reflection

Reflection exists when electromagnetic waves reverse its direction when it reach the interface between two media. Reflection depends also on many factors such as the speed of waves and the optical properties of the medium such as the density, atomic structure and band structure [22].

2.3.5 Diffraction

Diffraction results from the interference of secondary waves within the electromagnetic or light beam. This results in appearing of bright and dark fringes which constitute the diffraction pattern. Diffraction takes place when the dimensions of slits or particles or atoms are less than the wave length of the wave used [23].

2.3.6 Refractive index

Light that is transmitted into the transparent materials experiences a change in the speed , and, as a result, is bent at the interface; this phenomenon is called refraction. The refractive index n of a material is defined as the ratio of the velocity in a vacuum c to the velocity in the medium v

$$n = \frac{c}{v} \qquad (2.4)$$

The magnitude of n depends on the wavelength of the light as well as the atomic and crystal structure. Each color and wave length is deflected by a different amount as it passes out of the medium, which results in the separation of the colors. Not only does the index of refraction affect the optical path of light, but also, as explained shortly, it influences the fraction of incident light that is reflected at the surface [24].

2.3.7 Relation between Incident, Reflected and Refracted Beam

When electromagnetic waves impinge and incident on the interface between two media they may be reflected back. The reflection angle of wave from the reflecting surface is equal to the angle of incidence. The angles are defined with respect to the normal to the reflecting plane and the incident and reflected waves.

When light radiation passes from one medium into another having a different indexes of refraction, some of the light is scattered at the interface between the two media even if both are transparent. The reflectivity R represents the fraction of the incident light that is reflected at the interface, or

$$R = \frac{I_R}{I_o} \qquad (2.5)$$

Where I_o and I_R are the intensities of the incident and reflected beams, respectively. If the light is normal (or perpendicular) to the interface, then

$$R = \left(\frac{n_2 - n_1}{n_{2+} n_1}\right)^2 \qquad (2.6)$$

Where n_1 and n_2 are the indices of refraction of the two media. If the incident light is not normal to the interface, R will depend on the angle of incidence. When light is transmitted from a vacuum or air into a solid s, then

$$R = \left(\frac{n_s - 1}{n_s + 1}\right)^2 \qquad (2.7)$$

because the index of refraction of air is very nearly unity. Thus, the higher the index of refraction of the solid, the greater the reflectivity.

The phenomena of absorption, reflection, and transmission take place for the passage of light through a transparent medium. For an incident beam of intensity I_o that impinges on the front surface of a specimen of thickness x and absorption coefficient, the transmitted intensity is given by:

$$I_T = I_o(1 - R)^2 e^{-\alpha x} \tag{2.8}$$

Where R is the reflectance.

2.4 Electric Conductivity and Permittivity:

When the electric field having intensity E is applied between the terminals of a conductor it causes electric current of density J to flow. The constant of proportionality is called conductivity σ where

$$J = \sigma E \tag{2.9}$$

The electric flux density D inside the conductor is given by:

$$D = \in E \tag{2.10}$$

Where $\in$ is the electric permitivit

If the electromagnetic field is propagated in vacuum. The displacement current density is

$$J = \frac{\partial D}{\partial t} = \in \frac{\partial E}{\partial t} = \in \frac{\partial E_o\, e^{-iwt}}{\partial t} = -iw \in E \tag{2.11}$$

Comparing (2.10) and (2.11)

$$\sigma = -iw \in \tag{2.12}$$

Thus the conductivity is a complex quantity as well as the electric permitivity.

Thus one can rewrite equation (2.18) in the form:

$$\sigma = \sigma_1 + i\,\sigma_2 = -iw(\in_1 + i \in_2) = w \in_2 - iw \in_1 \tag{2.13}$$

Thus :

$$\sigma_1 = w \in_2 \qquad \sigma_2 = w \in_1 \tag{2.14}$$

2.5 Magnetic Moment and Susceptibility

It is well known that the electric current produces magnetic field. The magnetic moment P_0 of the atom in which electrons revolving around the nucleus is defined, in terms of the current i and the area A enclosed by it, to be in the form;

$$P_0 = iA \tag{2.15}$$

The current generated by the electron of charge $-e$ moving around a nucleus in a circular orbit takes the form ;

$$i = -ef = \frac{e\omega}{2\pi} \tag{2.16}$$

f is the frequency.

Where the area is given by ;

$$A = \pi r^2 \tag{2.17}$$

On the other hand the orbital angular L is given by [21];

$$L = mvr = m\omega r^2 \tag{2.18}$$

Where m is the electron mass and v is its speed.

Inserting (2.2), (2.3) and (2.4) in (2.1) yields the magnetic moment in the form;

$$P_o = iA = -\frac{e\omega}{2\pi}(\pi r^2) = -\frac{e\omega r^2}{2}$$

$$P_o = \frac{-em\omega r^2}{2m} = -\frac{e}{2m}\vec{L} \tag{2.19}$$

If n atoms per unit volume align themselves along the x-axis thus the component of x is given by;

$$M_x = n\, P_m = -n\, \mu_B\, g_J \vec{J} \tag{2.20}$$

Where M_x changes from 0 to max value during a time$T$. According to M_x one can define the magnetic permeability μ.

The electron revolving around a nucleus in a circular path can produce a magnetic field of flux density$B$. If the electron revolves with frequency f in circular orbit of radius r, then according to Bio-Savart law it produces a magnetic field of flux density;

$$B_e = \frac{\mu_0\, i}{2r} \tag{2.21}$$

$$B_e = \frac{\mu_0\, f\, e}{2r} \tag{2.22}$$

Hence ;

$$i = fe$$

The magnetic moment produced by such an electron is given by ;

$$P_m = iA = i(\pi r^2) = \pi i r^2 \tag{2.23}$$

Where A is the area enclosed by the current i ;

$$A = \pi r^2 \tag{2.24}$$

For z electrons with mean radius r, the magnetic flux density of the atom (B_a) is given by ;

$$B_a = \frac{\mu_0\, zf\, e}{2r} \tag{2.25}$$

Thus the internal atomic magnetic field generated by one electron is $B_i = \frac{\mu_0 fe}{2r}$; and is related to the magnetic moment according to the relation ;

$$B_e = \frac{\mu_0 P_m}{2\pi r^3} \tag{2.26}$$

Since the current for the whole atom [23] is ;

$$i = zfe \tag{2.27}$$

Hence the field of the atoms is related to the magnetic moment also as follows;

$$B_a = \frac{\mu_0 \, P_m}{2\pi r^3} \tag{2.28}$$

But the magnetic moment M is defined in terms of the number of dipoles N divided by the volume V to be ;

$$M = \frac{N \, P_m}{V} \tag{2.29}$$

If the atomic radius is r, thus one atom exists in a volume V_a is given by ;

$$\frac{N}{V} = \frac{1}{V_a} = \frac{1}{\frac{4}{3} \, \pi \, r^3} = \frac{3}{4\pi \, r^3} \tag{2.30}$$

This ;

$$M = \frac{3P_m}{4\pi \, r^3} \tag{2.31}$$

Using (2.25), (2.27), and (2.28) in (2.29) yields ;

$$M = \frac{3}{4\pi r^3}\,\frac{B_a}{\mu_0}\,(2\pi r^3) = \frac{3B_a}{2\mu_0}$$

(2.32)

Assume the proton is affected by nuclear force F_e beside internal magnetic field B_i and a resistive force γv_0 thus, the proton equation of motion ;

$$ma = F_e - B_i\, ev_0 - \gamma v_0$$

$$ma = \frac{mv_0^2}{r} = F_e - eB_i\omega_0 r - \gamma\,\omega_0 r$$

$$m\omega_0^2 r = F_e - eB_i\omega_0 r - \gamma\omega_0 r$$

$$F_e = m\omega_0^2 r + eB_i\omega_0 r + \gamma\omega_0 r$$

(2.33)

When an external magnetic field B_e is applied the frequency becomes ω, thus one gets ;

$$m\omega^2 r = F_e - eB_i\omega r - \gamma\omega r + Bev$$

$$= m\omega_o^2 r + eB_i\omega_o r + \gamma\omega_o r - eB_i\omega r - \gamma\omega r + B_e\omega r$$

$$m(\omega + \omega_0)(\omega - \omega_0)r = eB_i r(\omega_0 - \omega) + \gamma r(\omega_0 - \omega) + B_e\omega r$$

(2.34)

If the frequency ω is greater slightly than ω_0 it follows that ;

$$\omega_L = \omega - \omega_0 \qquad \omega \approx \omega_0$$

(2.35)

$$-2m\omega_0\omega_L = eB_i\omega_L + \gamma\omega_L + B_e\omega_0$$

$$-[2m\omega_0 + \gamma + eB_i]\omega_L = B_e\omega_0$$

$$\omega_L = -\frac{B_e\omega_0}{2m\omega_0 + \gamma + eB_i}$$

(2.36)

The magnetic susceptibility can be found by using;

$$i = -Zef = -\frac{Ze\omega_L}{2\pi}$$

$$P_m = Ai = \pi r_0^2 ef = -Ze\ \omega_L r_0^2$$

(2.37)

Where ;

$$x = y = z$$

$$x^2 = y^2 = z^2$$

Thus ;

$$r^2 = x^2 + y^2 + z^2$$

$$= z^2 + z^2 + z^2 = 3z^2$$

Hence ;

$$z^2 = \frac{1}{3} r^2$$

$$r_0^2 = r^2 - Z^2 = 3Z^2 - Z^2 = 2Z^2 = \frac{2}{3}\ r^2$$

(2.38)

$$M = nP_m = -\frac{2Zner^2\omega_L}{3}$$

$$M = -\frac{2Ze^2nr^2\omega_0 B}{3(2m\omega_0 + \gamma + eB_i)}$$

$$M = -\frac{2Ze^2n\omega r^2\mu_0}{3(2m\omega_0 + \gamma + eB_i)} H = \chi_m H$$

(2.39)

Then magnetic susceptibility is given by ;

$$\chi_m = -\frac{2Ze^2n\omega r^2\mu_0}{3(2m\omega_0 + \gamma + eB_i)}$$

(2.40)

2.6 Determination of Band Gaps

The fundamental absorption is related to the exaction transition from the valence to the conduction band. The transitions are classified into several types, according to the band structure of a material. The relation between absorption coefficient and optic band gap for direct transition (k=0) is given by Tauc equation [24]:

$$\sqrt{\alpha h\nu} = B(h\nu - E_g^{opt}) \tag{2.41}$$

And for indirect transition (k ≠ 0) the relation becomes

$$\alpha(h\omega) \propto \frac{(\hbar\omega - E_{gap})^2}{\hbar\omega} \tag{2.42}$$

From the αhν versus hν one obtains Eg and B parameters. B is also a useful diagnostic of the material since it is inversely proportional to the extent of the tail state (Δ E) at conduction and valance band edges.

2.7 Nano Materials

Nanotechnology is the application of nano science in technology. Nano science is the branch of science dealing with the material structure consisting of isolated nano particles having dimensions ranging from 1 to 300 nano meters. Nano materials being described by quantum laws have properties different from the bulk matter . Potential breakthroughs are possible in areas such as materials and manufacturing, medicine and healthcare, environment and energy, biotechnology and agriculture, electronics and information technology. The effect of nanotechnology on the health, and standard of living for people in this century could be at least as significant as microelectronics, medical imaging, computer-aided engineering, and man-made polymers [25].

2.8 Nanotechnology Goals

Nanotechnology will lead to promote the modern technology giving better understanding of nature; advances in fundamental research ; and significant changes in industrial manufacturing, and environmental management and sustainability. Examples of the promise of nanotechnology, with projected total worldwide market size of over $1 trillion annually in 10 to 15 years, include the following:

• Manufacturing: The nanometer scale is expected to become a highly efficient length scale for manufacturing once Nanoscience provides the understanding and Nano engineering develops the tools. Materials with high performance, unique properties and functions will be produced that traditional chemistry could not create [26].

2.9 Definition of Nanotechnology

Nanotechnology is an active resesearch dealing with the **applications of nano science in technology**. Nanotechnology a term encompassing the science, engineering, and applications of submicron materials – involves the harnessing of the unique physical, chemical properties of Nano materials . The economic and societal promise of nanotechnology has led to investments by governments and companies around the world.

A nanometer is one-billionth of a meter. For example, a sheet of paper is about 100,000 nanometers thick; a single gold atom is about a third of a nanometer in diameter. Dimensions between approximately 1 and 100 nanometers are known as the Nanoscale. Nanotechnology is the understanding and control of matter structure at the dimensions between approximately 1 and 100 nanometers, where unique phenomena enable novel applications. Encompassing.

2.10 Nanoscale Science, Engineering and Technology

Nano science deals with manipulating matter at this length scale. Unusual physical, chemical, and biological properties can emerge in materials at the Nanoscale. These properties may appear dramatically different in important ways from the properties of bulk materials and single atoms or molecules. Using structures designed at this extremely small scale, there exist opportunities to build materials, devices, and systems with Nano properties that can not only enhance existing technologies but also offer novel features with potentially far-reaching technical, economic, and societal implications.

Nanotechnology products can be used for the design and processes in various areas. It has been demonstrated that nanotechnology has many unique characteristics, and can significantly fix the current problems which the non-nanotechnology faced. Nanotechnology deals with the production and applications at scales ranging from a few nanometers to submicron dimensions . The conventional analytic aspects of nanotechnology must yield a certain synthetic approach, which is similar with non-nanotechnology[27]. This action will be conducive to the creation of new functions exhibited by Nanoscale structural units through their mutual interactions, even though these functionalities are not properties of the isolated units **(Huges, 2005**) [28]. It is a technology system aimed at arranging Nanoscale structural units, a group of atoms, molecules, or Nanoscale functional components, into a configuration that creates a novel functionality through mutual interactions among those units. These very small structures in Nanoscale are intensely interesting for many reasons .

Nanostructures are in a range of sizes in which quantum phenomena, especially quantum entanglement and other reflections of the wave character of matter, would be expected to be important.

The nanometer-sized, functional structures that carry out many of the most sophisticated tasks open up an exciting frontier of biology.

One set of considerations revolves around how nanotechnology is characterized, and how nanotechnology is understood as the emphasis moves toward the Nanoera. In the discussion of the Nanoera, there are divergent approaches to define and characterize the corresponding new features (**Lawrence, 2005)** [29]**.**

2.11 Importance of Nanomaterial

Nano science leads to the discovery of new materials with unique properties is the principal parameter for the sustained development of contemporary devices. In the last decade, intensive research efforts were made to create a large number of novel materials, notably those belongs to the nanometer regime. The outcome of the prolific research are the structures with reduced dimension, viz. two-dimensional structure, one-dimensional structure, and zero-dimensional structure. As the size of a material reduces to nanometer-scale dimensions then the material in general become superior to its bulk counterpart for many applications owing to its higher surface-to-volume ratio, size-dependent properties, and its potential for downscaling of device size. Among different elements, Carbon, placed at group 14 (IV A), has become one of the most important elements in the periodic table owing to its ability to form sp3, sp2, and sp hybrids which results in 3D (diamond and graphite), 2D (graphene), 1D [carbon nanotube (CNT)] [30].

2.12 Carbon Nanotube

CNT has become a center of attraction in the field of Nanoscale research in modern science. Nanotubes are nearly one-dimensional structure due to their high length to diameter ratio. CNTs exhibit a unique combination of electronic, thermal, mechanical (**RocoWilliams Alivisatos, 1999**) [31]..

2.13 Nanotechnology Basics

Nanotechnology is concerned with production of materials by controlling matter at the levels of atoms. This means that it is the use of very small particles of materials to create new large-scale materials (Treacy, Ebbeson, 1996) [32].

Nanotechnology are yet undefined as that technologies emerging from a new nanostructured material, or from the electronic properties of quantum dots, or from fundamentally new types of architectures – based on Nano devices for use in computation and information storage and transmission, The key issue is the size of particles because the properties of materials are dramatically affected by the scale of the nanometer (nm), 10-9 meter (m). Actually, nanotechnology is not a new science or technology with current development as we spoke of above. The research on nanotechnology has been very active in the recent two decades for two reasons.

The development and application of nanotechnology rely on the rapid development of other related sciences and technologies, such as physics and chemistry. According to (O. Lourie, Cox, and. Wagner, 1998) the subject of nanotechnology includes "almost any materials or devices which are structured on the nanometer scale in order to perform functions or obtain characteristics which could not otherwise be achieved." To better understand the differences among various scales with regards to nanotechnology just because materials can be made into very small particles does not immediately mean that they have any practical use (Krishram, 1998) [33]. According to quantum theory, materials at the Nanoscale, between 1 nm and 250 nm, lie between the quantum effects of atoms, molecules and the bulk properties of materials. Nanoscale is called 'No- Man's-Land' where many physical and electrical properties of materials are controlled by phenomena that have their own critical dimensions at the Nanoscale. Some 'Nano' definitions used in this paper

are listed below. 1) Cluster: A collection of units (atoms or reactive molecules) of up to about 50 units.

Colloids: A stable liquid phase containing particles in the 1-1000 nm range. A colloid particle is one such 1-1000 nm particle.

Nanoparticle: A solid particle in the range of 1- 100 nm that could be no crystalline, an aggregate of crystallites or a single crystallite.

Nanocrystal: A solid particle that is a single crystal in the nanometer range. With nanotechnology, scientists and engineers can influence, by being able to fabricate and control the structure of nanoparticles, the resulting properties and, ultimately, design materials to give designed properties. The electronic properties that can be controlled at this

Nanoscale are of great interest (Clolbert, K.A., Smith and Smalley 1999)[34].

The range of applications where the physical size of the particle can provide enhanced properties that are of benefit is extremely wide.

The science related to nanotechnology is new compared with other sciences. However, Nano sized devices and objects have existed on earth as long as life. The exceptional mechanical performance of biomaterials, such as bones or mollusk shells, is due to the presence of Nanocrystals of calcium compounds (Cheng, Bai, and Dresselhaus, 2000) [35].

2.14 New Features

Much of Nanoscience and nanotechnology is concerned with producing new or enhanced materials. Also, some nanotechnology-enabled products are already on the market and enjoying commercial success. These materials can behave quite differently at the Nanoscale compared to 7bulk. This is both because the small size of the particles dramatically increase surface area and therefore reactivity, and also because quantum effects start to become significant.

1) Three-dimensional Structure: Many materials with nm dimensions in 1D have been commercially available. Recent developments include producing three-dimensional (3D) particles two dimensional (2D (monolayer films, one-dimensional (1D) (wires and tubes) and zero dimensional (0D)(dots) for functional applications. This section will be concentrated on the developments and structures of 3D carbon particles. Carbon nanostructures have been the focus of much interest and research since they were first observed in the mid- 1980s (Vajtai and et al, 2002)[36].

The Buckminsterfullerene (C60) and its analogs show great promise as lubricants and, thanks to their cage structures, as drug delivery systems, as well as in Carbon C60 A Beautiful Molecule (Vajtai and et al, 2002).electronics. The same graphite sheet structure, which allows electrical conductivity, was discovered in the early 1990s (Vajtai and et al, 2002) [37].Fullerenes consist of 20 hexagonal and 12 pentagonal rings as the basis of an

2) Surface effects : In many sub-fields of nanotechnology, advances in structured materials occur both by evolutionary development of technologies and by revolutionary discoveries that generated new approaches to materials synthesis. As the particle size approaches to the 10 - 100 nm range, the surface to volume ratio increases and properties become size dependent.

Nanoparticles have a remarkable large surface area.

The calculated surface to nanoparticles bulk ratios for solid metal particles vs. the surface area imparts a serious change of surface energy and surface morphology. All these factors alter the basic properties and the chemical reactivity of the nanomaterial's (Falvo, Clary.,1997)[38].

The change in properties causes improved catalytic ability, tunable wavelength-sensing ability and better-designed pigments and paints with self-clean and self-healing features (Evans, L. 1998) [39].

The pressure, due to surface energy and the atomic structure of the surfaces, impacts density, phase transition temperatures,. Physicals Nanoparticles often have their own physical and chemical properties that are very different from the bulk matter .

With the continuous development of nanotechnology, the possibility for the bottom-up production of Nanoscale materials may result in some kind of self-assembly of structures similar to the self-assembly of phospholipid bilayers that resembles cellular membranes. On the basis of current knowledge, however, the spontaneous formation of artificial living systems through self-assembly and related processes, suggested by some prominent commentators, is considered highly improbable. The combination of self-replication with self-perpetuation in an engineered Nano system is extremely difficult to realize on the basis of current scientific knowledge (Binnig and Rohrer 1985) [40].

Nanotechnology is dependent on nanostructures that require creation and characterization. Two fundamentally different approaches for the controlled generation of nanostructures have evolved. On one hand, there is growth and self-assembly, from the bottom up, involving single atoms and molecules. On the other hand, there is the top-down approach in which the powerful techniques of lithography and etching start with large uniform pieces of material and generate the required nanostructures from them. Both methods have inherent advantages. Top down assembly methods are currently superior for the possibility of interconnection and integration, as in electronic circuitry. Bottom-up assembly is very powerful in creating identical structures with atomic precision, such as the super molecular functional entities in living organisms. In many different fields of Nano

scale science, e.g. the production of semiconductor quantum dots for lasers, the production of nanoparticles by a self-organization, and the generation of vesicles from lipids, self-organization is used for the generation of functional nanometer-sized objects. To date, manmade self-organized structures. remain much simpler than nature's complex self-organized processes and structures. As noted above, there is also no reason to believe that processes of self-assembly, which are scientifically very important for the generation of Nanoscale structures, could lead to uncontrolled self-perpetuation (Gang Wang,, 2018) [41].

Magnetic nanoparticles are a class of nanoparticles which can be manipulated by using magnetic field gradients. Such particles commonly consist of magnetic elements such as iron, nickel and cobalt and their chemical compounds. While nanoparticles are smaller than 1 micrometer in diameter (typically 5500 nanometers), the larger microbe ads are 0.5500 micrometer in diameter. Magnetic nanoparticle clusters which are composed of a number of individual magnetic nanoparticles are known as magnetic Nano beads with a diameter of 50200 nanometers Pankhurst. Connolly.

The physical and chemical properties of magnetic nanoparticles largely depend both on the synthesis method and chemical structure. In most cases, the particles range from 1 to 100 nm in size and may display super par magnetism (Chem, 1999).

Types of Nano materials Carbon

Carbon black accounts for the largest tonnage of engineered nanomaterial and carbon blacks are used in a wide variety of applications, including printing inks, toners, coatings, plastics, paper and building products. Dependent on the size and chemistry of the particles, carbon-black-containing plastics can be electrically conducting or insulating and have

significant reinforcing characteristics. Carbon black is a very fine particulate form of elemental carbon

. Although carbon black is still valued today for its coloring attributes, it is primarily used to provide reinforcement and other properties, especially to rubber articles. All carbon black is produced either by incomplete combustion or thermal decomposition of a hydrocarbon feedstock.

Two important characteristics of carbon black are surface area, an indirect measure of particle size, and structure, a measure of the degree of particle aggregation or chaining. Surface areas of carbon blacks can range from c. 10 m2 g-1, for use as reinforcing fillers, up to c. 1100 m2 g-1, for use as electrically conductive fillers. Surface area and structure are dependent on the type of process to manufacture the carbon black and they define the performance of the carbon black in its application. The mass production of carbon blacks started in the first half of the twentieth century in the wake of the expanding type industry. Carbon blacks were used as reinforcing fillers to optimize the physical properties of type and make them more durable. Even today the type industry uses at least 70% of the carbon blacks manufactured worldwide. The remainder finds use in a range of applications. Carbon blacks are now widely used for plastics master batch applications for use in conductive packaging, films, fibers, moldings, pipes

Chapter Three

Literature review

3.1 Introduction:

The applications of nano science covers a wide variety of physical branches including solid state physics, material science [42, 43 , 44], and energy. In this chapter some of the researches done by scientists are exhibited [45 , 46 , 47].

3.2 Syntheses (Ba x Fe1-x Ti O_4) Nano size and Study Crystal properties, Optical Energy Gap and Optical & Electrical Conductivity

Abstract

In this work of some researchers a thin films of (BaxFe1-xTiO_4) (x=1, 0.1, 0.2, 0.3, 0.5, 0.6, 0.7,08, 0.9 and 0) were prepared by the sol- gel method. The influence of Fe concentration on the Nano, electrical and optical properties of the samples was studied by using x-ray diffraction (XRD), and UV-VIS spectroscopy. The X-ray diffraction (XRD) technique analyses shows that for all samples the average Nano size decrease with decreasing of iron concentration. UV-visible absorption spectra showed that the energy gap decreases from (2.074) eV to (2.046) eV as iron concentration decrease. The conductivity which reflects the electrical properties, increases when Fe concentration increases shorter wavelengths and decreases at long wavelength [48].

The (BaxFe1-xTiO4) (x=1, 0.1, 0.2, 0.3, 0.5, 0.6, 0.7,08, 0.9 and 0) Nano thin films compounds were prepared by the sol- gel method. Barium nitrate [Ba(NO3)2]], Iron(III) nitrate [Fe(NO3)3.9HO2] and titanium oxide were used as starting material, distilling water as dissolving medium and nitric acid as adjusting of PH less than 5 PH . First Barium nitrate and iron nitrate

were weighted separately, each one followed by the addition of suitable quantity of distilling water to make solution, which was stirred and heated after PH was adjusted to 5.0 at70c0 for one hour. Secondly the two solutions were mixed and added 3.0g of titanium oxide, the product mixture was heated and stirred at 70c0 continuously about one hour, the last one was deposited for one day then filtered. Then the solution was slowly evaporated to form sol by continues in heat treatment convert to gel at150c0 after two hours. Finally the gel was dried and grinded to powder. The structural properties were determined by using XRD and Riveted. Ultra-visible spectrometer (UV) was used to study optical properties. The spectra for different electrical and optical properties were displayed below

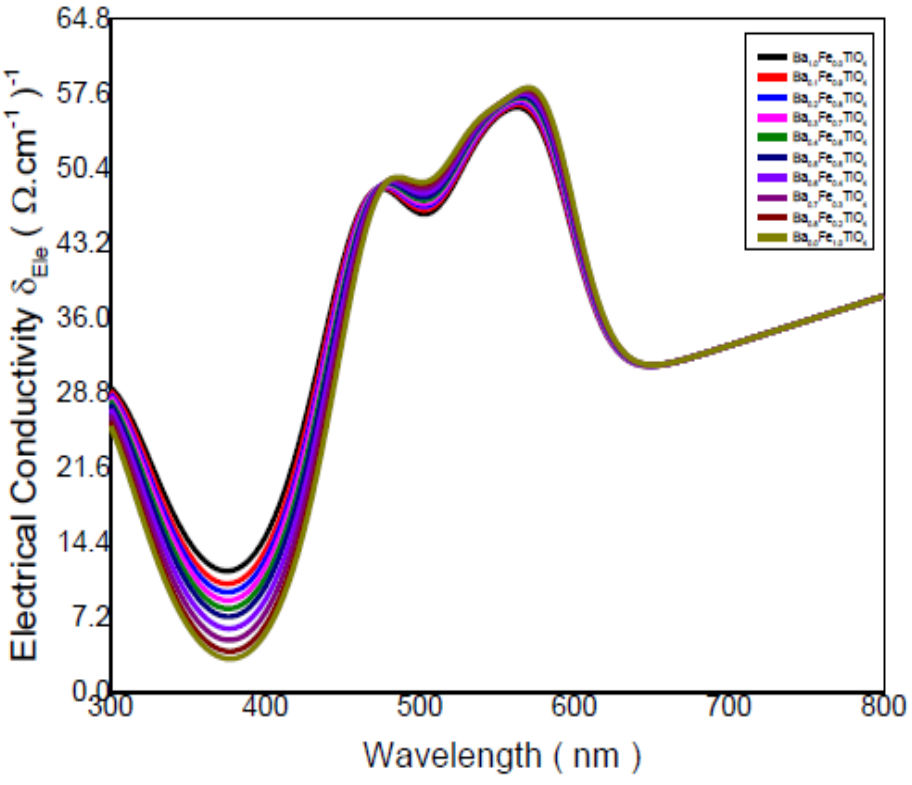

Fig (3.1) Electrical Conductivity spectrum of all (Ba_x $Fe_{(1-x)}$ TiO_4)

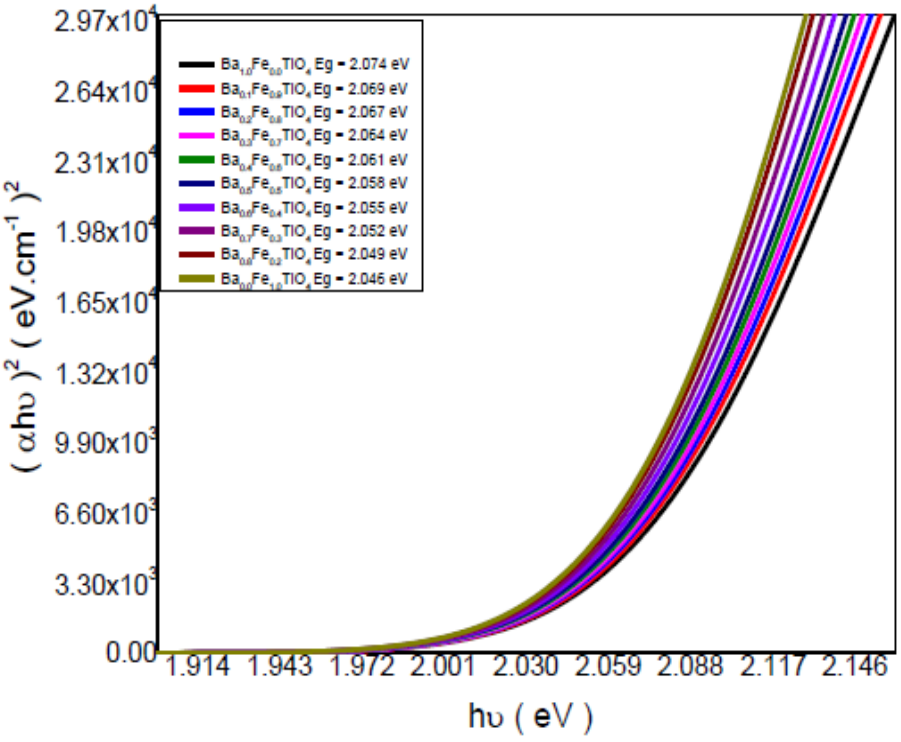

Fig (3.2) Optical Energy Band spectrum of all (Ba_x $Fe_{(1-x)}$ TiO_4) samples

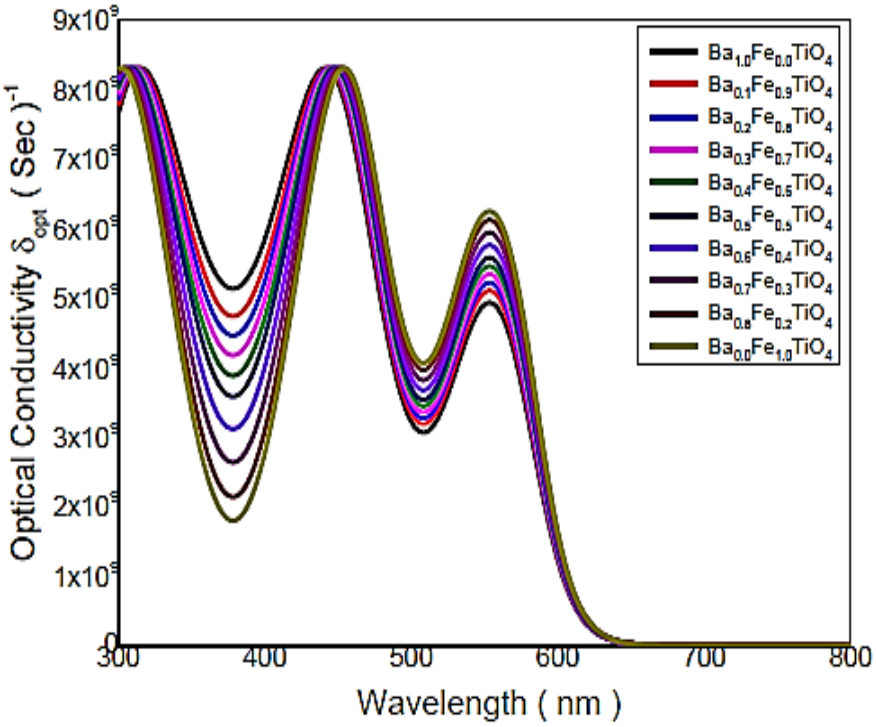

Fig (3.3) Optical Conductivity spectrum of all (Ba_x $Fe_{(1-x)}$ TiO_4)samples

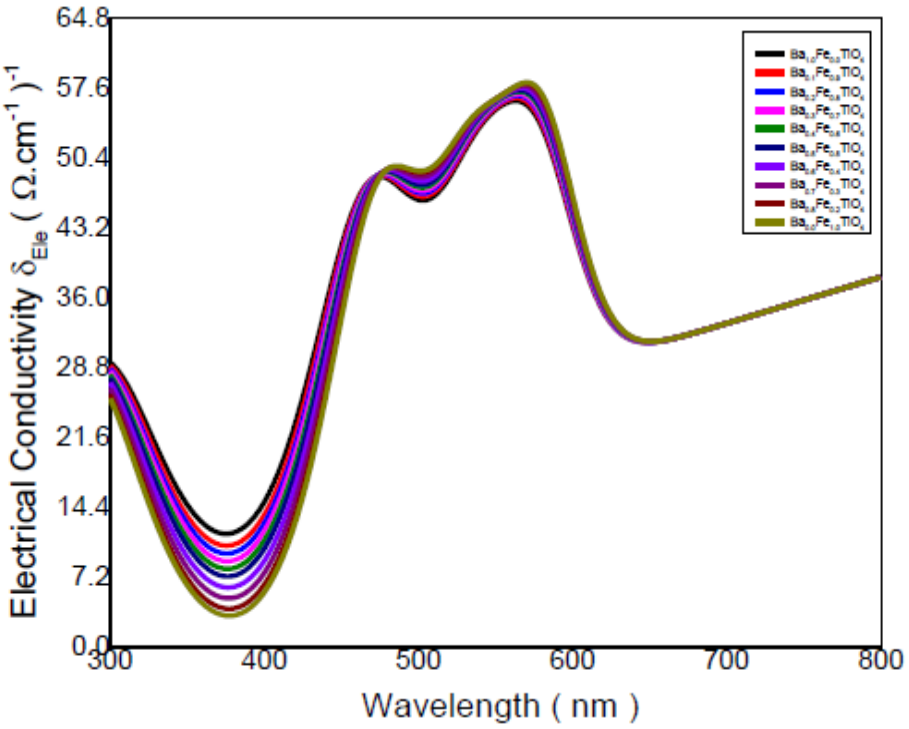

Fig (3.4) Electrical Conductivity spectrum of all (Ba_x $Fe_{(1-x)}$ TiO_4)samples

The energy band gap decreases as the average Nano size decreases. The conductivity increases upon increasing Fe concentration and the Nano size as well.

Different studies confirm this work [49, 50 , 51].

3.3 The Effect of Fe Concentration on Crystal size, Crystal Spacing, Nano Size, and Absorption Coefficient for (Ba x Fe1-x Ti O 4)

In this work, The (BaxFe1-xTiO4) (x=1, 0.1, 0.2, 0.3, 0.5, 0.6, 0.7,08, 0.9 and 0) samples were prepared by the sol- gel method and technique . The effect of Fe concentration on the Nano structure and optical properties of the samples were studied by using x-ray diffraction (XRD), and UV-VIS spectroscopy. The X-ray diffraction (XRD) analyses. The results obtained indicate and show that for all samples the average Nano size decreases upon decreasing iron concentration. UV-visible absorption spectra shows

that decreasing iron concentration increases absorption coefficient. Moreover decreasing Nano size, increases absorption coefficient [52]. The spectrum which shows the absorption coefficient and the effects of changing the nano size are displayed in the figures below

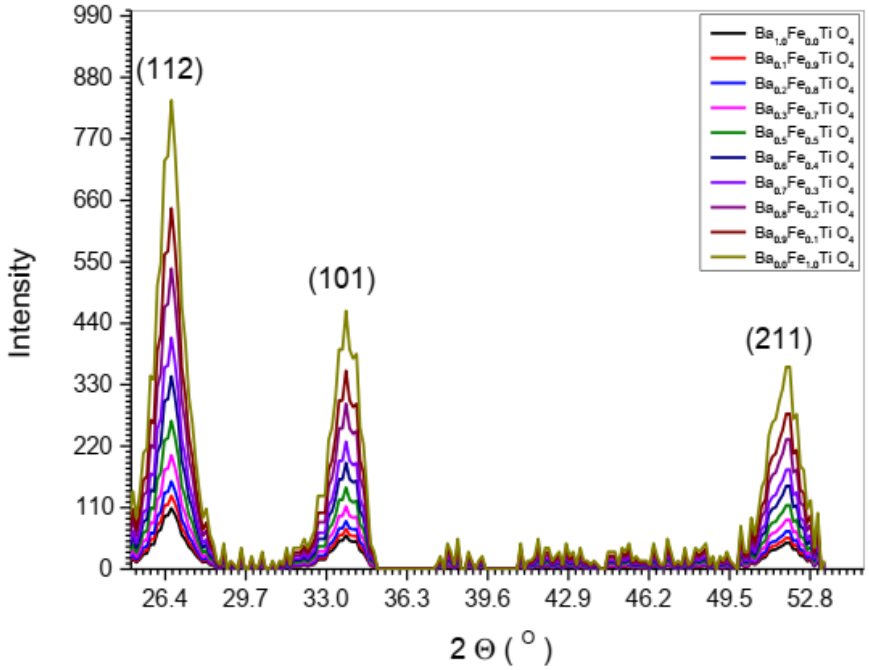

Fig (3.5) XRD spectrum of all (Ba x $Fe_{(1-x)}$ Ti O_4) samples

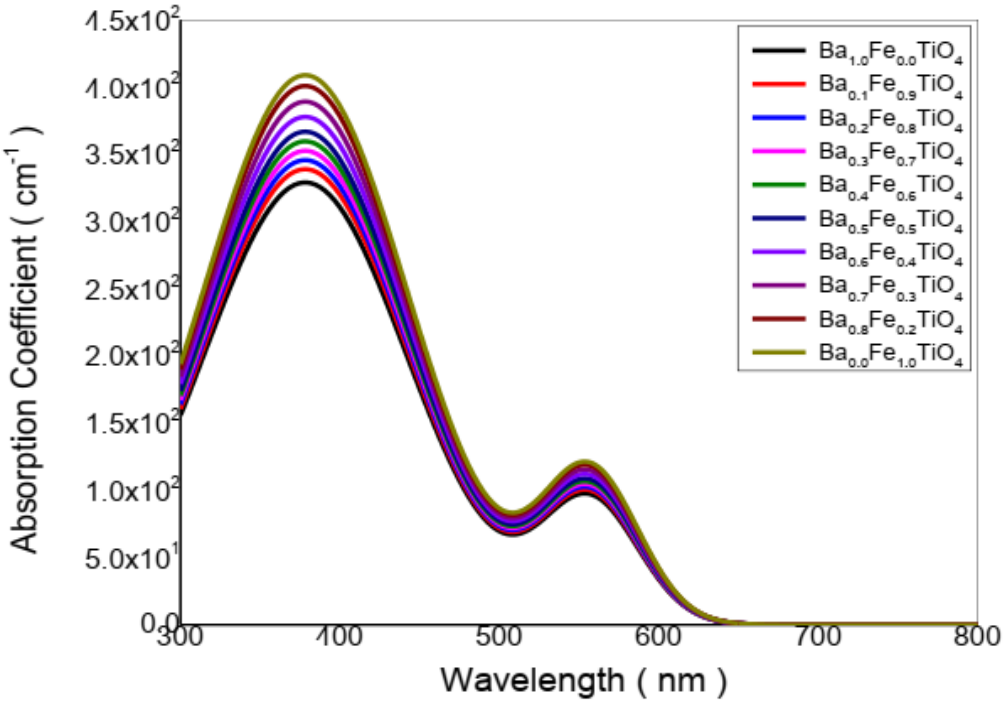

Fig (3.6) Absorption Coefficient spectrum of all (Ba x Fe $_{(1-x)}$ Ti O4) samples

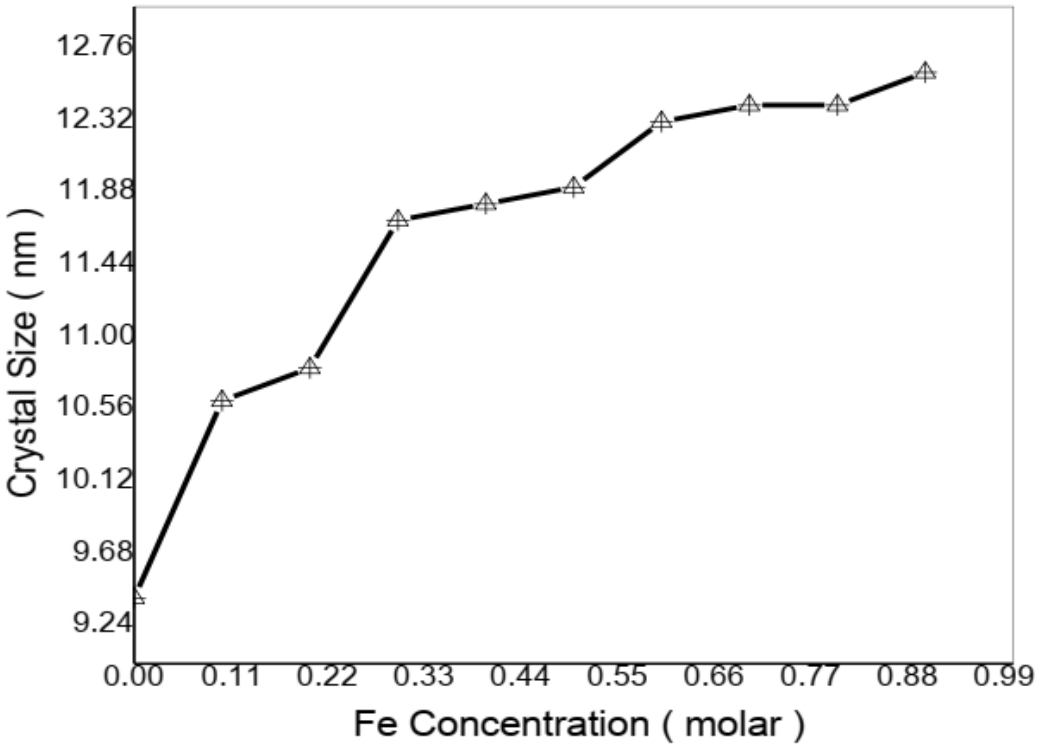

Fig (3.7) relationship between the Fe Concentration and Crystal Size Of all (Ba x Fe $_{(1-x)}$ Ti O_4) sample

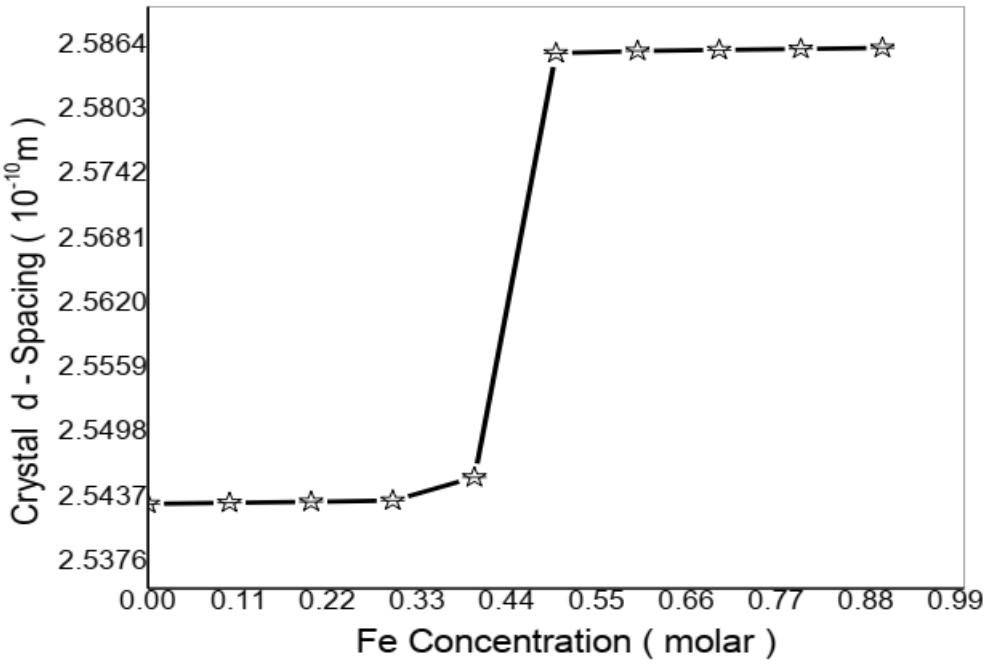

Fig (3.8) relationship between the Fe Concentration and Crystal d-Spacing Of all (Ba x Fe $_{(1-x)}$ Ti O_4) sample

Increasing Fe concentration increases crystal size and crystal spacing. The absorption coefficient decreases upon increasing Fe concentration and crystal size. This study was confirmed by many papers [38 , 39 , 40].

3.4 The Effect of Changing Concentrations of Al_2O_3 On The (ZnO)X(Al_2O_3)1-X Thin Films Absorption And Energy Gap

Thin films samples of (ZnO)x (Al2O3)1-x deposited on glass substrates by Sol-gel method were prepared and formed. Eleven samples were prepared by changing ZnO concentration from 0 to 1 in steps of 0.1. The UV spectral technique was used to determine the absorption coefficient and the energy gap for different wave lengths . The nano crystal size and the crystal spacing of the deposited particles was found by using the x-ray diffraction (XRD) technique. The results obtained show and indicate that the absorption coefficient decreases upon decreasing the nano crystal size and the energy gap decreases when the ZnO concentration decreases from 0.9 to 0.3 [41].

The results obtained are displayed in the figures below

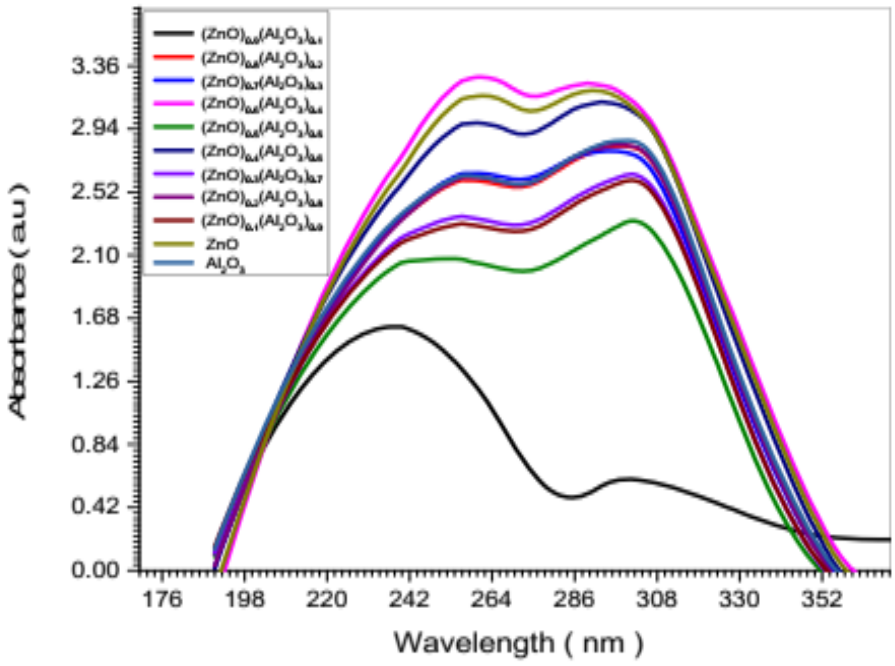

Fig.(3.9) The relation between absorbance and wavelengths of eleventh (ZnO)x $(Al_2O_3)_{1-x}$ samples

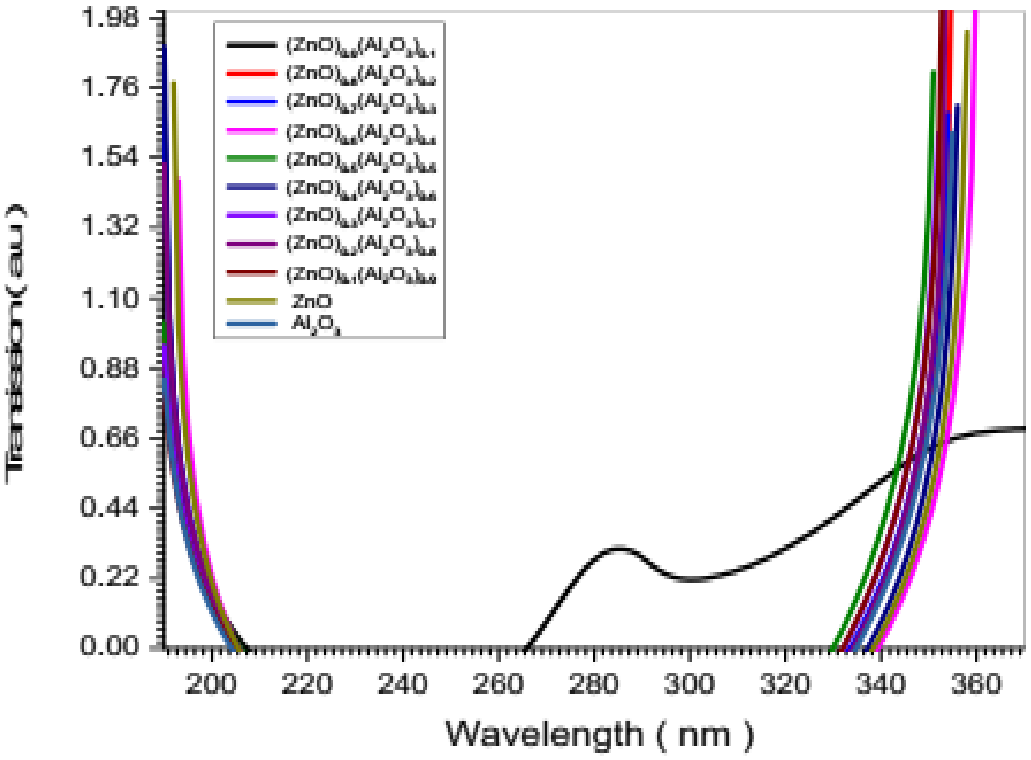

Fig.(3.10) The relation between transmission and wavelengths of eleventh $(ZnO)x\ (Al_2O_3)_{1-x}$ samples

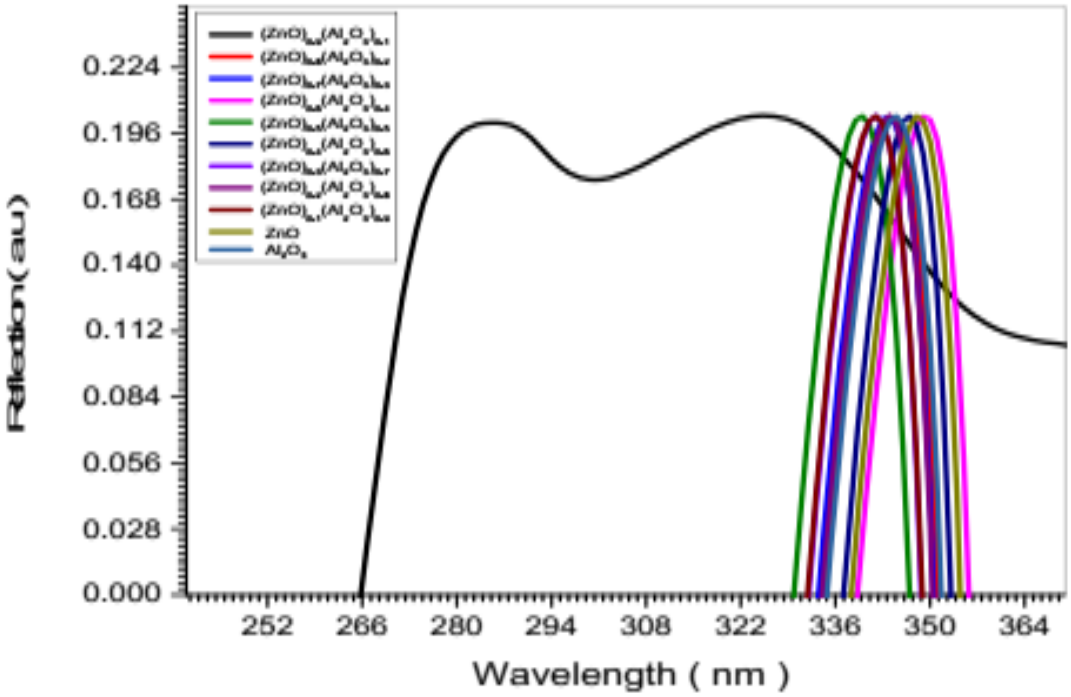

Fig.(3.12) The relation between reflection and wavelengths of eleventh $(ZnO)x\ (Al_2O_3)_{1-x}$ samples

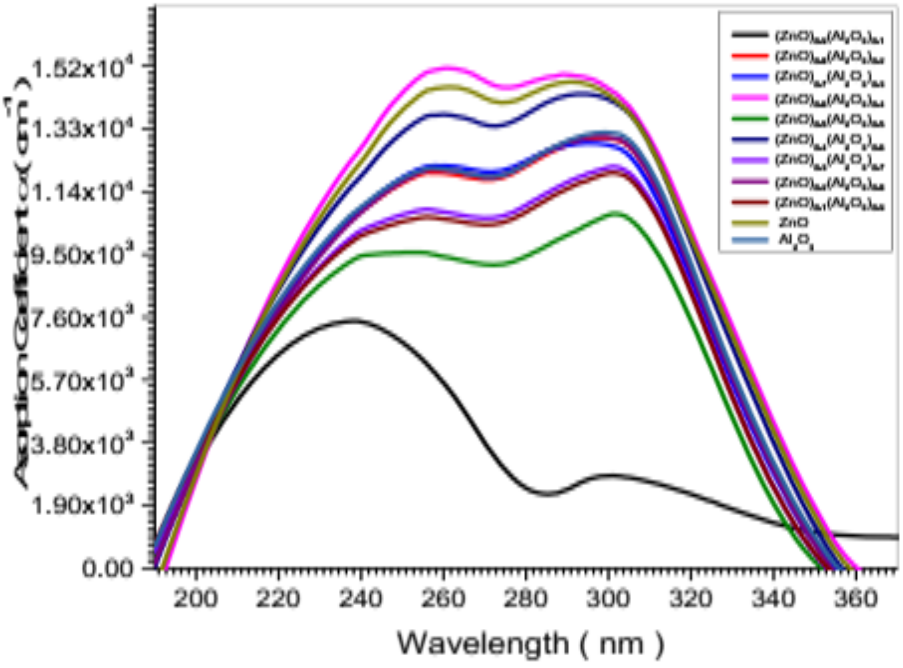

Fig.(3.13) The relation between absorption coefficient wavelengths of eleventh (ZnO)x $(Al_2O_3)_{1-x}$ samples

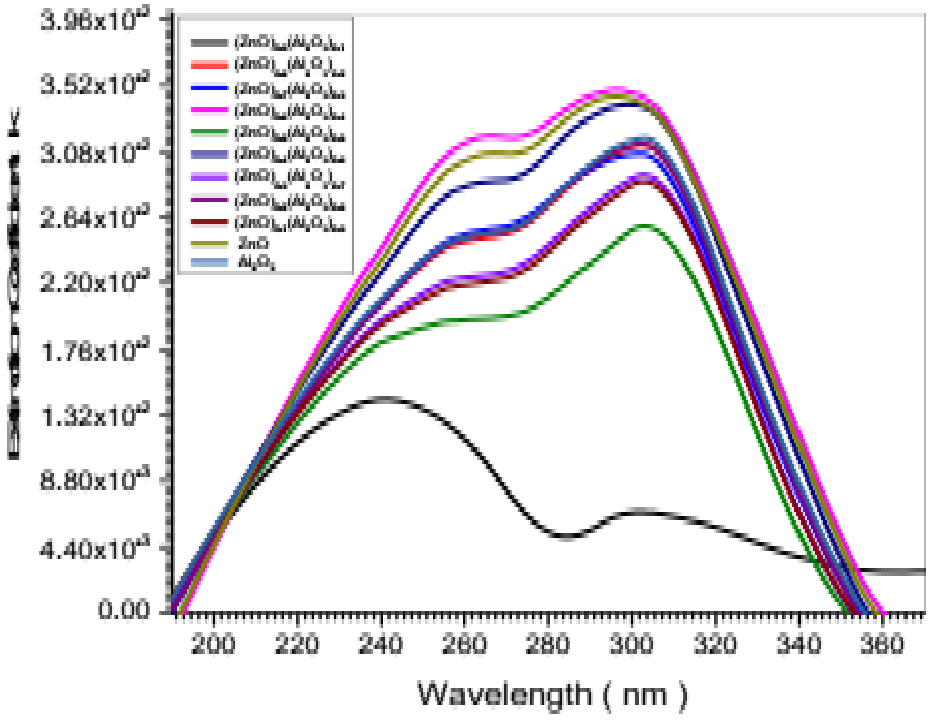

Fig.(3.14) The relation between extinction coefficient (α) and wavelengths of eleventh (ZnO)x $(Al_2O_3)_{1-x}$ samples

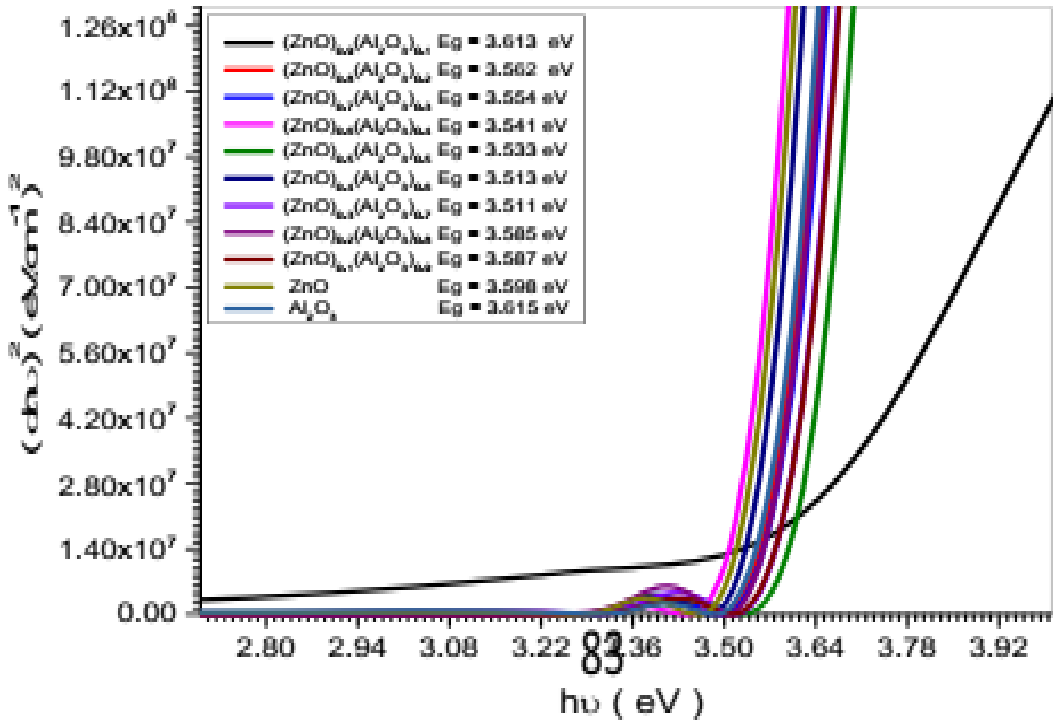

Fig(3.15)The optical energy band gab of elevanht (ZnO)x (Al2O3)1- x samples

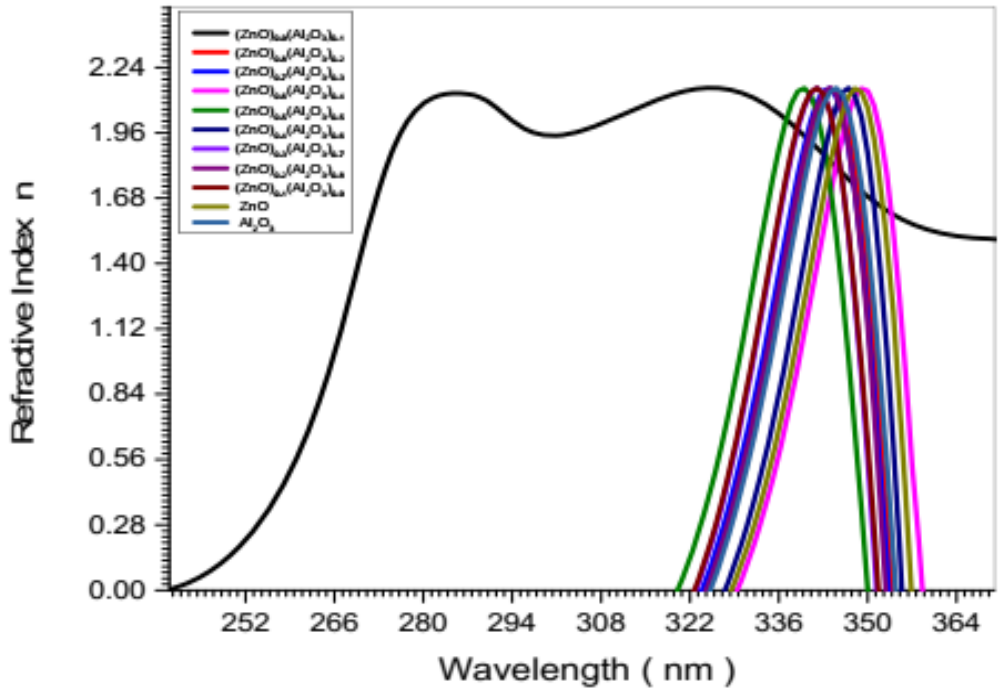

Fig (3.16)The relation between refractive index and wavelengths of eleventh $(ZnO)_x (Al_2O_3)_{1-x}$ samples

The figures indicated that the absorption coefficient of (ZnO)x(Al2O3)1-x thin film decreases as the nano crystal size decreases. The energy gap decreases when ZnO concentration decreases up to 0.3. Thus to get more transported film one must decrease nano crystal size. This work is confirmed by many papers [42 , 43 , 44].

3.5 Deposition of zinc oxide as an electron transport layer in planar perovskite solar cells by spray and SILAR methods comparable with pin coating

CH3NH3PbI3 planar-structure perovskite solar cells were prepared and fabricated with the configuration FTO/ZnO/ CH3NH3PbI3/Au. ZnO nanoparticles. The thin films were synthesized by the precipitation method. Three different deposition methods including spin-coating, spraying and successive ionic layer adsorption and reaction (SILAR) were applied to fabricate the ZnO films as an electron effective transport layers. Nano and spectral analyses, such as XRD, SEM, FESEM, UV-visible and I–V measurements, were carried out and used to evaluate the performance of the cells. The best cell performance is that fabricated from the perovskite solar cell with a ZnO film coated by the spin method. The average efficiency was found to be 7% without using any hole transport materials and 10.25% using spiro-OMeTAD as a hole transport material. The average efficiencies of the cells coated by the spraying and SILAR methods using spiro-OMeTAD, were found to be 8.64% and 7.7% respectively. This study demonstrates the versatility and importance of the spray and SILAR coating methods and their potential for fabricating low-cost, large scale, flexible and mass produced perovskite solar cells [45].

The crystal structure and the spacing of the ZnO NPs and their size were determined and found by X-ray diffraction (XRD) PANalytical X'Pert Pro MPD multipurpose instrument. SEM and FESEM images of the ZnO NPs

were taken and manipulated by a scanning electron microscope (TESCAN, Vega3, Czech).

Absorption spectra of the ZnO lms were prepared by an Ocean Optics spectrometer model HR 4000 in order to observe their absorption and calculate the band gap of them. The whole cell was characterized by SEM images and the UV-visible spectra of the perovskite lms. The current–density potential (J–V) of the curves was measured by Keithley Model 2400 under AM 1.5G 100 mW cm2 using a solar simulator from Sharif Solar Co calibrated with a silicon reference cell.

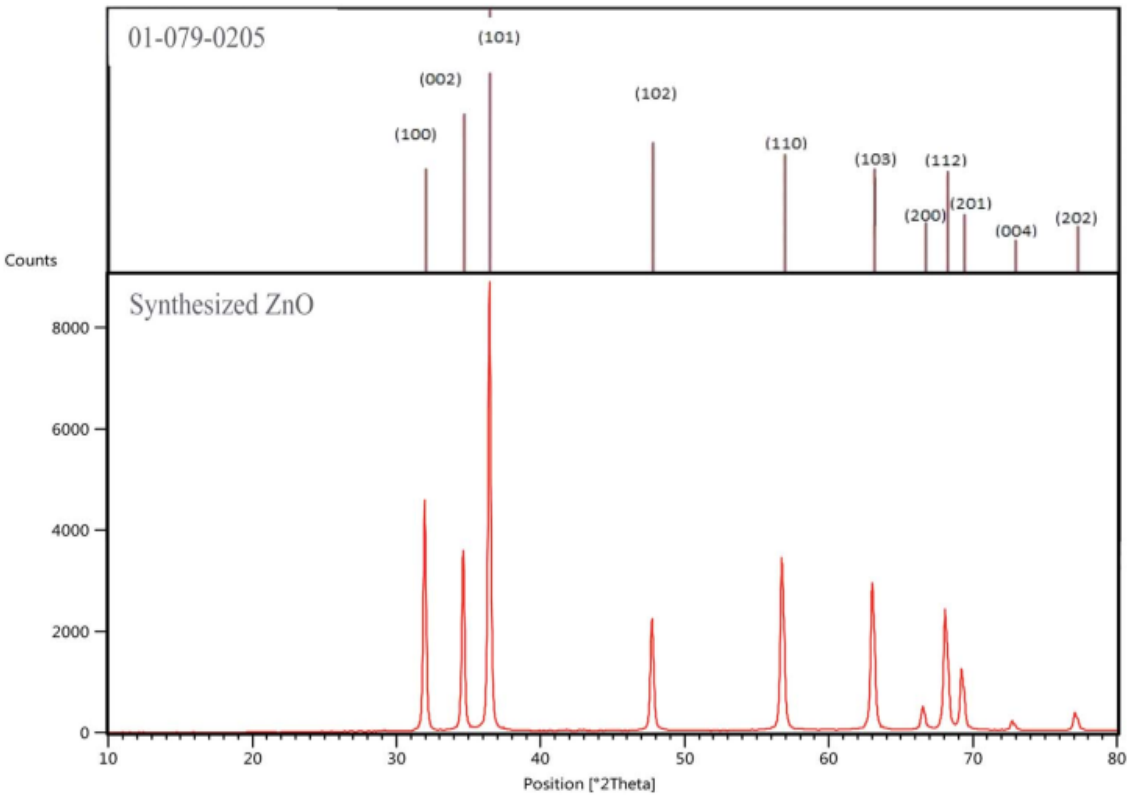

Fig. (3.17) XRD patterns of the synthesized ZnO nanoparticles.

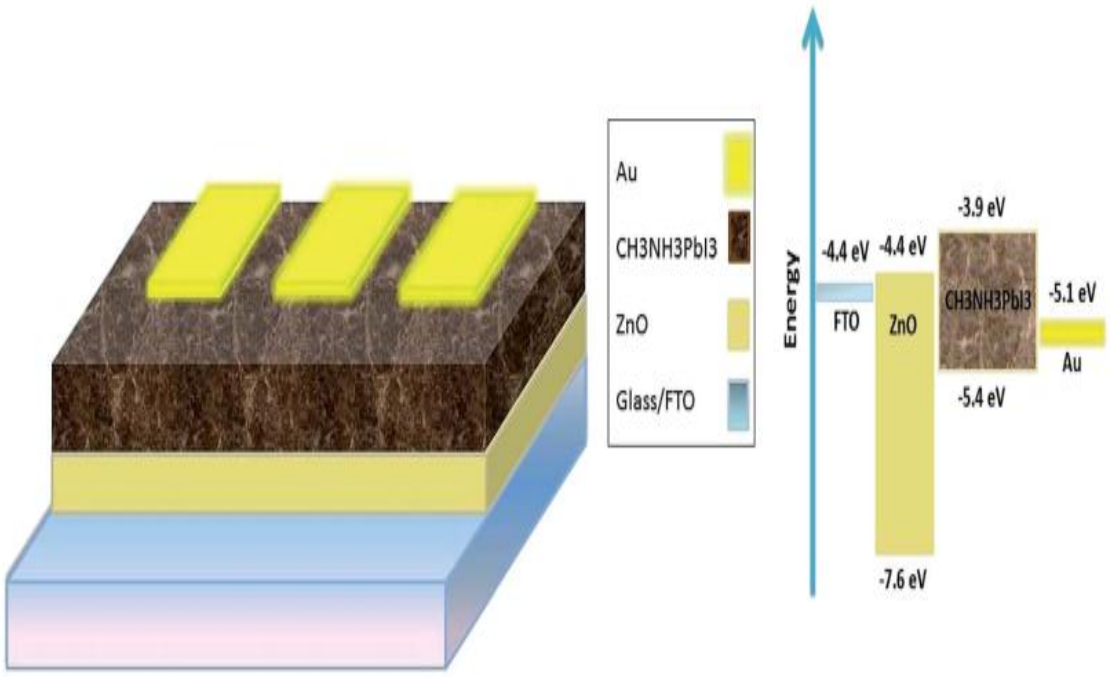

Fig.(3.18) (a) Schematic illustration of the architecture of the perovskite devices fabricated in this study: FTO front contact, ZnO ETL, CH3NH3PbI3

Film and Au back contact, and (b) energy levels of the individual device components and possible electronics.

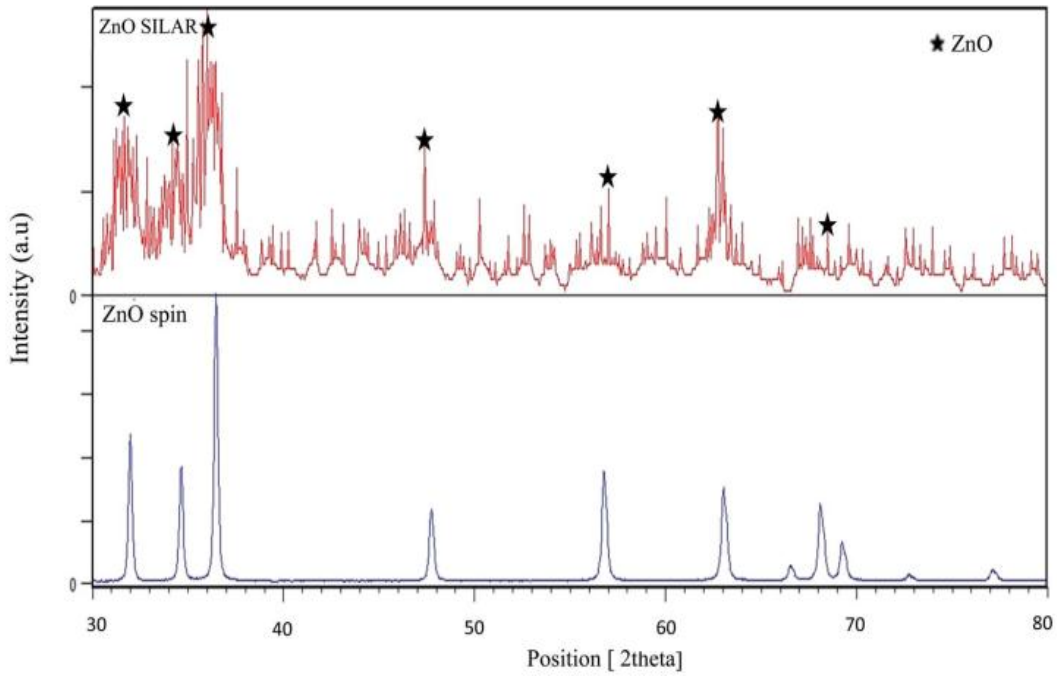

Fig.(3.19) XRD patterns of the ZnO layer deposited by SILAR method compared with spin coating method

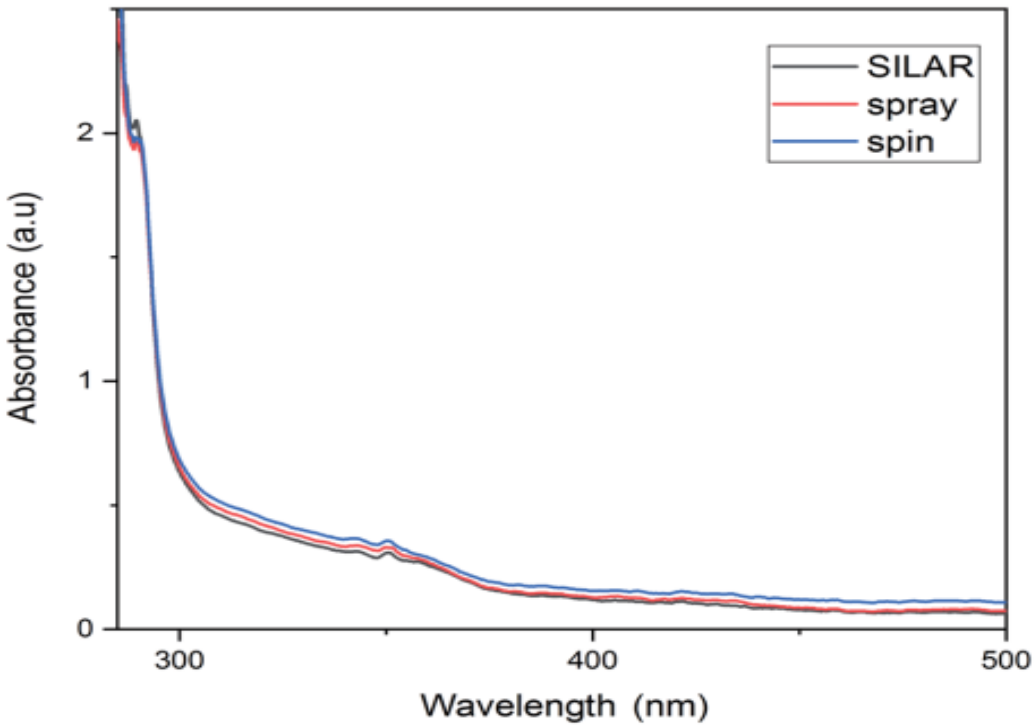

Fig.(3.20) UV-visible spectra of the ZnO thin films coated by different methods

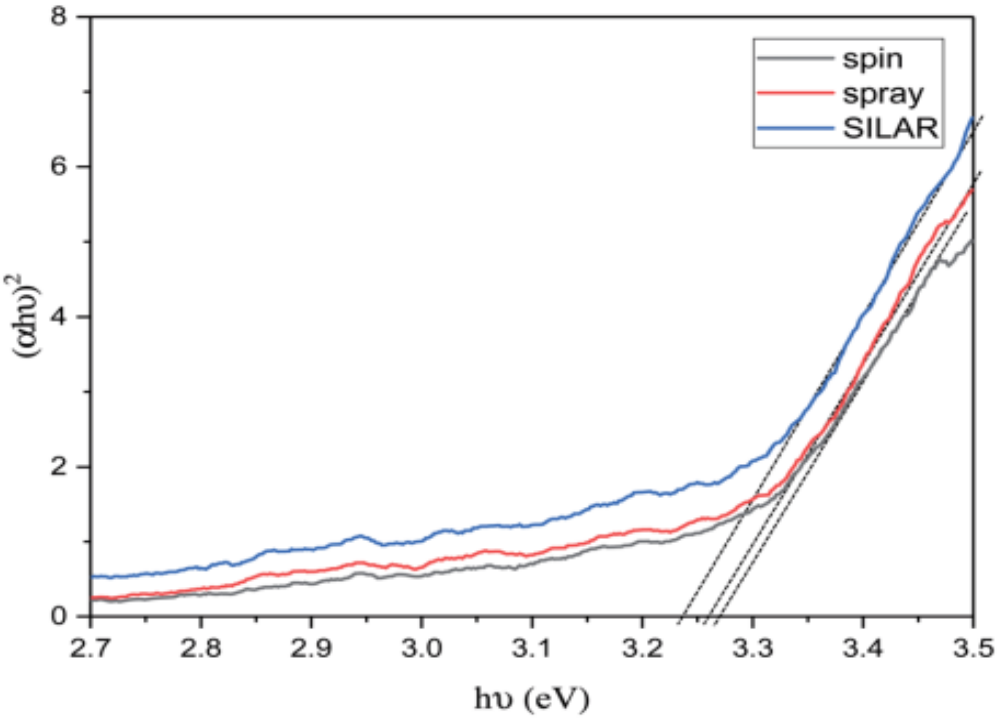

Fig. (3.21) Plot of (ahn)2 vs. the photon energy (hn) of the ZnO films based on different coating methods. The band gap values are obtained by extrapolating the linear part of the curves

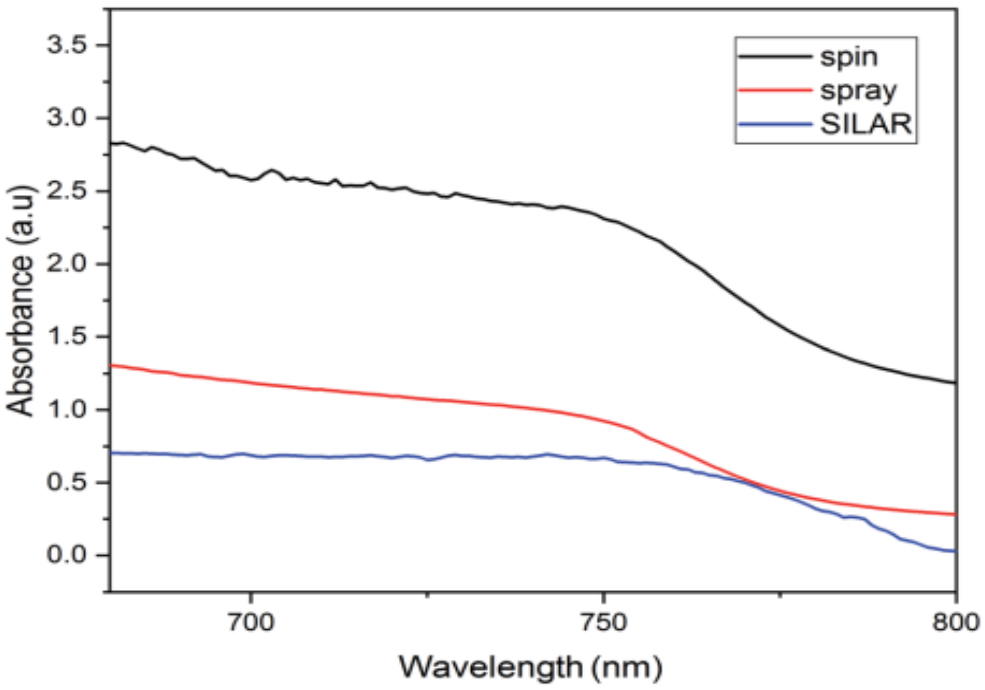

Fig. (3.22) UV-visible spectra of the perovskite layers coated on the ZnO

films with different coating methods

In summary, perovskite solar cells were fabricated at a processing temperature of less than 120 C. Three most common deposition methods of coating layers were compared to achieve a low-cost, efficient and capable procedure for the mass production of cells and the selection of exible substrates, which are the requirements for commercialization of perovskite solar cells. According to the results, the cells fabricated by the spin-coating method showed higher efficiency. The performance of the cells made through spray and SILAR coating methods was also noticeable. On the basis of the results, it can be claimed that fabrication of PSCs by applying ZnO, as an electron transport layer, and through spray and SILAR coating methods ensures such advantages as efficiency, low cost, and ease of production. The procedure used in this study can be of benet for both selection of exible substrates and large-scale production of solar cells. Many researchers agree with this study [46 , 47 , 48].

3.6 The Relationship between Energy Gab & Efficiency in Dye Solar Cells

In this work dye sensitized solar cells are fabricated and made from: Ecrchrom Black T, DDTTC, Rohadamin B,and Coumarin 500,with Al and TTO electrodes were fabricated. The energy gap of these dyes samples were found and determined using UV Spectrometer. The energy gap for: Ecrchrom Black T, DDTTC, Rohadamin B, and Coumarin 500 ; were found 2.16 eV ,2.20 eV ,3.27 eV and 3,60 respectively .

The V- I characteristics for these cells and their performance were also used to find the cells efficiencies . The efficiency:

Ecrchrom Black T, DDTTC, Rohadamin B, Coumarin 500 were found to be 1.66,1.62, 1.49 and 1.31. It is realized that; the efficiency increased when energy gab decreased [49,50,51,52].of Engy gaps of : Ecrchrom Black T, DDTTC, Rohadamin B, and Coumarin 500 were found using UV spectrometer as shown in figures (1), (2),(3) and (4)

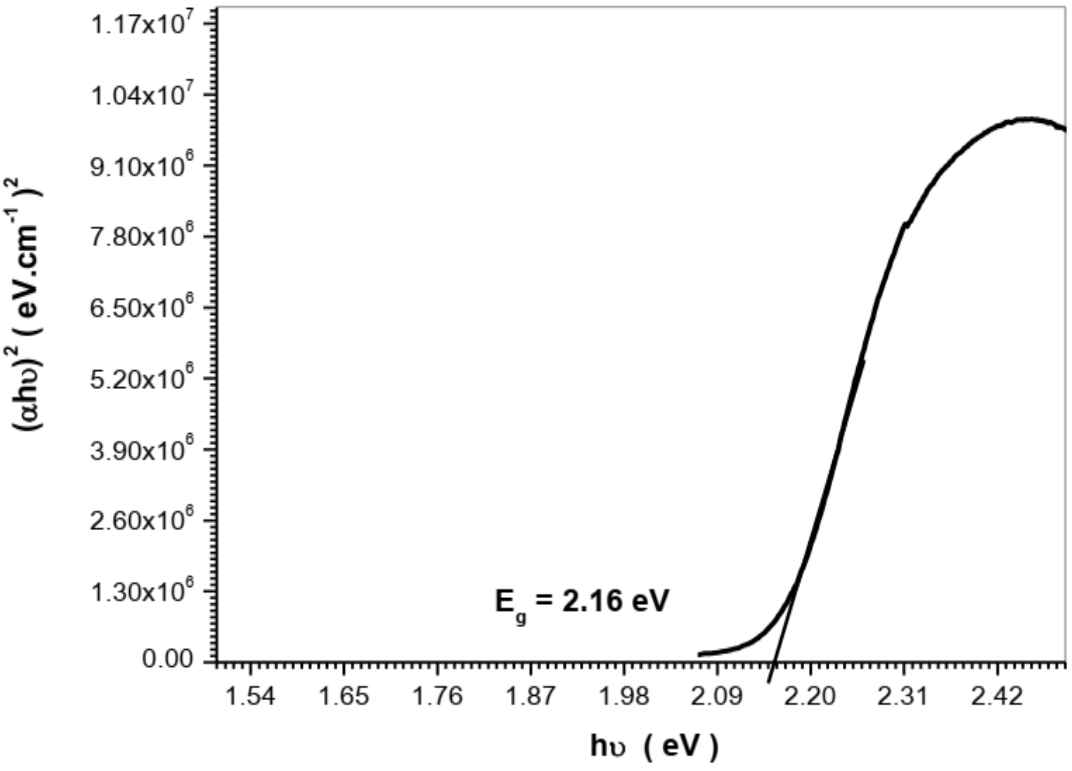

Fig(3.23) The optical energy gap (Eg) value of Ecrchrom Black

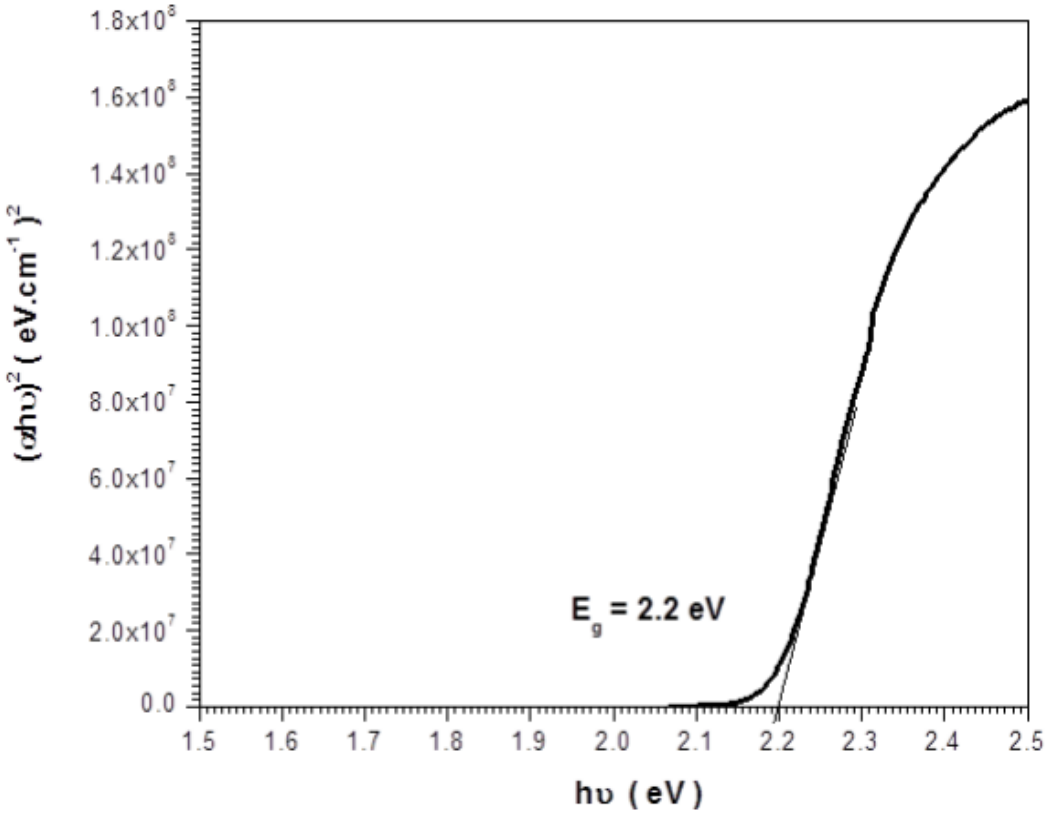

Fig (3.24) the optical energy gap (Eg) value of DDTT

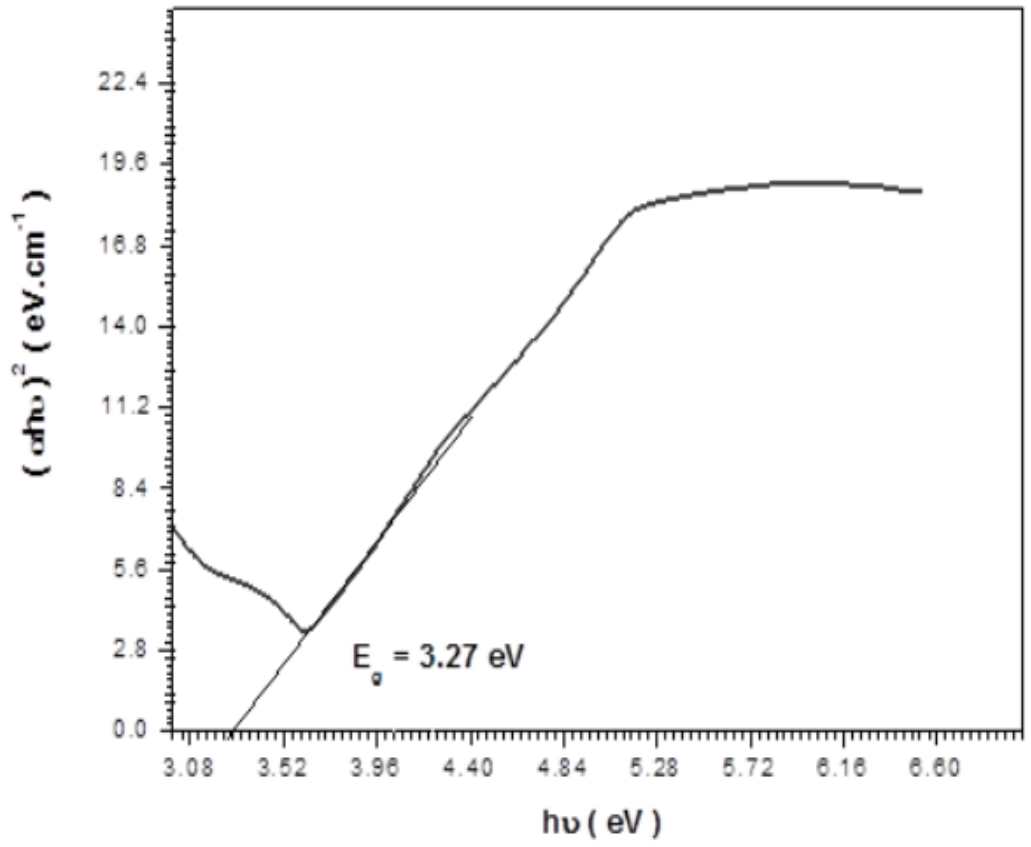

Fig (3.25) the optical energy gap (Eg) value of Rohadamin

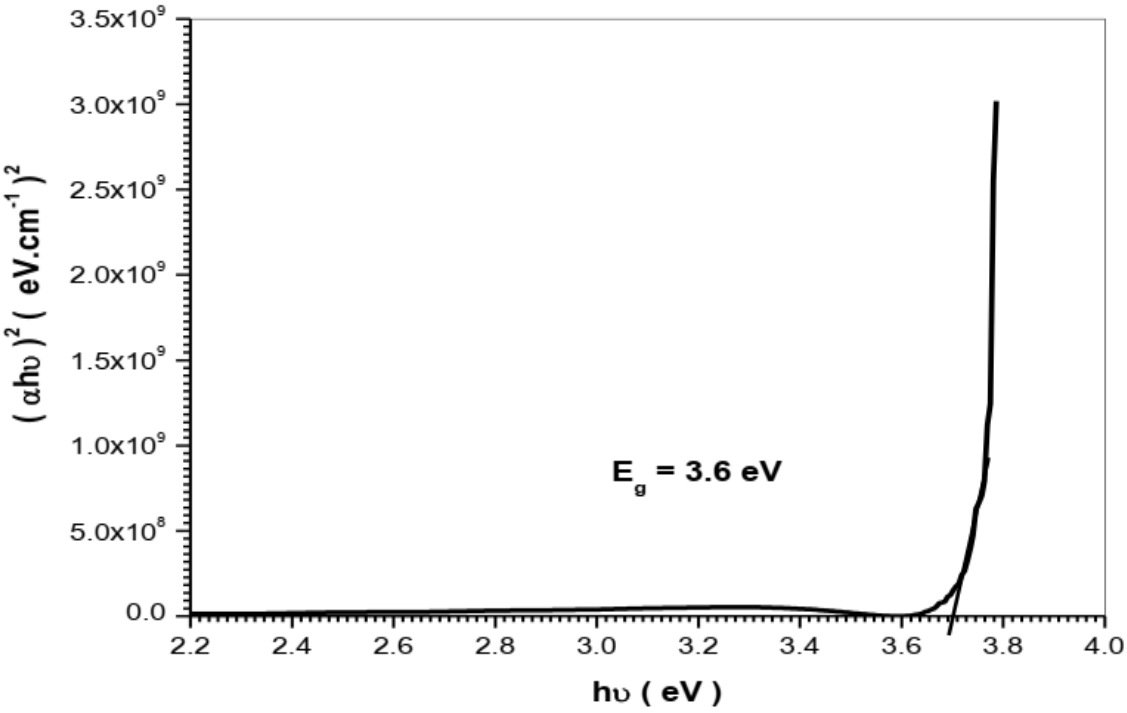

Fig (3.26) the optical energy gap (Eg) value of Coumarin 500

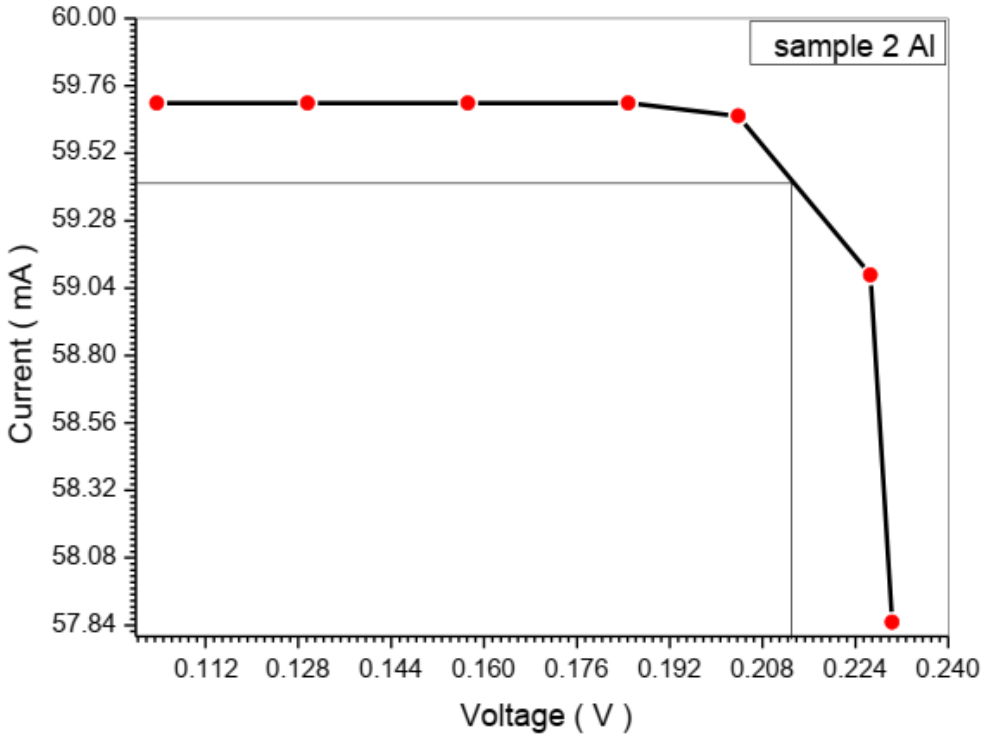

Fig (3.27) I-V characteristic curve for sample 1(Ecrchrom Black T) with Al electrode

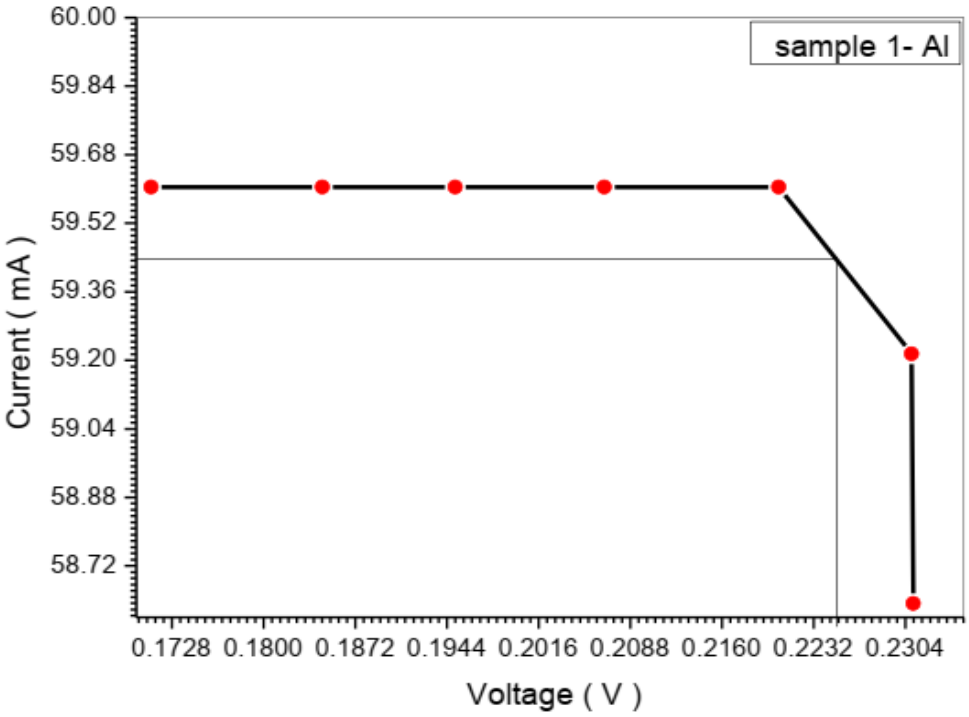

Fig (3.28): I-V characteristic curve for sample 2 (DDTTC) with Al electrode

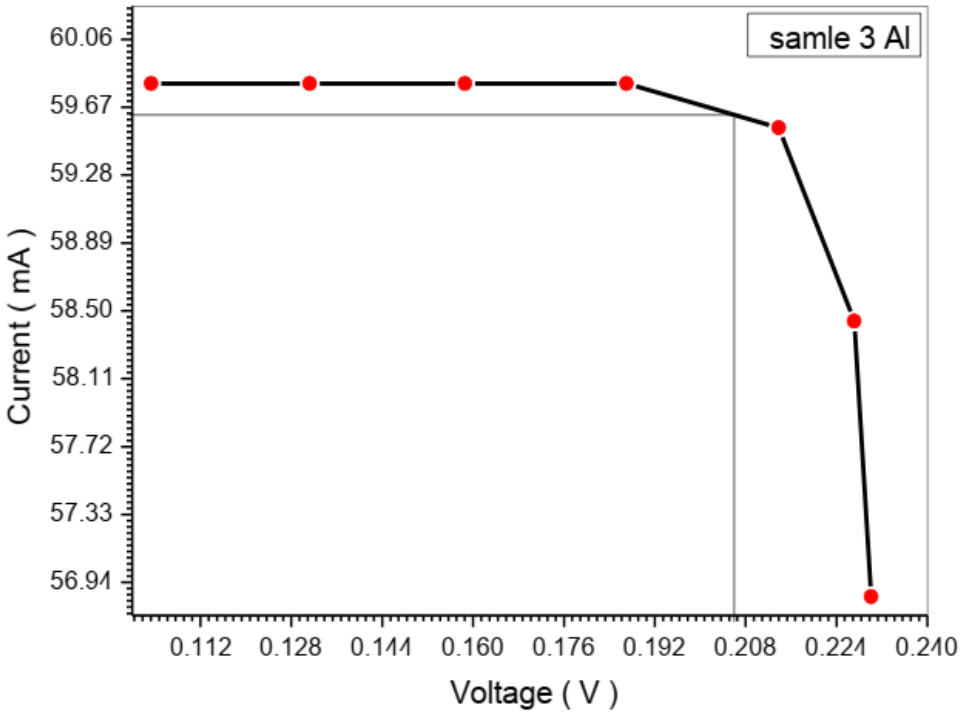

Fig (3.29): I-V characteristic curve for sample 3(Rohadamin B) with Al electrode

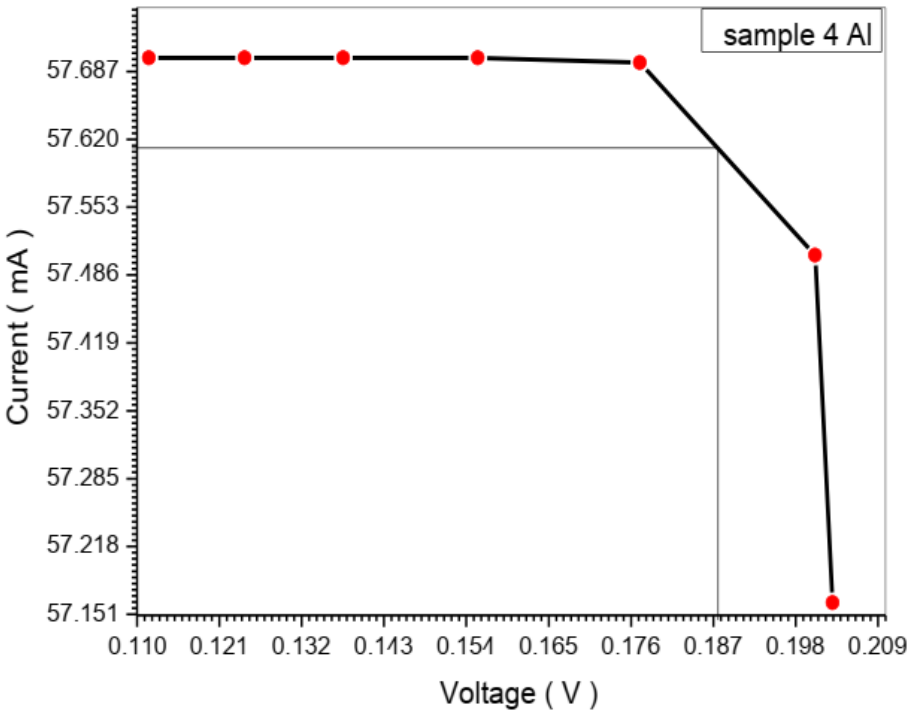

Fig (3.30): I-V characteristic curve for sample 4 (Coumarin 500) with Al electrode

3.7 The effect of Annealing Temperature, Doping Carbon Nanotubes with Tio_2, cuo, zno, and mgo, on its conductivity and electrical primitively

In this work Tio2, cuo, zno, and mgo , were used and prepared to dope carbon nano tube at differeat annealing temperatures.450 ,500 ,550 ,and 600C0 . The spectrum of the conductivity and dielectric constants were displayed using UV spectrometer at different annealing temperatures. It was found that the conductivity and dielectrics constants decrease when the temperature is increased for all samples except for mgo where they increase. These relations conform with physical laws and are explained theoretically [53]

.

Theoretical model for explaining the experimental work

Consider the electron of mass m and charge is affected by and electric field intensity E and resistive medium of coefficient γ. The equation of motion is thus given by:

$$m\,\ddot{x} = e\,E - \gamma\,\dot{x} \quad \text{\_\_\_\_(1)}$$

$$\text{Let } x = x_0\,e^{-i\,wt}\ ,\dot{x} = -i\,wx, \ddot{x} = -w^2x \quad \text{\_\_\_\_\_(2)}$$

Thus:

$$-m\,w^2x = eE + i\gamma wx$$

$$-(mw^2 + i\gamma w)x = eE \quad \text{\_\_\_\_\_(3)}$$

Thus:

$$x = \frac{-eE}{(mw^2 + i\gamma w)}$$

$$x = \frac{-e[mw^2 - i\gamma w]E}{m^2w^4 + \gamma^2w^2} \quad \text{\_\_\_\_\_(4)}$$

Hence, the electric dipole moment takes the form

$$P = n_e ex = \frac{e^2n_e[-mw + i\gamma]}{m^2w^3 + \gamma^2w} = \varepsilon_0 xE \quad \text{\_\_\_\_\_(5)}$$

$$= \varepsilon_0(x_1 + ix_2)E \quad \text{\_\_\_\_\_(6)}$$

If the concentration no is related to γ via The relation:

$$\gamma = \gamma_0 n_0 \quad \text{\_\_\_\_\_(7)}$$

Thus:

$$x_1 = \frac{-e^2n_e mw}{\varepsilon_0(m^2w^3 + \gamma_0^2n_0^2w)}$$

$$x_2 = \frac{e^2n_e n_0\gamma_0}{\varepsilon_0(m^2w^3 + \gamma_0^2n_0^2w)} \quad \text{\_\_\_\_\_(8)}$$

On the other hand, the current density due to dipole oscillation is given by:

$$J = \frac{\partial P}{\partial t} = xE_0\,\frac{\partial e^{-iwt}}{\partial t} = -iw(x_1 + ix_2)E$$

$$= w_2x_2E - iwx_1E$$

$$= \sigma E = (\sigma_1 + i\sigma_2)E$$

Thus

$$\sigma_1 = wx_2 , \qquad \sigma_2 = -wx_1 \text{ \_\_\_\_\_(9)}$$

But the electric flux density is given by:

$$D = (\varepsilon_1 + i\varepsilon_2)E = \varepsilon_0 E + \varepsilon_0(x_1 + ix_2)E \text{ \_\_\_\_\_(10)}$$

Thus:

$$\varepsilon_1 = \varepsilon_0\varepsilon_{r_1} = \varepsilon_0(1 + x_1) \quad ,$$
$$\varepsilon_2 = \varepsilon_0\varepsilon_{r_2} = \varepsilon_0 x_2 \text{ \_\_\_\_\_(11)}$$

Since:

$$I = I_0 e^{-\gamma x} = |E|^2 = E_0^2\, e^{-2k_2 x}$$

It follows that the $\propto = 2k_2$ _____(12)

Sorption coefficient is given by using the relation:

$$k^2 = (k_1 + ik_2)^2 = \frac{w^2}{v^2} w^2(\mu\varepsilon) = w^2(\mu_0\varepsilon_0.\varepsilon_r)$$

$$= k_1^2 - k_2^2 + 2k_1k_2i = \frac{w^2}{c^2}(\varepsilon r_1 + i\varepsilon r_2) \text{ \_\_\_\_\_(13)}$$

On gets

$$\propto = 2k_2 = \frac{w^2}{c^2 k_1}\varepsilon_{r_2} = \frac{w^2}{c^2 k_1}\, x_2 \text{ \_\_\_\_\_(14)}$$

$$\propto$$

$$= \frac{w^2 e^2 n_e n_0 \gamma_0}{c^2 k_1^2 \varepsilon_0 (m^2 w^3 + \gamma_0^2 n_0^2 w)} \qquad \text{\_\_\_\_\_(15)}$$

4. Results

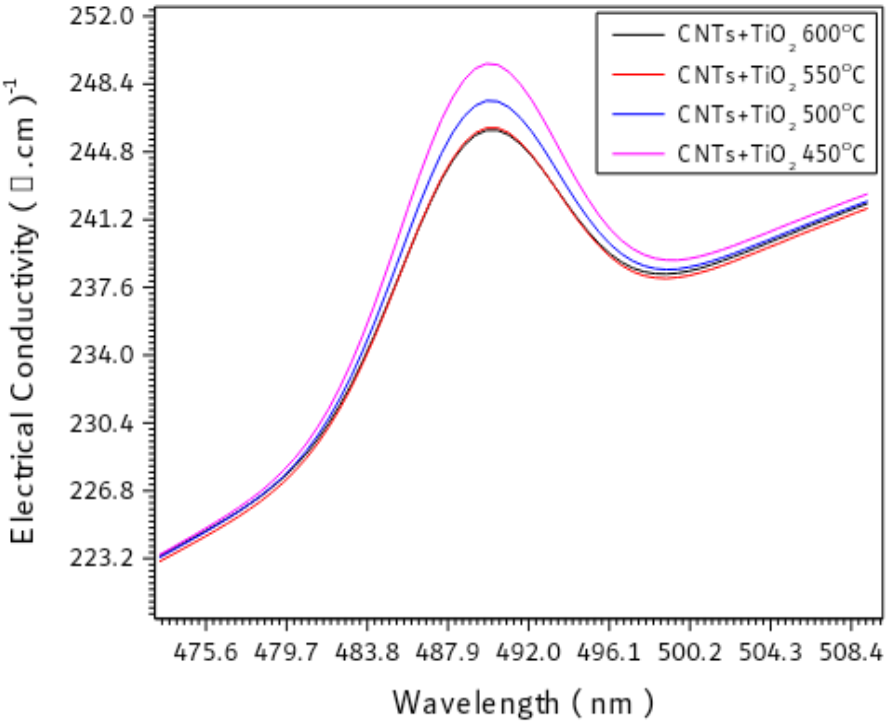

Fig (3.31) the electrical conductivity spectra of CNTs doping by TiO_2 thermal annealing by rate (450,500,550 and 600^{O}C)

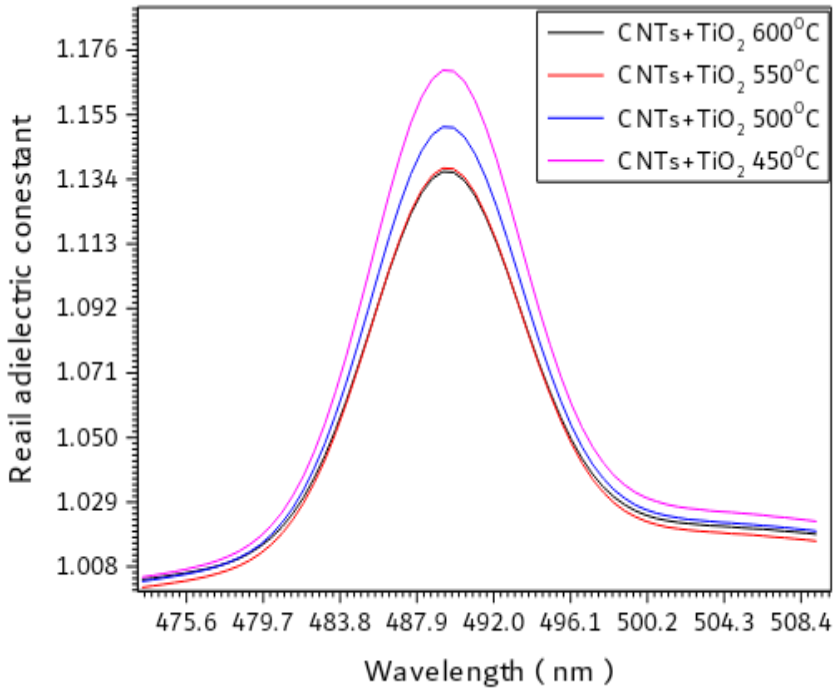

Fig (3.32) the real dielectric constant spectra of CNTs doping by TiO_2 thermal annealing by rate (450,500,550 and 600^{O}C)

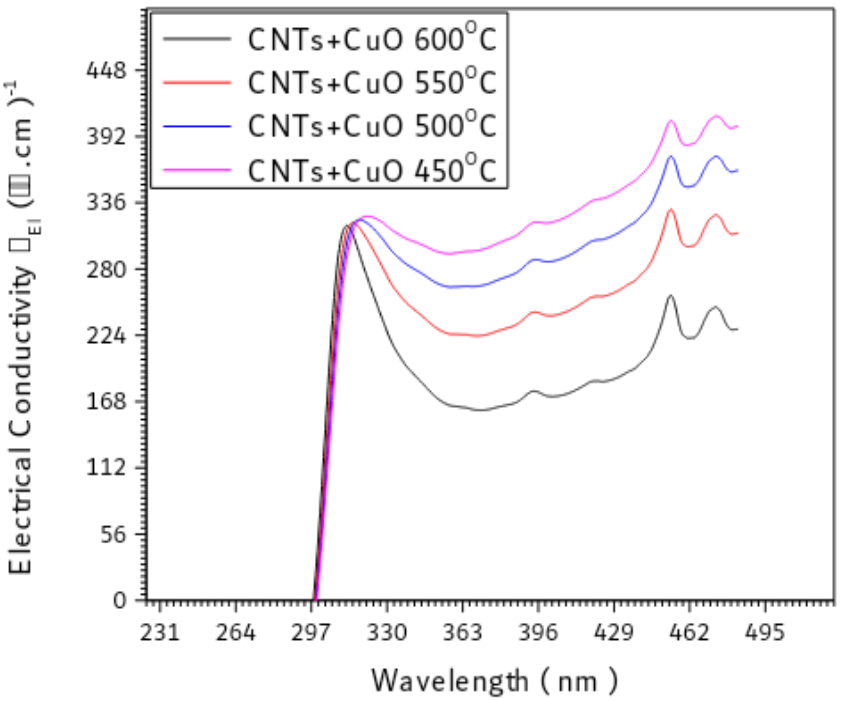

Fig (3.33) the electrical conductivity spectra of CNTs doping by CuO thermal annealing by rate (450,500,550 and 600^{O}C)

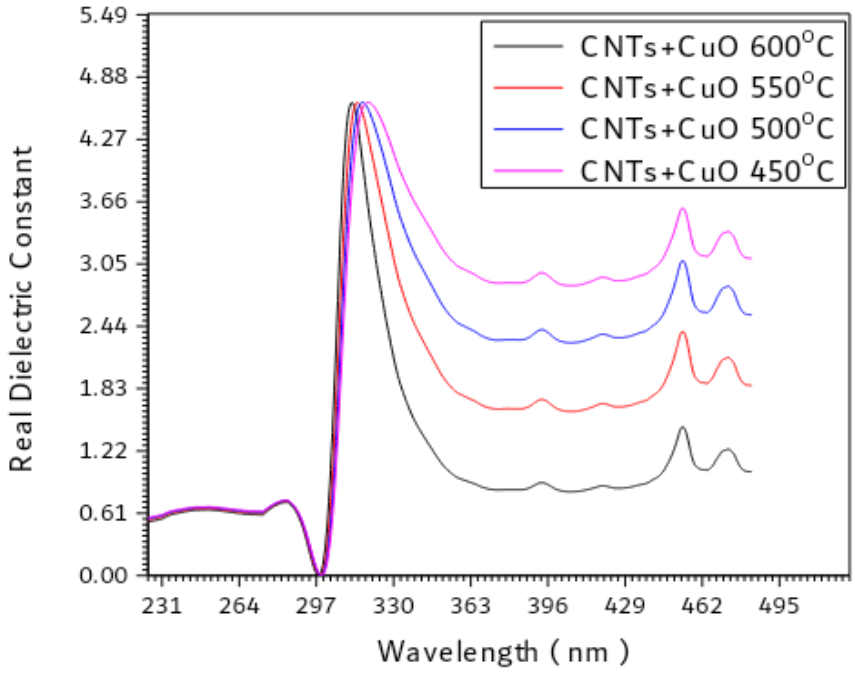

Fig (3.34) the real dielectric constant spectra of CNTs doping by CuO thermal annealing by rate (450,500,550 and 600^{O}C)

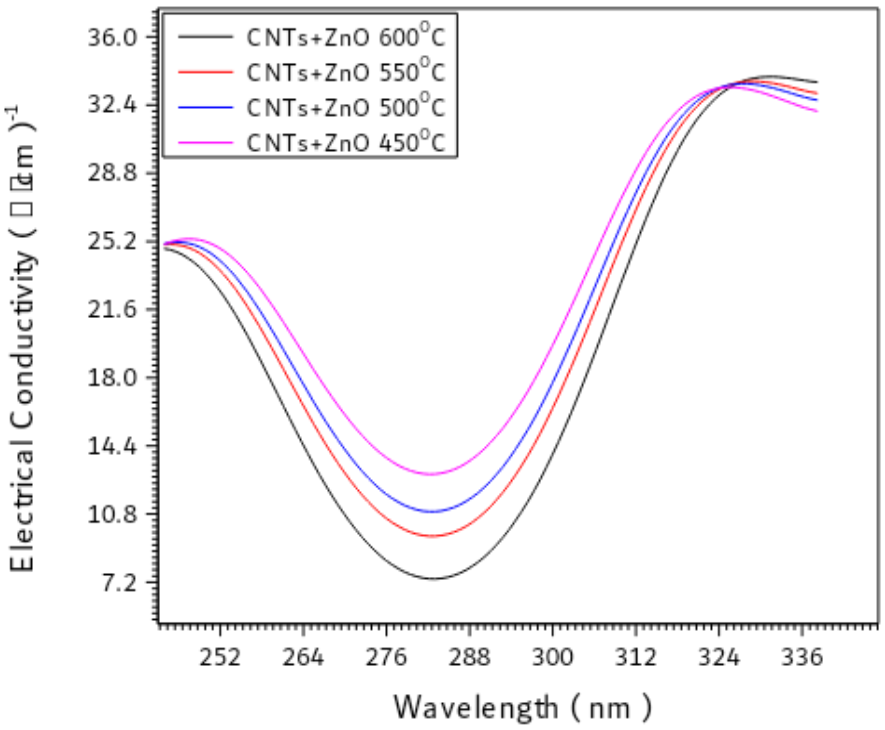

Fig (3.35) the electrical conductivity spectra of CNTs doping by ZnO thermal annealing by rate (450,500,550 and 600^{O}C)

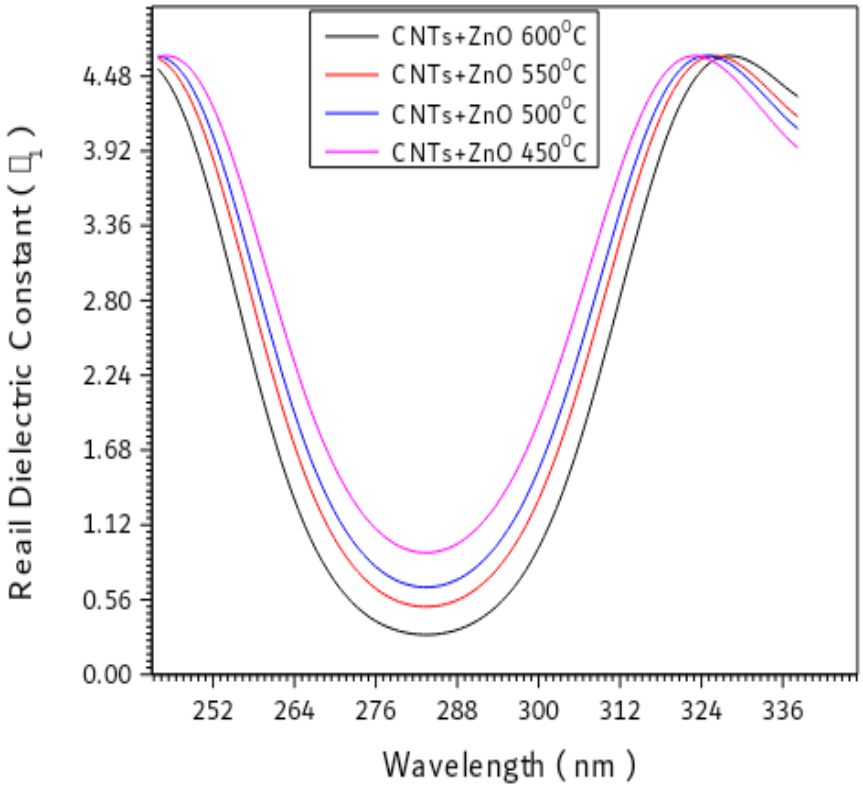

Fig (3.36) the real dielectric constant spectra of CNTs doping by ZnO thermal annealing by rate (450,500,550 and 600^{O}C)

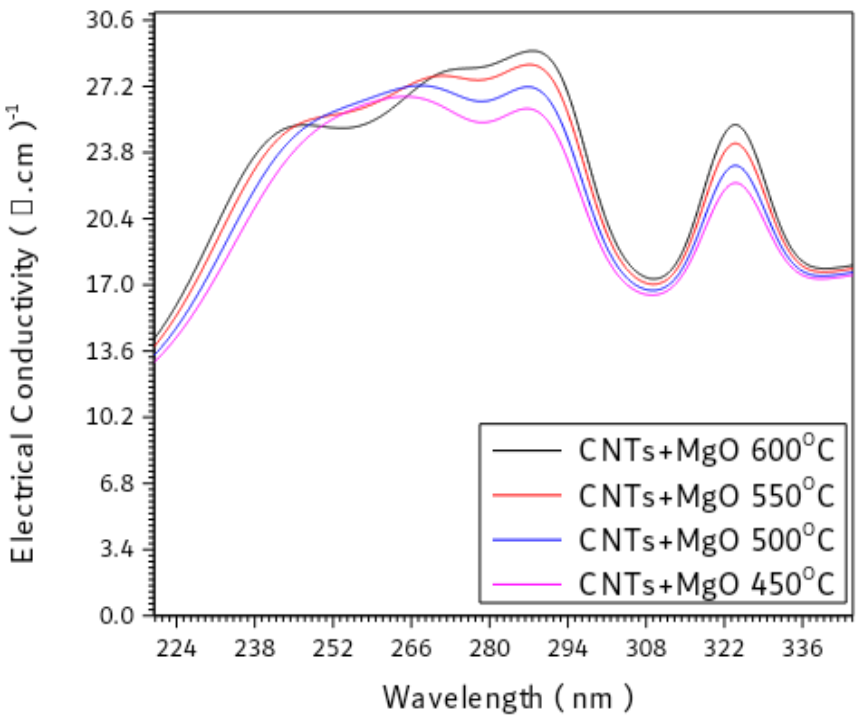

Fig (3.37) the electrical conductivity spectra of CNTs doping by MgO thermal annealing by rate (450,500,550 and 600^{O}C)

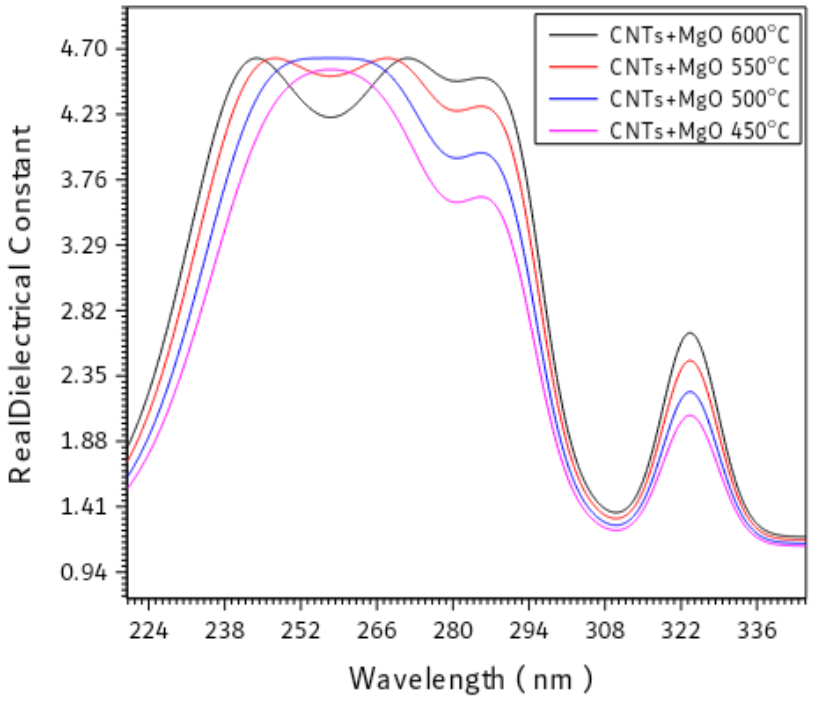

Fig (3.38) the real dielectric constant spectra of CNTs doping by MgO thermal annealing by rate (450,500,550 and 600^{O}C)

The theortical relation shows the following results

For Tio2, cuo, and zno the increase of temperature T decreases conductivity. This may be explained by equations (8) and (9).

When one assumes that $mw < \gamma_0 n_0$

In this case

$$\sigma_1 \sim \frac{1}{n_0} \qquad \text{\_\_\_\_\_} (16)$$

Thus, increasing temperature allows more atoms (n_0) to penetrate. Thus increases n_0 , thus decreases conductivity. This may also be explained by assuming that the increase of atoms increases collision, which in turn increases resistivity. This decreases of course conductivity.

For Mgo the conductivity decreases upon increasing temperature

This may be explained by assuming Mgo to act as magnetic dipoles, which leads to splilling of energy levels of the surrounding carbon atoms. This causes the lower edge of the conduction band and the upper edge of the valence band to enter the energy gap.

This causes E_g to decrease by an amount

$$2\Delta E = 2n_0 \beta g H \text{\_\_\_\_\_} (17)$$

Where ΔE is the splitting width above and below the original level. Thus the new energy gap is given by

$$\widetilde{E_g} = E_g - 2n_0 \beta g H \text{\_\_\_\_\_} (18)$$

This narrowing of gap allows large number of electrons n to enter the conduction band. Thus increases conductivity according to the relation

$$\sigma = \frac{ne^2\tau}{m} \text{\_\_\_\_\_} (19)$$

The real dielectric constant ε_1 decreases with temperature T, for Tio_2, cuo and zno. This may be explained by assuming that these molecules acts as

electric dipoles opposing the applied electric field E . If the susceptibility per atom is x_a . Thus

$$D = \varepsilon E = \varepsilon_0 E + p = \varepsilon_0 E - \varepsilon_0 n_0 x_a E = \varepsilon_0 (1 - n_0 x_a) E = \varepsilon E \_\_\_\_\_ (20)$$

$$\varepsilon_1 = \varepsilon = \varepsilon_0 (1 - n_0 x_a) \_\_\_\_\_ (21)$$

This means that increasing temperature allows more atoms (n_0) to penetrate. This cause $\varepsilon_1$to decrease according to equation (21) for Mgo One can assume that molecules align themselves in the direction of the external field. Thus, the flux density is given by

$$D = \varepsilon E = \varepsilon_0 E + p = \varepsilon_0 E + \varepsilon_0 n_0 x_a E = \varepsilon_0 (1 + n_0 x_a) E \_\_\_\_\_ (22)$$

$$\varepsilon_1 = \varepsilon = \varepsilon_0 (1 + n_0 x_a) \_\_\_\_\_ (23)$$

3.8 The effect of doping soda lime glass with iron oxide on its physical properties

The iron oxide Fe3O2 was prepared with melt quenching technique. The Archimedes method shows increase of glass density and decrease of molar volume upon increasing the iron oxide density. The refractive index increases and the energy gap decreases upon increasing the iron oxide concentration [54]. This work was confirmed by many previous studies [55 , 56].

3.9 Summary and critique:

The electrical magnetic [57 , 58 , 59] and optical properties and matters [60,61 , 62] can be studied by using spectrometers [63 , 64 , 65]. This properties can be control using nano science [66 ,67] to fabricate nano solar cells [68].

This means that nano technology is very important for are modern electronics and energy transducers.

Chapter Four

Materials and Methods

4.1 Introduction

This chapter is devoted for the experimental work which includes materials used, the equipment's used for measurements and sample preparation. In this work 8 samples of (Nacl) were prepared by cruching them.

4.2 Materials

Row sodium chloride (Nacl) was crushed then the powder passed through different milles having different micro sizes.

4.3 Equipment's used

The crystal and nano structures of the samples where characterized by X-ray diffraction (XRD) while the optical properties like absorption and energy gap were determined by using UV-visible absorption spectrophotometer

4.3.1. X-ray diffract Meter

X-ray diffraction is a technique to study crystal structures like atomic spacing and the distance between crystal planes beside the nano crystal size. The X-ray diffract meters consists of three basic elements: x –ray tube, a sample holder, and x- ray detector.

X- rays is generated when the heating filament produces electrons, that are accelerated towards a target by applying a voltage. The accelerated electrons bombard the a target material. When electrons have sufficient energy to dislodge inner shell electrons of target material, characteristic x-ray spectra are produced. These spectra consist of several components, the most common being k_α and k_β. k_α Consist in part of $k_{\alpha 1}$ and$k_{\alpha 2}$. $k_{\alpha 1}$ has slightly shorter wavelength and twice the intensity as Kα2. The specific

wavelengths are characteristic of the target material. Filtering, by foils or crystal monochrometers, is required to produce monochromatic X-rays needed for diffraction. Kα1and Kα2 are sufficiently close in wavelength such that a weighted average of the two is used. Copper is the most common target material for single-crystal diffraction, with Cu Kα radiation = 1.5418Å. These X-rays are collimated and directed onto the sample. As the sample and detector are rotated, the intensity of the reflected X-rays is recorded. When the geometry of the incident X-rays impinging the sample satisfies the Bragg Equation, constructive interference occurs and a peak in intensity occurs. A detector records and processes this X-ray signal and converts the signal to a count rate which is then output to a device such as a printer or computer monitor [69].

Fig (4.1) X-Ray diffract meter: XRD (wavelength 1.54 A°),

4.3.2. Ultraviolet -Visible Spectrometer (UV-Vis)

Ultraviolet and Visible Spectrometer is an absorption spectroscopy using electromagnetic radiations having wave length in the rage between 190 nm to 800 nm and is divided into the ultraviolet (UV, 190-400 nm) and visible (VIS, 400-800 nm) regions. Since the absorption of ultraviolet or visible radiation by a molecule leads transition among electronic energy levels of the molecule, it is also often called as electronic spectroscopy [70]. In general, the UV-visible spectra, measures absorbance. Absorption can take place due to electronic, vibrational, and rotational transition [71].

The absorption spectra determined is this work use Shimadzu spectrophotometer (UV mini 1240) in 190-800nm range see Figure (4.2).

Figure (4.2): UV mini 1240 spectrometer shimadzu

4.4 Crushing Machine and severs

The crushing machine is shown in figure (4.9). it consists of metallic crusher which crush any materials into small tiny particles transforming it into a powder see figure (4.6), figure (4.8). The severs consist of metallic screen or mech for purification and for splitting different particles having different micro sizes see figure (4.4).

4.5 Experimental procedures

1- Row sodium chloride (NaCl) salt was brought from the market.
2- To be purified the NaCl salt was dissolved in wate4r which is forced to flow through a sever. After that the salt was dried using drying machine.
3- The salt NaCl is then crushed into small micro sizes using crushing machine see figure (4.5),figure (4.7).
4- The powder was split into different powders having 8 different micro sizes to form 8 samples see figure (4.3).
5- The nano size of each sample was found using XRD.
6- The optical and electrical properties depending on the absorption spectra was determined using UV-VIS spectrometer beside some computer programs.
7- The chemical bonds were found using FTIR.
8- The results obtained were recorded in tables and displayed graphical.

Figure (4.3): The samples of NaCl

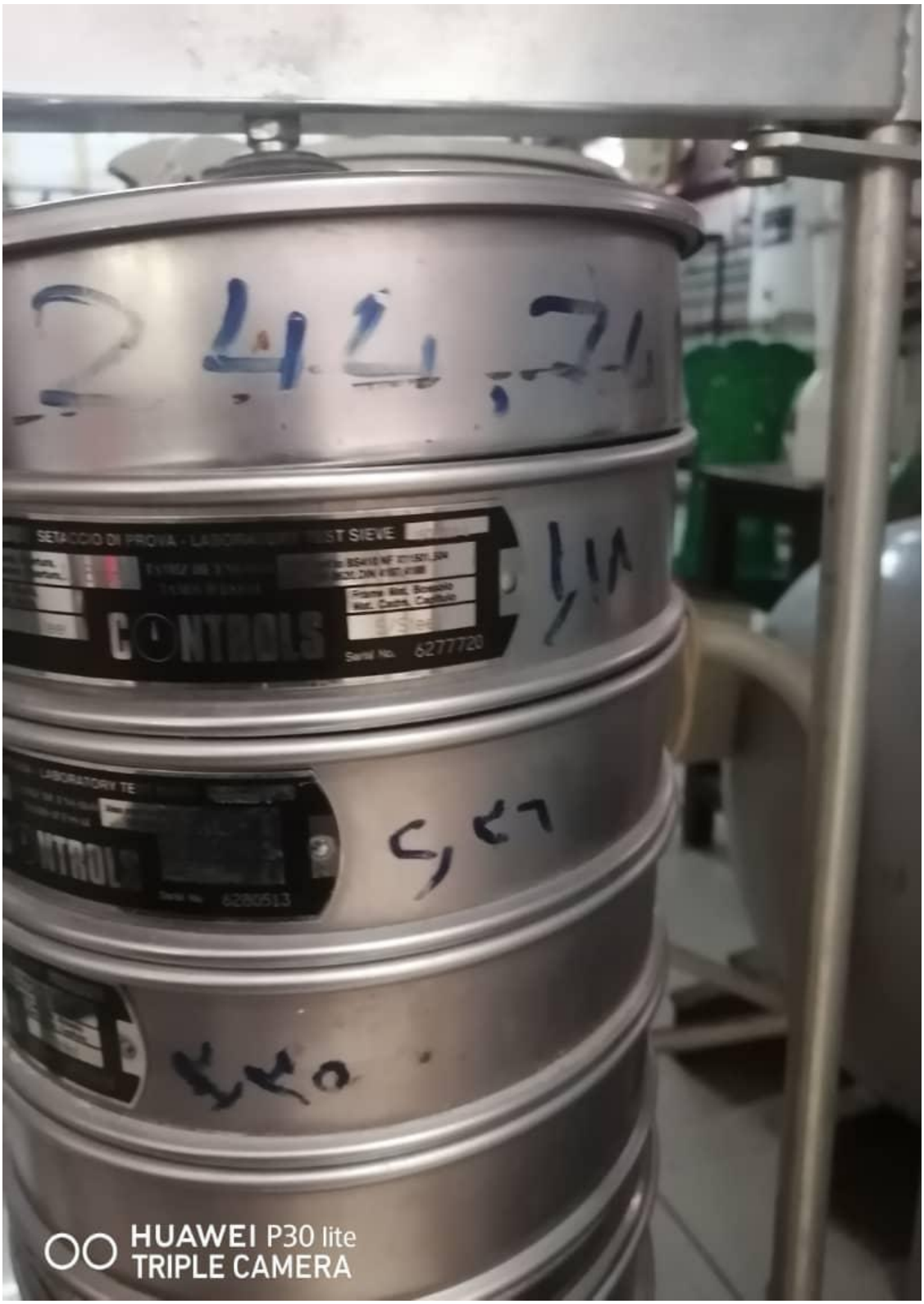

Figure (4.4): The metallic mesh of NaCl

Figure (4.5): The spray drier of NaCl

Figure (4.6): The metallic sever of NaCl

Figure (4.7): The drying machine of NaCl (side view)

Figure (4.8): The metallic sever of NaCl (side view)

Figure (4.9) crushing machine

Chapter Five

Results and Discussion

5.1 Introduction

In this chapter the main results that have been obtained from the experiments made from two types of sodium chloride crushed at different size. The data of X-ray diffraction (XRD) have been analyzed by to gated crystal structure and lattice parameters of samples, the FT-IR data have been carried to investigate the chemical bonds within atoms, and the data of UV-visible used to evaluate the optical parameters. At last, though optical results calculated.

5.2 XRD Results of Sodium Chloride (NaCl) crushed at different size

The result blow shows the XRD of ten samples for sodium chloride crushed at different size

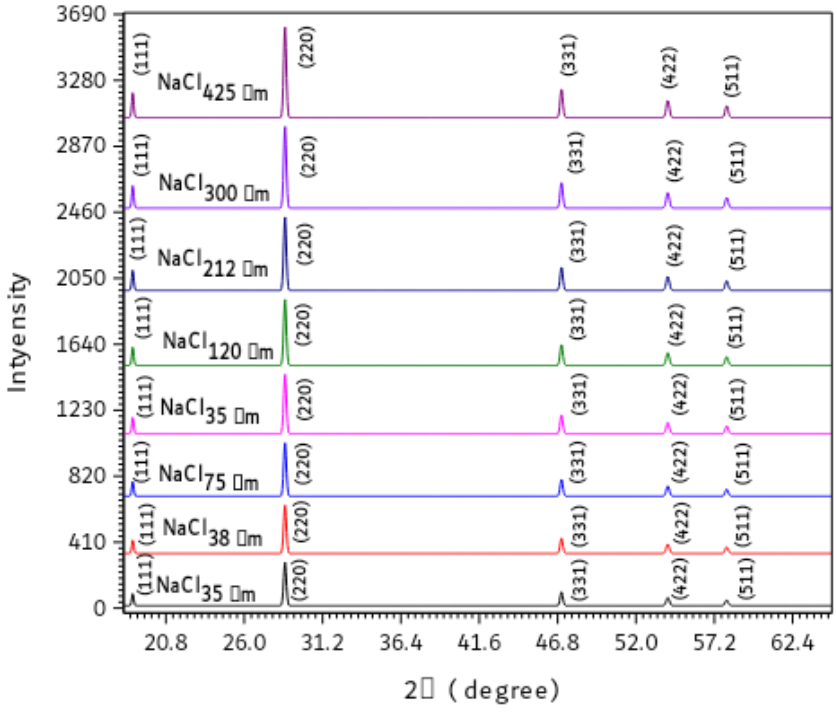

Fig (5.1) XRD spectrum of sodium chloride crushed at different size

Table (5.1) Lattice parameters of sodium chloride crushed at different size

XRD Data		S1	S2	S3	S4	S5	S6	S7	S8
Space Group		Fm -3m (225)	Fm -3m (225)	Fm -3m (225)	Fm -3m (225)	Fm -3m (225)	Fm -3m (225)	Fm -3m (225)	Fm -3m (225)
Crystal System		cubic	cubic	cubic	cubic	cubic	cubic	cubic	cubic
Cell Parameters 10^{-10} m	a	8.287	8.287	8.287	8.287	8.287	8.287	8.287	8.287
	b	8.287	8.287	8.287	8.287	8.287	8.287	8.287	8.287
	c	8.287	8.287	8.287	8.287	8.287	8.287	8.287	8.287
Density ($g.cm^{-3}$)		3.42	3.31	3.24	3.11	2.96	2.81	2.79	2.73
Volume $(10^{-10})^3$		569.1	569.4	569.7	569.9	570.1	570.3	570.6	570.9
d (10^{-10} m)		2.58	2.62	2.68	2.73	2.79	2.84	2.88	2.93
Cell Angular	alpha	90	90	90	90	90	90	90	90
	beta	90	90	90	90	90	90	90	90
	gamma	90	90	90	90	90	90	90	90

The crystal structure of all samples characterized at room temperature using a Philips PW1700 X-ray diffract meter (operated at 40 kV and current of 30 mA) and samples were scanned between 18^{O} and 65^{O} for sodium chloride at different size at scanning speed of 0.06 ^{o} C/s using Cu Kα radiation with λ = 1.5418Å. The representative XRD charts of all samples were shown in fig (5.1). Crystallites have cubic crystal structure for all sodium chloride at different size samples crystal structure as shown in table (5.1). from describe the (density, volume and d-space) of sodium chloride at different size samples it was observed that all samples have different density value, that d-space and volume are increase when sodium chloride crushed size increase, but density approximately decrease when sodium chloride at different size samples increase.

5.3 FTIR Results of Sodium Chloride (NaCl) at different size

After constructed eight Sodium Chloride (NaCl) crushed at different size samples, Fourier transforms infrared spectroscopy (FTIR) to study the vibrational frequencies as shown in fig (4.2) results blow, the functional groups of all samples display from table (5.1) as shown below.

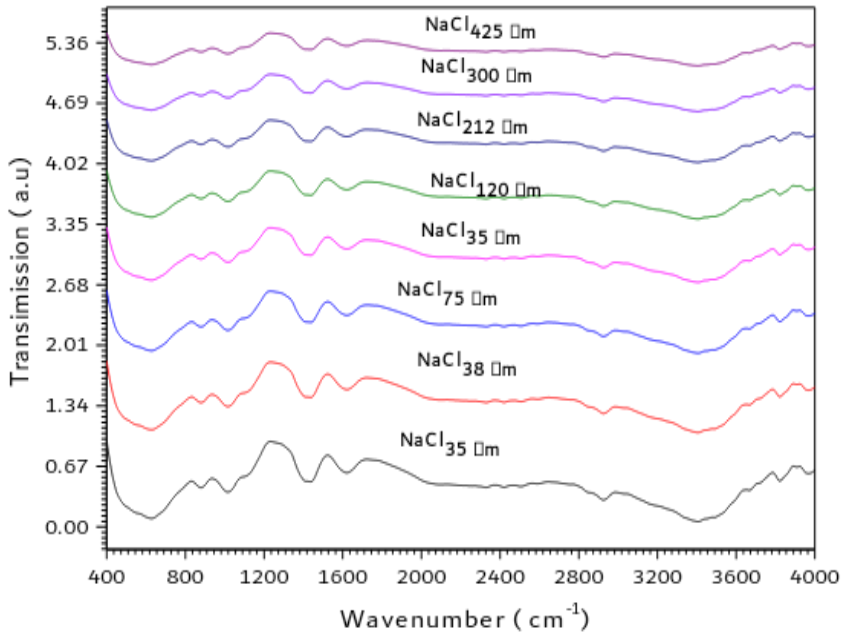

Fig (5.2) IR spectrum of sodium chloride crushed at different size

Table (5.2) Table of Characteristic IR sodium chloride crushed at different size samples

No	Wavenumber (cm-1)	Functional Group Names	Type of Vibration
1	615	alkyl halides	C–Br stretch
2	890	Aromatics	C–H “oop”
3	1112	aliphatic amines	C–N stretch
4	1426	Aromatics	C–C stretch (in–ring)
5	1377	Alkanes	C–H rock
6	1620	1° amines	N–H bend
7	2325	Nitriles	C≡N stretch
8	2415	Thiol	S-H (very weak)
9	2510	carboxylic acids	O–H stretch
10	2925	Alkanes	C–H stretch
11	3400	alcohols, phenols	O–H stretch, H–bonded
12	3830	Water	O–H stretch, free hydroxyl
13	3960	Water	O–H stretch, free hydroxyl

Fourier Transform Infrared spectroscopy is a technique used to measure the vibrational frequencies of bonds in the molecule. The FTIR spectra for sodium chloride crushed at different size were shown in Fig (5.2). The O–H stretch of alcohol group intensity peaks vibration at 3400 cm^{-1} for all sodium chloride crushed at different size samples, but O–H stretch, free hydroxyl of water intensity peaks vibration at (3830 and 3960) cm^{-1} for all sodium chloride crushed at different size samples. The characteristic peaks of alkanes C–H stretch positioned at 2925 cm^{-1} and 1377 cm^{-1} for all samples. The intensity peak assigned to carboxylic acids O–H stretch at 2510 cm^{-1} for all samples. for thiol S-H (very weak) at 2415 cm^{-1} for all samples. The intensity peak assigned to nitriles C≡N stretch at 2325 cm^{-1}

for all samples, at 1620 cm^{-1} intensity peaks vibration 1° amines N–H bend, and at 1426 cm^{-1} . Aromatics bond C–C stretch (in–ring) positioned at 2925 cm^{-1} , but aliphatic amines C–N stretch intensity peaks vibration at 1112 cm^{-1} and aromatics C–H "oop" peaks vibration at 1112 cm^{-1} for all sodium chloride crushed at different size samples. At last, the C–Br stretch of alkyl halides group intensity peaks vibration at 615 cm^{-1} for all sodium chloride crushed at different size samples

5.4 Optical Results of Sodium Chloride at Different Size Samples

The optical results of ten samples for sodium chloride at different size samples obtained using UV-VIS spectrometer as showing blow

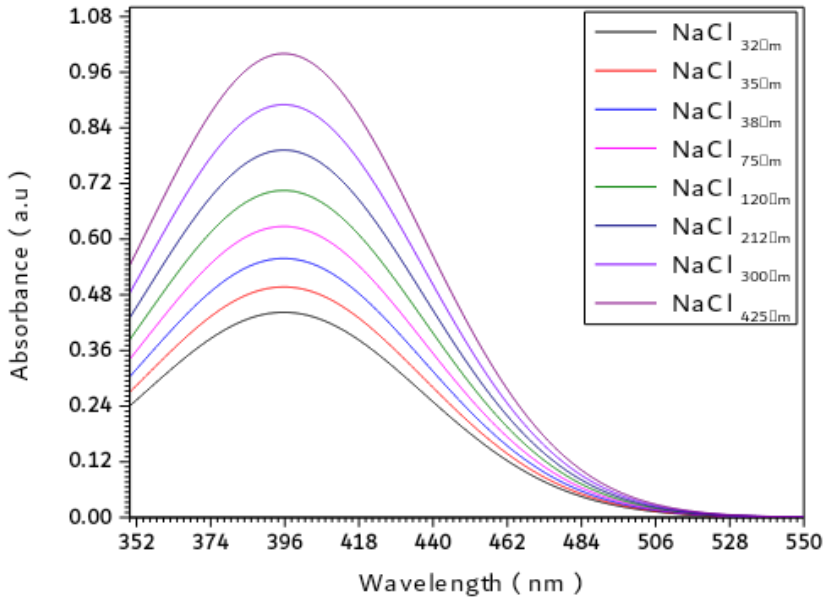

Figure (5.3) absorbance spectra of sodium chloride crushed at different size samples

Fig (5.3) display the absorbance of sodium chloride crushed at different size samples, the absorbance value decreases from 1.006 (a.u) at wavelength 396 nm for NaCl $_{425\mu m}$ sample to 0.441 (a.u) for NaCl $_{32\mu m}$ at same wavelength and this agree with the fact the decreases in absorbing surface lade to decrease in the absorbance.

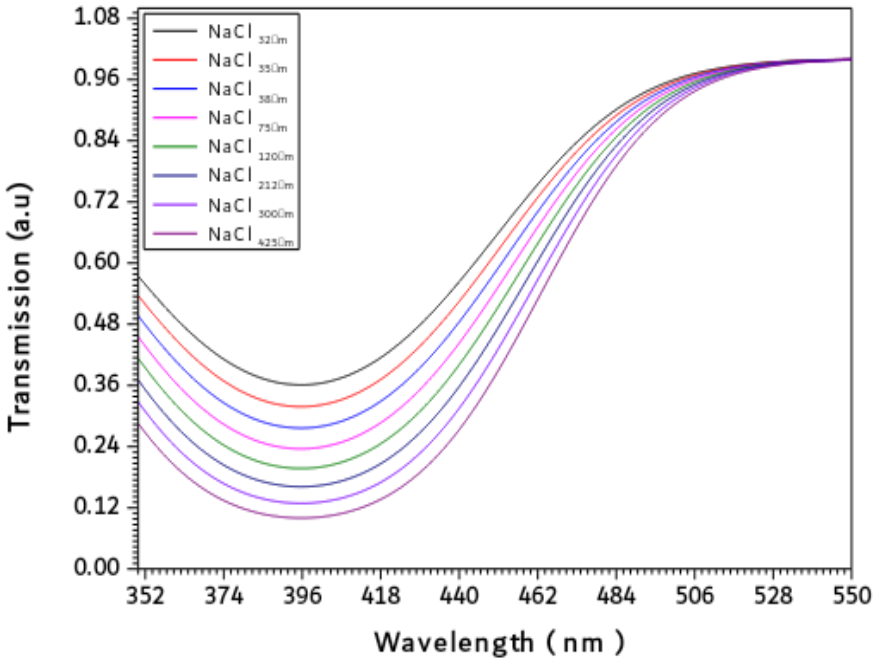

Figure (5.4) Transmission spectra of sodium chloride crushed at different size samples

The transmission of sodium chloride crushed at different size samples were shown in fig (5.4), transmission is opposite process of absorbance this means that the sample which has high absorbance will has minimum transmission.

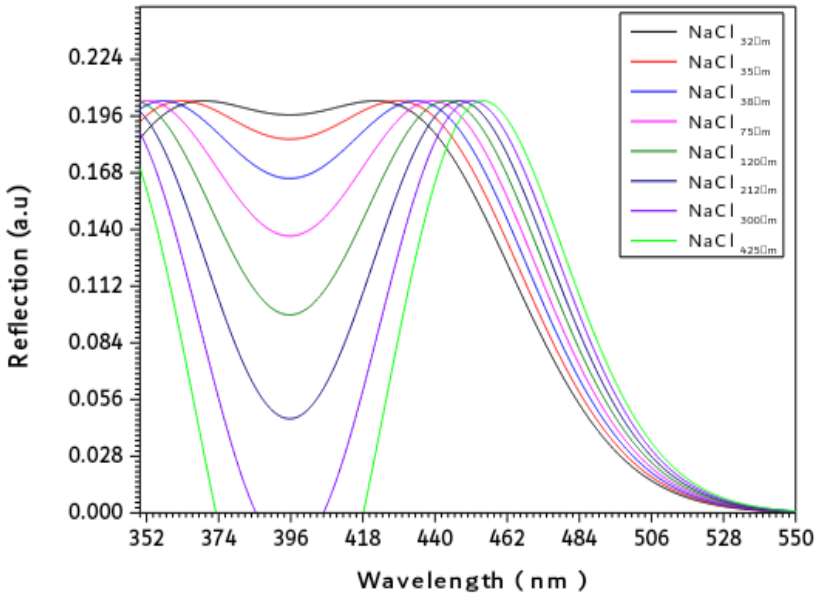

Figure (5.5) Reflection spectra of sodium chloride crushed at different size samples

Fig (5.5) show the reflection of sodium chloride crushed at different size samples; the reflection of all samples was 0.204 (a.u) ranged from 424.78nm for NaCl $_{32\mu m}$ to 454.82 nm NaCl $_{425\mu m}$.

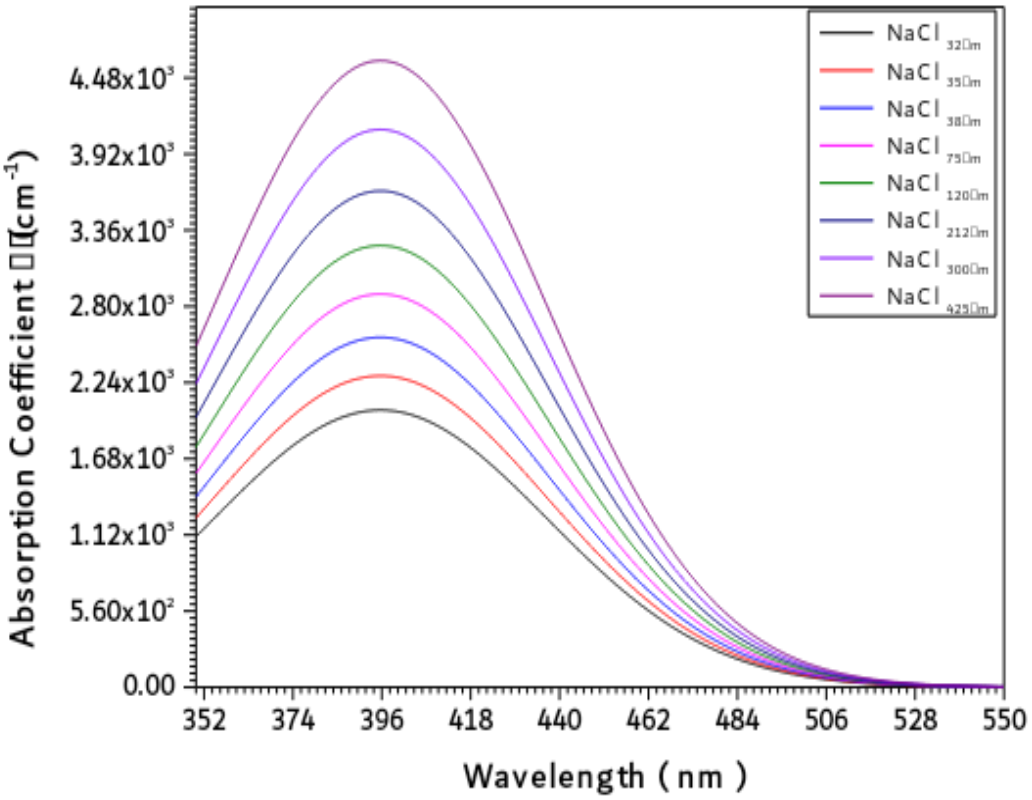

Figure (5.6) Absorption coefficient of sodium chloride crushed at different size samples as a function in wavelength

Fig (5.6) show the absorption coefficient of sodium chloride crushed at different size samples; the absorption coefficient decreases from 4.617×10^{3} cm^{-1} (a.u) at wavelength 396.2 nm for NaCl $_{425\mu m}$ sample to 2.049×10^{3} cm^{-1} (a.u) for NaCl $_{32\mu m}$ at same wavelength

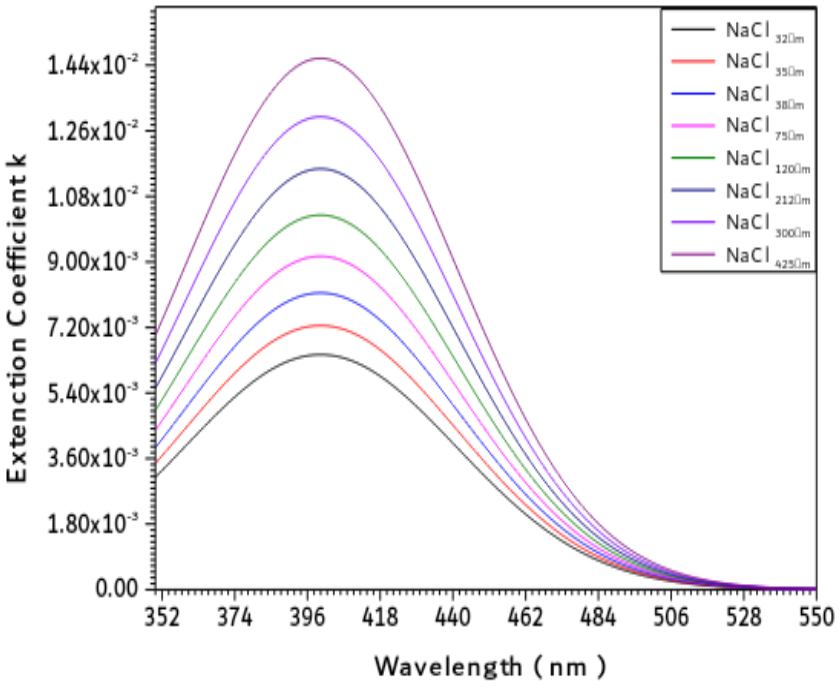

Figure (5.7) Extinction coefficient of sodium chloride crushed at different size samples as a function in wavelength

The extinction coefficient of sodium chloride crushed at different size samples was shown in fig (5.7) the extinction coefficient decreased when the size of sodium chloride decreased, the maximum value of extinction coefficient is 1.46×10^{-2} for NaCl $_{425\mu m}$ at 400.12nmm while the minimum value is 6.5×10^{-3} for NaCl $_{32\mu m}$ at same wavelength.

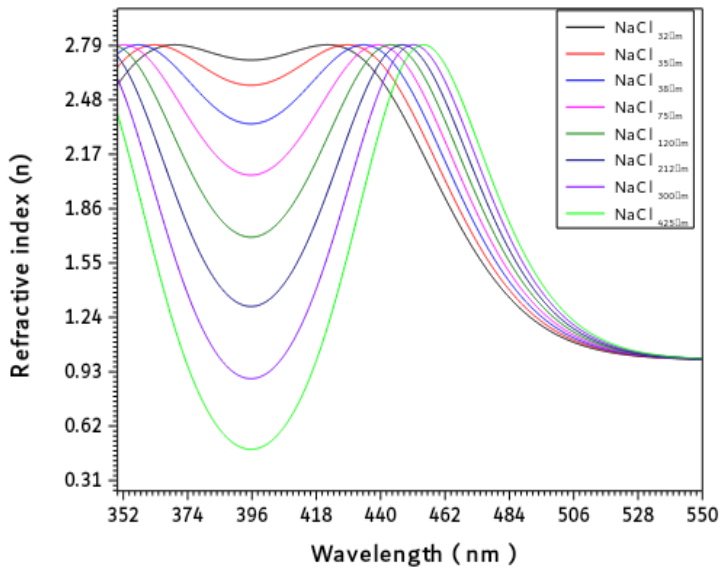

Figure (5.8) Refractive index of sodium chloride crushed at different size samples as a function in wavelength

The refractive index (n) is the relative between speed of light in vacuum to its speed in material which does not absorb this light. The value of n was calculated from the equation

$$n = \left[\left(\frac{(1+R)}{(1-R)}\right)^2 - (1+k^2)\right]^{\frac{1}{2}} + \frac{(1+R)}{(1-R)}$$

Where (R) is the reflectivity. The variation of (n) vs (λ) for sodium chloride crushed at different size samples was shown in fig.(4.8), the maximum value of refractive index is (2.803) for all samples at wavelength ranged (350 to 455) nm.

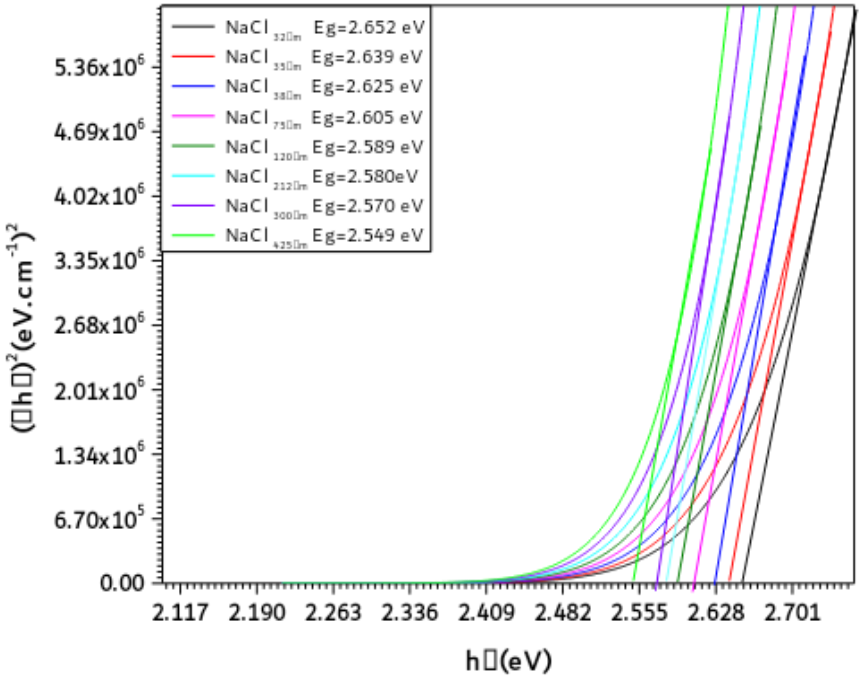

Fig(5.9) optical energy band gap of sodium chloride crushed at different size samples

The optical energy gap (Eg) has been calculated by the relation $(\alpha h\upsilon)^2 = C(h\upsilon - Eg)$ where (C) is constant. By plotting $(\alpha h\upsilon)^2$ vs photon energy ($h\upsilon$) as shown in fig.(5.9) for sodium chloride crushed at different size samples, and by extrapolating the straight thin portion of the curve to intercept the energy axis ,the value of (Eg) decresed from 2.652 eV for NaCl $_{32\mu m}$ to 2.549 eV for NaCl $_{4252\mu m}$. It was observed that the different crushed size sodium chloride samples confirmed the reason for the band gap shifts .

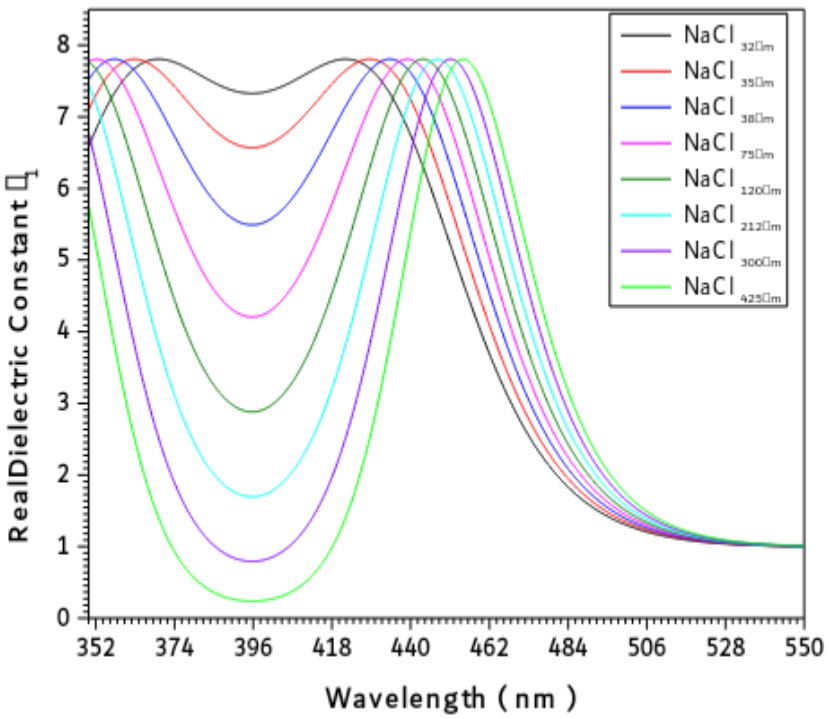

Figure (5.10) Real dielectric constant of sodium chloride crushed at different size samples as a function in wavelength

In Fig(5.10) shows the variation of the real dielectric constant (ε_1) with wavelength of sodium chloride crushed at different size samples which calculated from the relation $\varepsilon_1 = n^2 - k^2$ Where the real the dielectric (ε_1) is the normal dielectric constant . From fig (4.10) the maximum value of (ε_1) for all samples equal (7.85) at wavelength ranged (350 to 455) nm, the variation of (ε_1) is follow the refractive index where the absorption of the samples at these wavelength is small, but the polarization was increase.

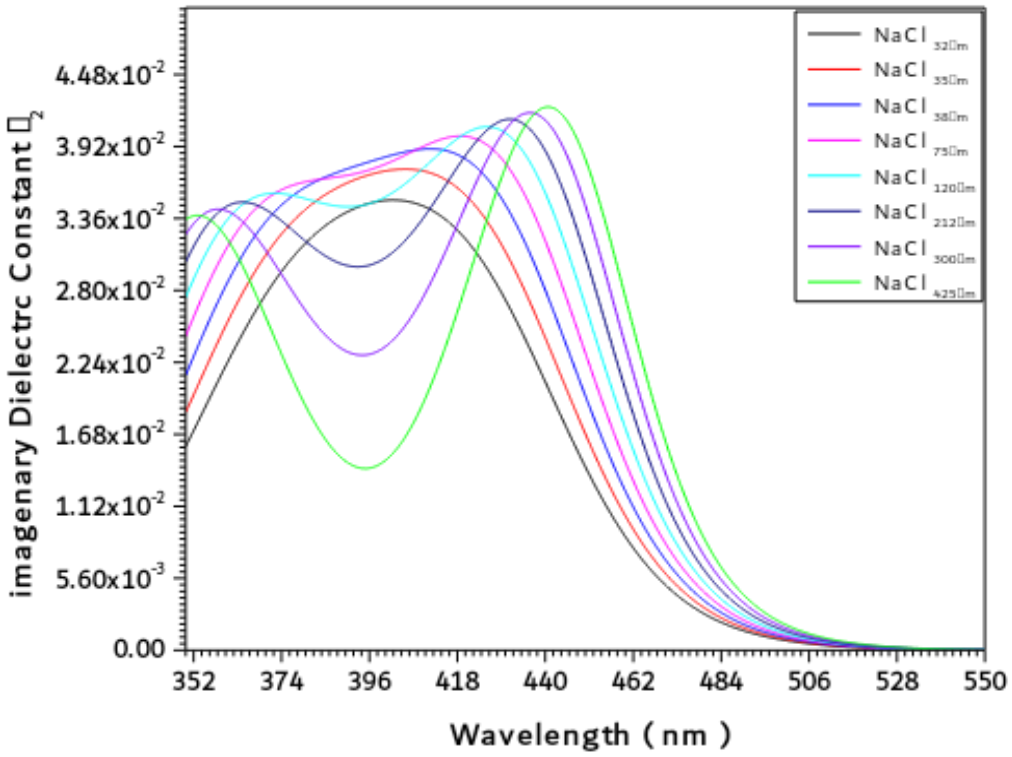

Figure (5.11) Imaginary dielectric constant of sodium chloride crushed at different size samples as a function in wavelength

The imaginary dielectric constant (ε_2) vs (λ) was shown in fig(5.11) this value calculated from the relation $\varepsilon_2 = 2nK$ (ε_2) represent the absorption associated with free carriers.As shown in fig(5.11). these behavior may by related to the different absorption mechanism forfree carriers. The value of imaginary dielectric constant decresed from 4.27×10^{-2} to 3.33×10^{-2} in range (350 to 455) nm for all samples. ,these behavior may by related to the different absorption mechanism for free carriers.

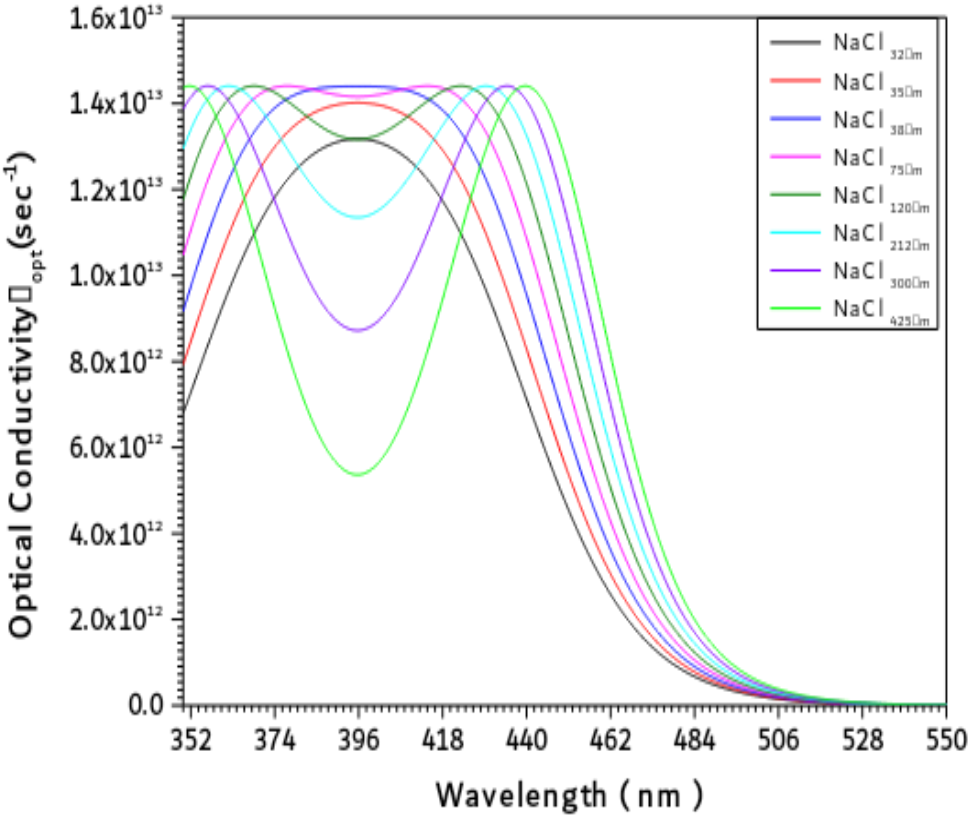

Figure (5.12) Optical conductivity of sodium chloride crushed at different size samples as a function in wavelength

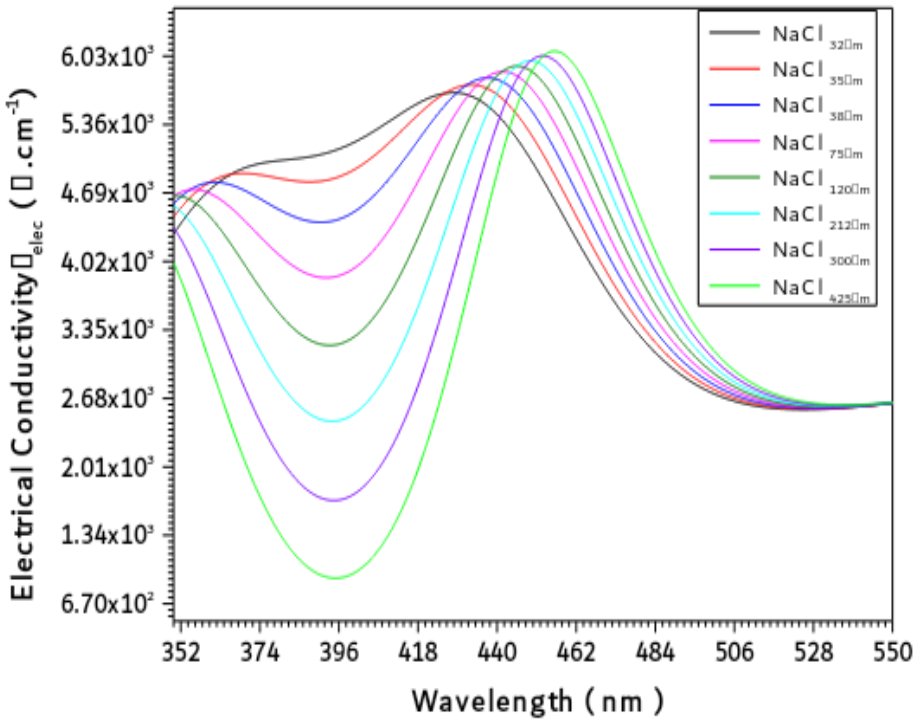

Figure (5.13) Electrical conductivity of sodium chloride crushed at different size samples as a function in wavelength

The optical conductivity is a measure of frequency response of material when irradiated with light which is determined using the following relation, $\delta_{opt} = \frac{\alpha nc}{4\pi}$ Where (c) is the light velocity. The electrical conductivity can be estimated using the following relation $\delta_{ele} = \frac{2\lambda\delta_{opt}}{\alpha}$.

The high magnitude of optical conductivity for all samples (1.44×10^{13} sec^{-1}) in range (350.13 to 440.8)nm confirms the presence of very high photo-response of the conductivity of sodium chloride crushed at different size samples.

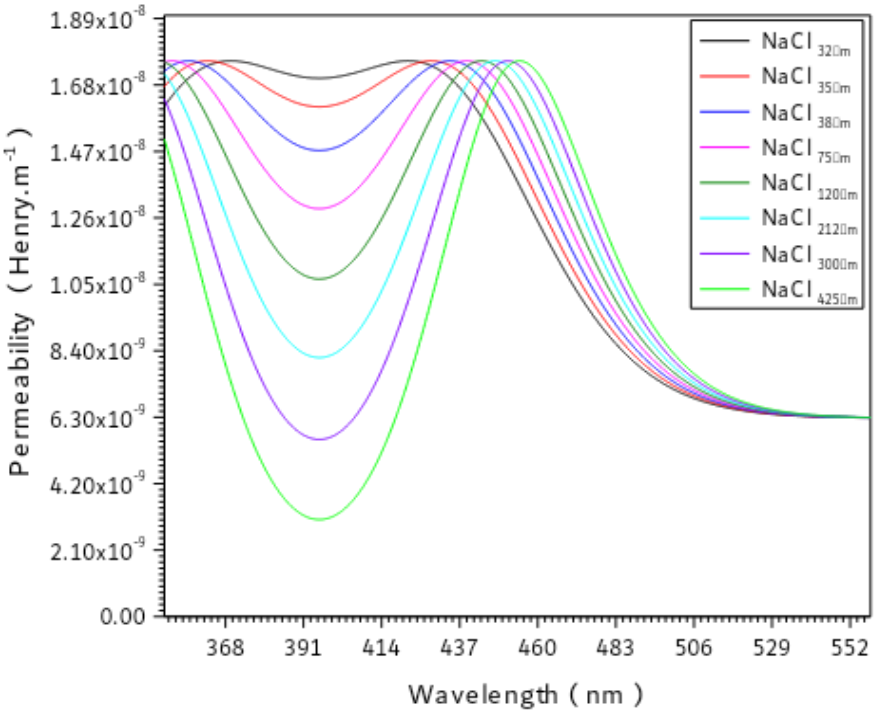

Figure (5.14) Electrical permeability of sodium chloride crushed at different size samples as a function in wavelength

The value of electrical permeability (μ) was calculated from the equation $\mu_r = \frac{\sqrt{n}}{\varepsilon_o}$ Where (μ_o) is vacumm permeability equal (1.257×10^{-6} henry /m) . The variation of electrical permeability (μ) vs (λ) for sodium chloride crushed at different size samples was shown in fig.(5.14), the maximum value of electrical permeability (μ) is (1.759×10^{-8} henry/m) for all samples at wavelength ranged (350 to 455) nm.

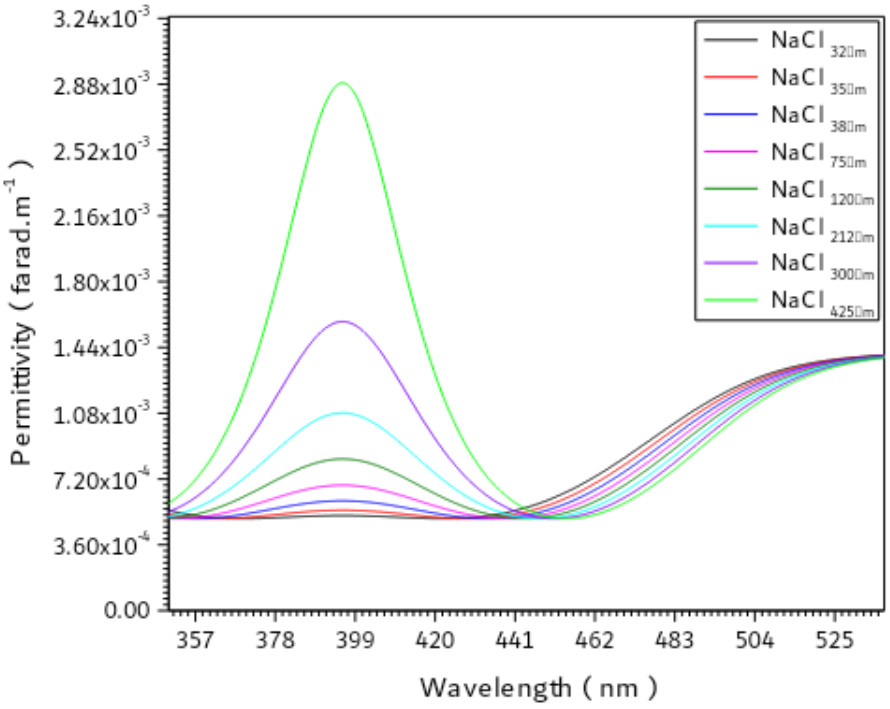

Figure (5.15) Magmatic permittivity of sodium chloride crushed at different size samples as a function in wavelength

The value of magmatic permittivity (ε_r) was calculated from the equation $\varepsilon_r = \frac{1}{\sqrt{n}\ \varepsilon_o}$ Where (ε_o) is vacumm permittivity equal (8.85×10^{-12} farad/m) . The variation of magmatic permittivity (ε_r) vs (λ) for sodium chloride crushed at different size samples was shown in fig.(5.15), the maximum value of magmatic permittivity (ε_r) is (2.899×10^{-3} farad/m) for sample NaCl $_{425\mu m}$ at wavelength 395 nm, while for sample NaCl $_{32\mu m}$ equal (5.264×10^{-4} farad/m).

5.5 Effect of Crushed Size on Properties of Sodium Chloride Samples

Table (5.3) Structurer, optical, electrical and magnetic properties of sodium chloride crushed at different size samples (all properties studied at wavelength 395 nm).

Sample	d-space 10-10m	Density mg.cm-3	Volume (10-10m)3	Eg eV	Refractive Index	Electrical Conductivity ×103(Ω.m)-1	electrical permeability (μ) (10-8 henry/m)	magmatic permittivity (εr) (10-3 farad/m)
NaCl 32μm	2.58	3.42	569.1	2.652	2.71	5.12	1.70	0.53
NaCl 35μm	2.62	3.31	569.4	2.639	2.56	4.84	1.60	0.55
NaCl 38μm	2.68	3.24	569.7	2.625	2.35	4.41	1.50	0.61
NaCl 75μm	2.73	3.11	569.9	2.605	2.05	3.88	1.30	0.69
NaCl 120μm	2.79	2.69	570.1	2.589	1.70	3.19	1.10	0.84
NaCl 212μm	2.84	2.81	570.3	2.580	1.30	2.45	0.80	1.09
NaCl 300μm	2.88	2.79	570.6	2.570	0.89	1.69	0.50	1.59
NaCl 425μm	2.93	2.73	570.9	2.549	0.48	0.89	0.30	2.90

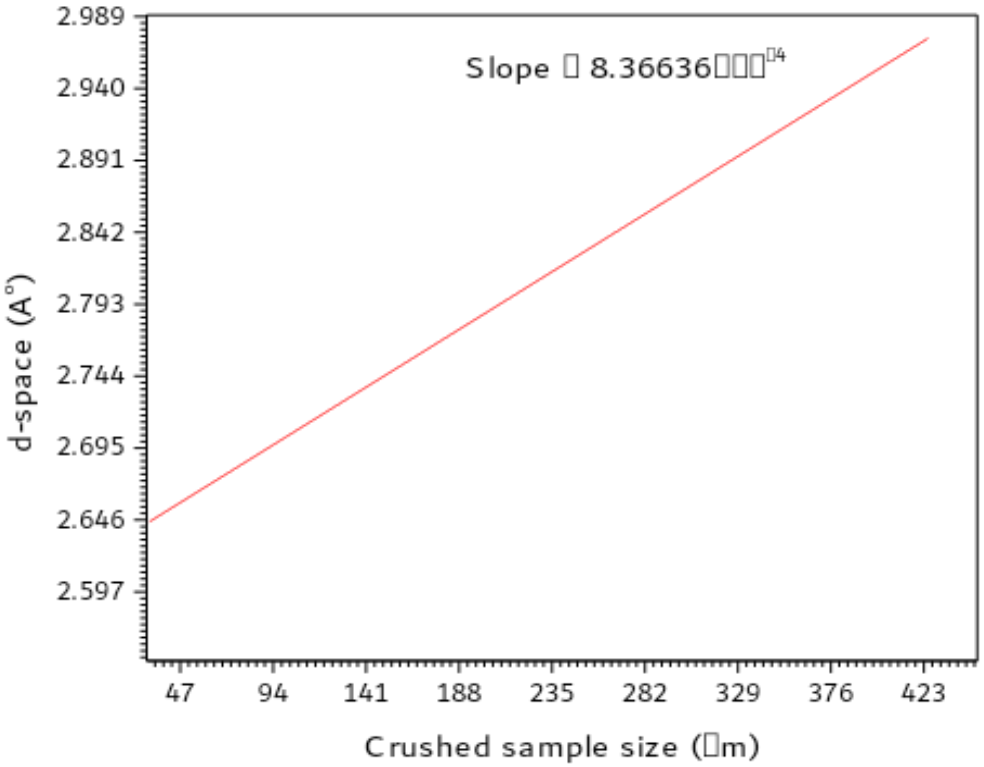

Figure (5.16) Relationship between crushed size of sodium chloride samples and d-space

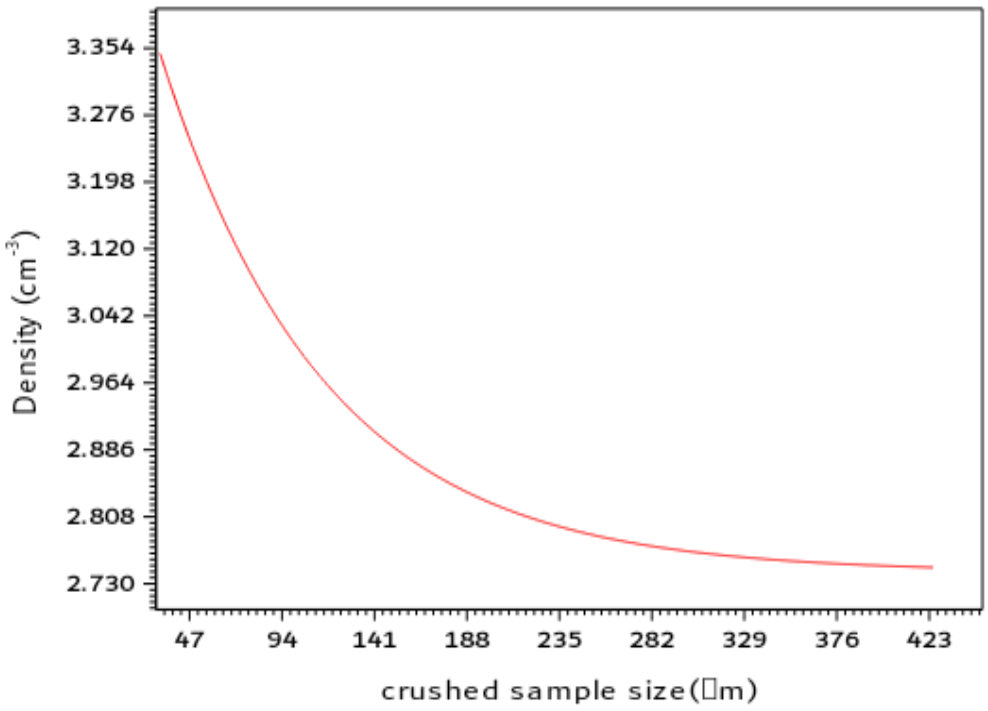

Figure (5.17) Relationship between crushed size of sodium chloride samples and density

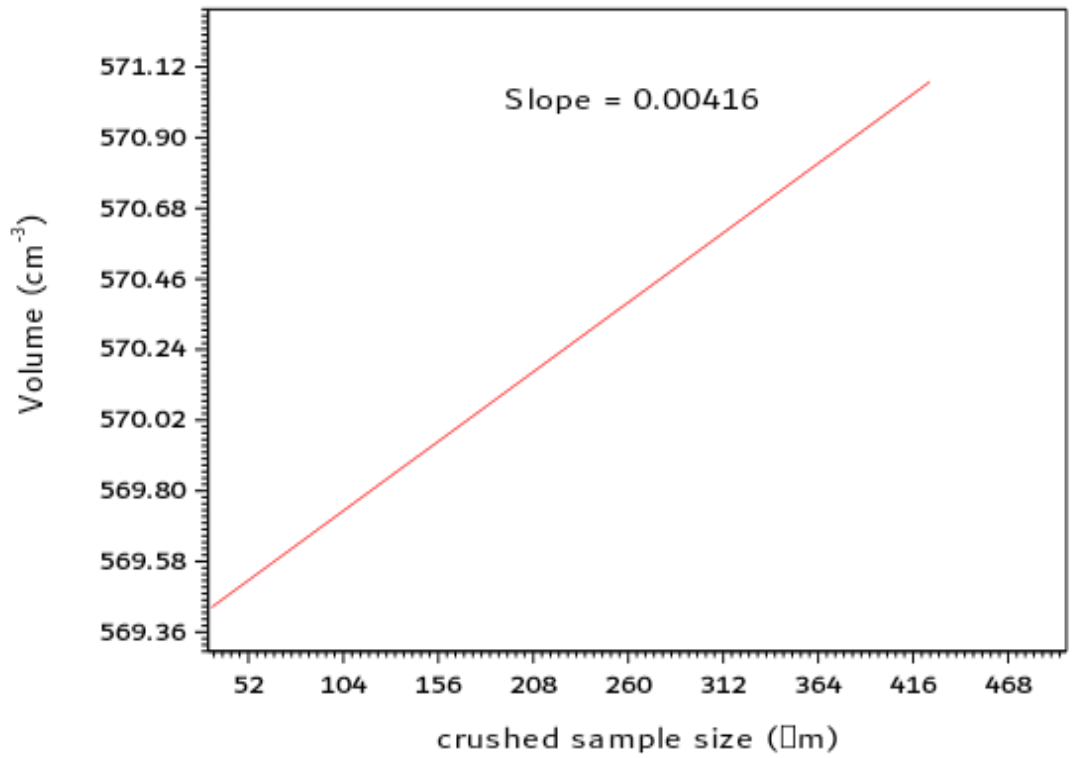

Figure (5.18) Relationship between crushed size of sodium chloride samples and volume

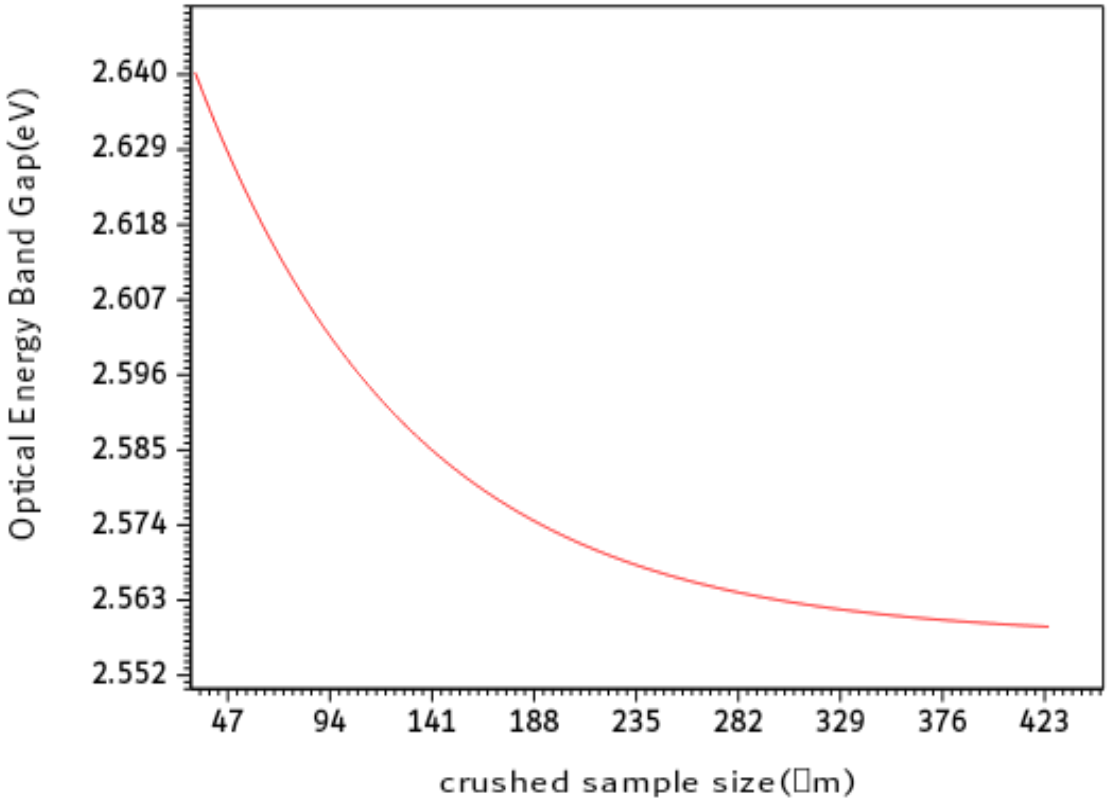

Figure (5.19) Relationship between crushed size of sodium chloride samples and optical energy band gap

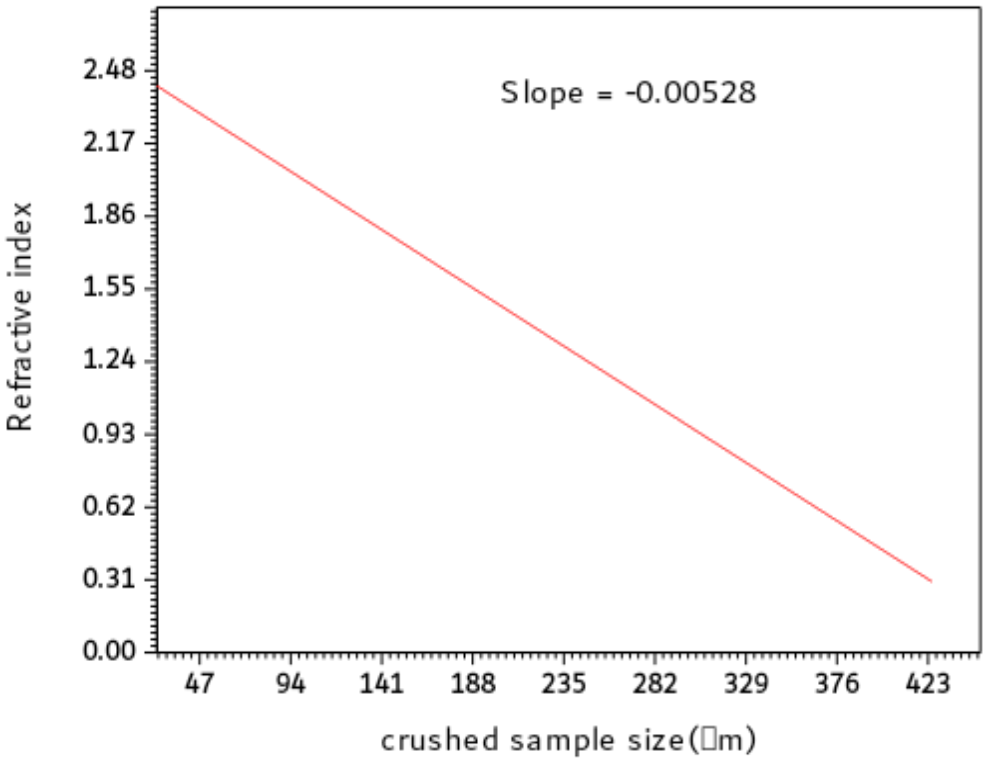

Figure (5.20) Relationship between crushed size of sodium chloride samples and refractive index

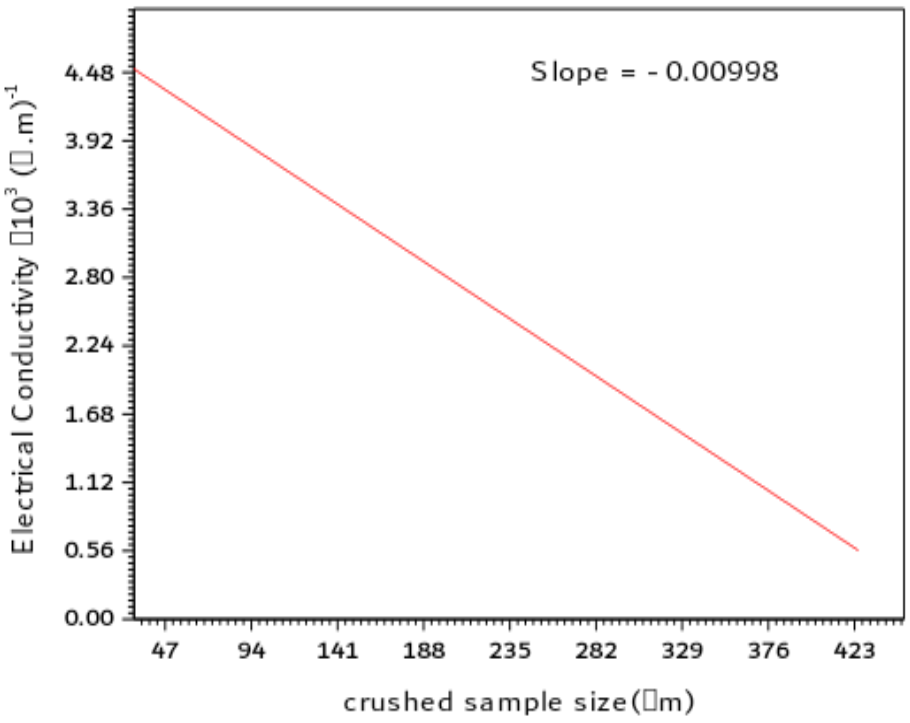

Figure (5.21) Relationship between crushed size of sodium chloride samples and electrical conductivity

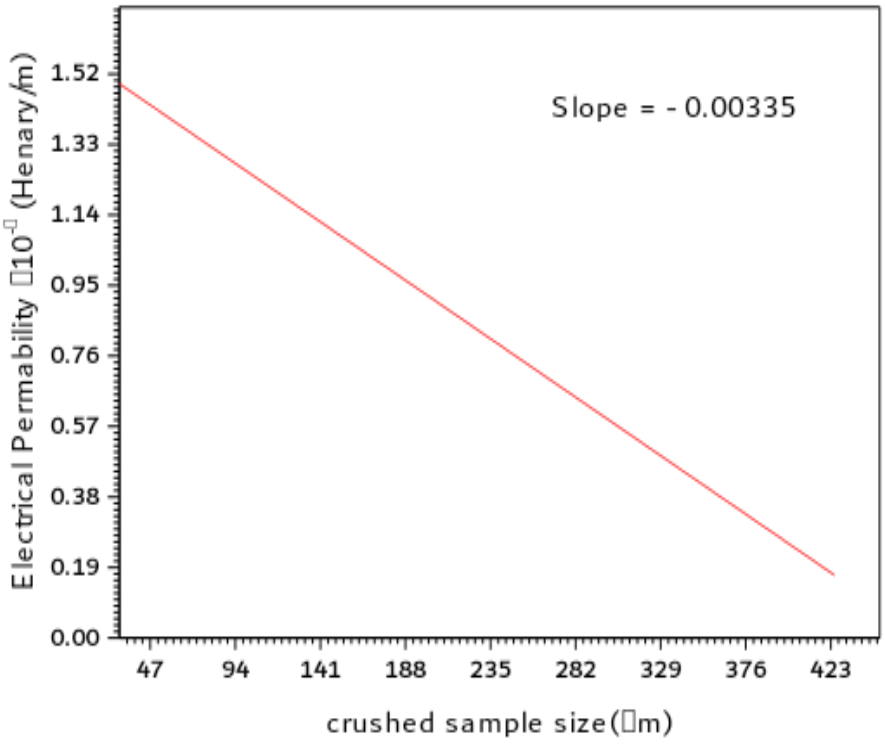

Figure (5.22) Relationship between crushed size of sodium chloride samples and electrical permeability

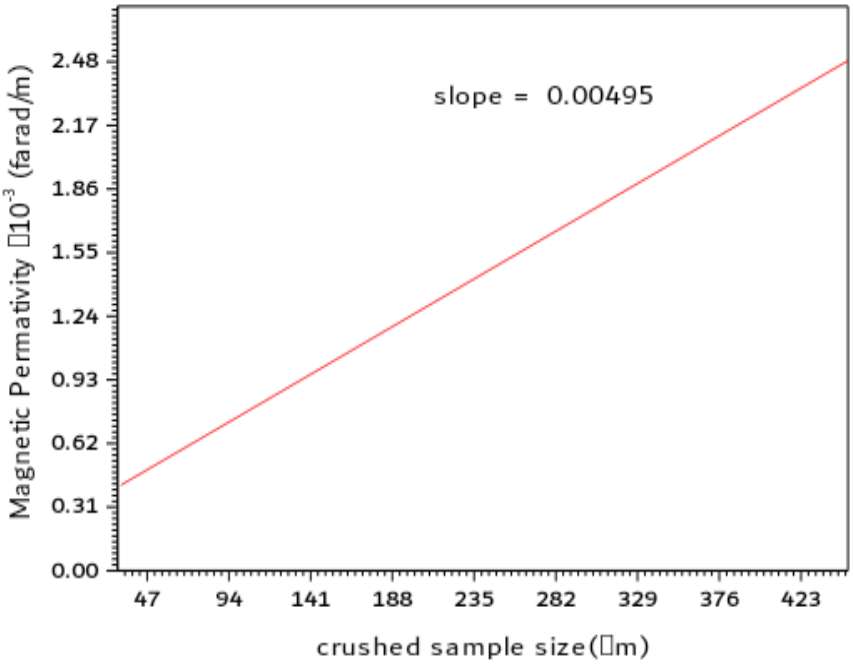

Figure (5.23) Relationship between crushed size of sodium chloride samples and magnetic permittivity

5.6 Discussion

The change of some optical and electrical properties of the 8 samples of Nacl when crushed shows very interesting properties. Using UV spectrometer the change of absorption coefficient α, refractive index n, energy gap Eg, electric permittivity ε, optical and electric conductivities σ_{0p} and σ_{eL}beside magnetic permittivity were displayed graphically against the wavelength λ for different Nacl crushed sizes (32, 25, 28, 75, 120, 212, 300, and 425μm). According to figure (5.6) the absorption coefficient increases upon increasing the crush size. This may be attributed to the fact that increasing crush size increases the density and number of absorbing atoms. The refractive index in figures (4.8, 4.20) decreases upon increased the crush size in the wave length 352 – 462 nm after that it increases.

The energy gaps in figures (5.9, 5.19) shows that Eg decreases upon increasing the crush size.

The electric permittivity in figure (5.10, 5.22) decreases upon increasing the crush size in the range 352 – 462 nm after that it increases with the crush size.

The optical and electrical conductivities shows almost similar behavior. Figure (5.12) for the optical conductivity indicates that for the wave length range 352 – 374nm and. After 462nm the optical conductivity increases upon increasing the crush size.

The electrical conductivity in figure (5.13 , 21) indicates that it decreases upon increasing crush size in the range 352 – 462nm. After 462nm it increases with the crush size.

The magnetic permeability in figure (5.14, 23) decreases upon increasing crush size in the range 360 – 462nm, while it increases with the crush size for wave lengths more than 462nm figures (5.16) and (5.18) shows that both crystal spacing d and nano crystal volume V increases upon increasing

the crush size. However the density decreases upon increasing crush size according to figure (5.17).

5.7 Conclusion

The crushing of Nacl into small particles having different micro sizes shows that this causes their physical properties to change. Ti was found that their nano size increases upon increasing their micro size, where each micro particle consists of aggregates of nano crystals. The absorption coefficient, crystal spacing increases upon increasing the nano and micro size. The energy gap decreases upon increasing the nano and micro size. The energy gap decreases upon increasing the nano and micro size. The optical conductivity also increases for a wide range of wavelengths. The electric conductivity, permittivity, refractive index and magnetic permeability decreases for short wavelengths and increases for long wave lengths upon increasing the nano and micro size.

5.8 Future work

1. This study of this work can be extended for other materials which are used in industry.
2. Other studies including thermal properties beside mechanical properties are needed also.
3. The applications of this work in industry is also very important.

References

[1] Li, B., Wang, L., Kang, B., and Qiu, Y .(2006), Solar Energy Materials and Solar Cells, Wiley-VCH.

[2] Dalven, Richard. (1980) "Introduction to applied solid state physics. Topics in the applications of semiconductors, superconductors and the nonlinear optical porperties of solids." New York: Plenum Press.

[3] G.Aruld has, (2009) Quantum Mechanics, and edition, PHI private limited, New Delhi.

[4] Partanen, Mikko, Hayraynen, Teppo, Oksanen, Jani, Tulkki Jukka, (2017) photon mass drag and the momentum of light in a medium, physical reviewA (Atomic, Molecular and optical physics), 95 (6), [063850].

[5] Ratna Tantra (2016), Nanomaterial , Wiley & sons, New York .

[6] Bhushan, B, Luo, D, Schricker, S.R.,Sigmung, W., Zauscher, S., (2014) Hand book of Nanomaterials properties, Heidelberg; London, Springer;.

[7] Ratna Tantra (2016) , Nanomaterial characterization, first published April Wiley & sons, Inc9, New York ISBN978111875354York

[8] Neha Srivastava, Manish Srivastava, P. K. Mishra and Vijai Kumar Gupta. Green Synthesis of Nanomaterials for Bioenergy Applications, First Edition. 2021 John Wiley & Sons Lt8, New York.

[9] Li, B., Wang, L., Kang, B., and Qiu, Y.(2006), Solar Energy Materials and Solar Cells, Wiley-VCH.

[10] Schawbl, F., quantum Mechanics third edition,(2016) springer, Berlin (2005).

[11] L.I.Schiff, Quantum Mehanics (2005) Mc Graw Hill, Tokyo .

[12] K. Uuang, Quantum field theory (2010), wiley VCH, Weinheim .

[13] David J. Griffith, Introduction to quantum mechanics (2005), prentice Hall, New Jersy .

[14] A. Beiser, concept of modern physics(2002), Mc Graw Hill, London

[15] Levich, B. G., theoretical physics(1696), John wiley and sons, New York .

[16] principles of physics,(1998) USA, F. Bueche,

[17] Bohren, C., & Huffman, D. (2008). Absorption and scattering of light by small particles (First Edit). Arizona: A Wiley-Interscience Publishers.

[18] Paul Lorrain and Dale R. Corson, Electromagnetic fields and waves(1970), W.H.Ferman and company san Francis co .

[19] Aldén, M. (2011). Lecture 7. Rayleigh scattering and applications in combustion measurements. Combustion Summer School Lecture.

[20] Seeger, Karlheinz. Semiconductor physics(2013), Springer Science & Business Media,.

[21] Wu, Jyh-Ming, et al. "Thermal evaporation growth and the luminescence property of TiO2 nanowires." Journal of crystal Growth 281.2-4 (2005): 384-390.

[22] Raymond A. serway, physics(2004), Saunders College publishing, califomia .

[23] Shakib, S. A., & Eshrah, I. A. (2011). Electromagnetic Scattering from Conductors : the Recursive Iterative Surface Equivalence Approach. IEEE, (2), 1–4.

[24] Klaus Grobe and Michael Eiselt. (2014). Wavelength division multiplexing; A practical engineering guide. Wiley.

[25] Kamat, P.V., et al., Nanoparticles, in Handbook of Nanostructured Materials and Nanotechnology., Academic Press: New York.2010.

[26] Liu, Xiaolan, et al. "Hybrid energy harvester with bi-functional nano-wrinkled anti-reflective PDMS film.

[27] Sabu Thomas, Aparna Thankppan, perovskite photovoltaics, 2018 Elsevier Inc.

[28] Shisode, M.V., et al., Investigations of magnetic and ferroelectric properties of multiferroic Sr-doped bismuth ferrite. Applied Physics A, 2018. 124(9): p. 603

[29] Gibin George, Zhiping Luo,Sivosanara Roo Ede fundamentals of perovskite Oxides, 2020 by CRC Press.

[30] Bhandari, K.P., R.J. An overview of Hybrid –organic – inorganic metal Halide perovskite solar cells. Academic Press: Cambridge, MA, USA, 2018, pp.233-254.

[31] Richard J. D. Tiley, perovskite: structure – property relationships, first published 2016 Wiley & sons, Inc. ISBN 97811189535651

[32] Bhoyar, D.N., et al., Structural, infrared, magnetic and ferroelectric properties of Sr0· 5Ba0· 5Ti1-xFexO3 Nano ceramics: Modifications via trivalent Fe ion doping. Physical B: Condensed Matter, 2020. 581: p. 411944.

[33] Amira Jad Elrb Ali, Mubarak Dirar Abdallah, Abdalsakhi S M.H, A. E. Mohamed Osman, Ahmed H .Alfaki, Asim Ahmed Mohamed Fadol, Asma, Abd-Alla Mohamed Altambor, Syntheses (Ba x Fe1-x Ti O 4) Nano size and Study Crystal properties, Optical Energy Gap and Optical & Electrical Conductivity, IOSR Journal Of Applied Physics (IOSR-JAP)

[34] brinker,c.Jeffrey , sol –gel science :the physics and chemistry of sol-gel processing “, Boston, academic press, 2019.

[35] M. K. Jararaj, Nano structured Oxide and Devices: Optical and Electrical Properites1st ed. 2020 springer.

[36] Ye, Z.-G., Handbook of advanced dielectric, piezoelectric and ferroelectric materials: Synthesis, properties and applications. Elsevier, 2008

[37] Amira Jad Elrb Ali, Mubarak Dirar Abdallah, Abdalsakhi S M.H, A. E. Mohamed Osman Ahmed H .Alfaki, Asim Ahmed Mohamed Fadol, Asma Abd-Alla, Mohamed Altambor, The Effect of Fe Concentration on

Crystal size, Crystal Spacing, Nano Size, and Absorption Coefficient for (Ba x Fe1-x Ti O4), IOSR Journal of Applied Physics (IOSR-JAP) e-ISSN: 2278-4861.Volume 13, Issue 6 Ser. II (Nov. – Dec. 2021), PP 14-18

[38] Chen, K., Chen, X., Xue, D., Hydrothermal route to crystallization of FeOOH nanorods via FeCl36H2O: effect of Fe3+ concentration on pseudocapacitance of ironbased materials, 2015.

[39] Arico AS, Bruce P, Scrosati B, Tarascon J-M, Schalkwijk WV Nanostructured materials for advanced energy conversion and storage devices. (2005) Nat Mater 4:366–377.

[40] Claassen, J.O., Sandenbergh, R.F.(2007), Influence of mixing on the quality of iron precipitates in zinc-rich solutions. Hydrometallurgy.

[41] Zohal E. M. Ebnouf, Mahmoud.H.M .Hilo, Mubarak Dirar Abdallah, Ahmed H.Alfaki, Abdalsakhi S M.H & Sawsan Ahmed Elhouri Ahmed, The Effect of Changing Concentrations of Al2O3 On The (ZnO)X(Al2O3)1-X Thin Films Absorption And Energy Gap, International Journal of Scientific Engineering and Applied Science (IJSEAS) – Volume-3, Issue-3, March 2019.

[42] Guang Zhu , Likun Pan, perovskite materials:(2016) synthesis, characterization, properties and application BoD- books on Demand.

[43] brinker,c.Jeffrey , sol –gel (2019) science :the physics and chemistry of sol-gel processing “ , Boston , academic press.

[44] M. K. Jararaj, (2020) springer Nano structured Oxide and Devices: Optical and Electrical Properites1st ed.

[45] M. Dehghanab and A. Behjat *ab, 2019, 9, 20917–20924 Deposition of zinc oxide as an electron transport layer in planar perovskite solar cells by spray and SILAR ethods comparable with spin coating, RSC Adv.

[46] A. K. Chandiran, A. Yella, M. T. Mayer, P. Gao, M. K. Nazeeruddin and M. Gratzel, Adv. Mater., 2014, 26, 4309–4312.

[47] T. Sahoo, M. Kim, M.-H. Lee, L.-W. Jang, J.-W. Jeon, J. S. Kwak, I.-Y. Ko and I.-H. Lee, J. Alloys Compd., 2010, 491, 308–313.

[48] H.-S. Kim, C.-R. Lee, J.-H. Im, K.-B. Lee, T. Moehl, A. Marchioro, S.-J. Moon, R. Humphry-Baker, J.-H. Yum, J. E. Moser, M. Gr¨atzel and N.-G. Park, Sci. Rep., 2012, 2, 591.

[49] Sakina Ibrahim Ali, Mubarak Dirar Abdallah, Sawsan Ahmed Elhouri Ahmed, The Relationship Between Energy Gab & Efficiency in Dye Solar Cells, International Journal of Current Trends in Engineering & Research (IJCTER) e-ISSN 2455–1392 Volume 2 Issue 7, July 2016 pp. 82 – 89.

[50] Hino, Y., Kajii, H. & Ohmori, Y. (2006). Transient characteristics of polyfluorene-based polymer light-emitting diodes and their application for color tunable devices.

[51] Hoke, E. T. Vandewal, K., Bartelt, J. A., Mateker, W. R., Douglas, J. D., Noriega, R., Graham, K. R., Fréchet, J. M., Salleo, A. & McGehee, M. D. (2013). Recombination in Polymer:Fullerene Solar Cells with Open-Circuit Voltages Approaching and Exceeding 1.0 V. Adv. Energy Mater. 3,220–230.

[52] Hino, Y., Kajii, H. & Ohmori, Y(2006). Transient characteristics of polyfluorene-based polymer light-emitting diodes and their application for color tunable devices. Thin Solid Films.

[53] Azza Abdalwahab Abdalla, Ali Sulaiman Mohamed, Mubarak Dirar Abdallah, Abdalsakhi Suleman & Sawsan Ahmed Elhouri Ahmed.

[54] Physical properties of carbon nanotubes by Saito, Dresselhaus and Dresselhaus(1998). (Imperial CollegePress.

[55] Ali Salih Ali, Mubarak Dirar Abd-Alla, Mohammedaine Adam, December (2020) The effect of iron oxide on physical and optical properties of soda lime glass, Kordofan journal of Educational Sciences and Huminaties, I(1),V(1).

[56] Introduction to Carbon Nanotubes and Its Applications in Semiconductor Industry Author: Lo, SiO- On 5/10/2006.

[57] L. Solymar, D. Walshr R. R. A. Syms, (2014) electrical properties of materials, Ninth edition Oxford University Press, , ISBN 978–0–19–870278–8.

[58] M. K. Jayaraj, (2020) optical and electrical properties, material Horizons; from nature to nanomaterial, 1st edition, ISBN. 10-98115333x.

[59] Michael B. Heaney(2000) "Electrical Conductivity and Resistivity. "Copyright CRC Press LLC.

[60] Baumeister PW, (1961) Optical absorption of cuprous oxide, Physical Review.

[61] E.Y.Tsymbal,(1972) Optical properties of solids, academic press New York and London.

[62] Gonzale, W and Mancini, H.L, an introduction to materials science. Princeton university press (2004). ISBN 9780-691-07097-1

[63] Gunzler, H. and Gremlich, H.-U.,IR Spectroscopy: An Introduction, Wiley-VCH, Weinheim, Ger-many, 2002.

[64] Hollas, J. M. (1996),Modern Spectroscopy, , Wiley, Chichester, UK, 3rd Edition.

[65] N.B. Colthrup, L.H. Daly, S.E. Wiberley,(1990) Introduction to Infrared and Raman Spectroscopy, Academic Press, SanDiego, .

[66] J. O. Carneiro. S. Azevedo, F. Fernandes, E. Freitas, M. Pereira, C. J. Tavares, and S. Lanceros-Mendez and V(2014). Synthesis of iron-doped TiO2nanoparticles by ball-milling process: the influence of process parameters on the structural, optical, magnetic, and photocatalytic properties, Springer Science+ Business Media New York.

[67] Duangdao Channei1, Auppatham Nakaruk, Sukon Phanichphant, Pramod Koshy and Charles Christopher Sorrell. (2016) Effect of iron

doping on the structural and optical properties of CeO2films, Springer Science and Business Media New York.

[68] Stephen Lourduraj and Rayar Victor Williams (2017). Effect of iron doping on structural and optical properties of TiO2 thin film by sol–gel routed spin coating technique J. Adv. Dielect. 7, 1750024.

[69] BS Avinash, VS Chaturmukh, HS Jayanna, and CS Naveen, (2016) effect of particle size on band gap and DC electrical conductivity of TiO2 nanomaterial.

[70] L.H Omari and H. Lassri(2020). Structural and optical properties of Fe-doped ruddlesden – popper Ca3 Ti2-x Fex O7-δ nanoparticles Elsevier B. V.

[71] Nicholas O. Ongwen, Andrew O.Oduor1, and Elijah O. Ayieta, (2019) Effect of Concentration of Reactants on the Optical Properties of Iron Doped Cadmium Stannate Thin Films Deposited by Spray Pyrolysis; Published by Scientific & Academic Publishing 2019.